SAND74-0042
Unlimited Release
UC-70

Deep Rock Nuclear Waste Disposal Test: Design and Operation

R. D. Klett

MASTER

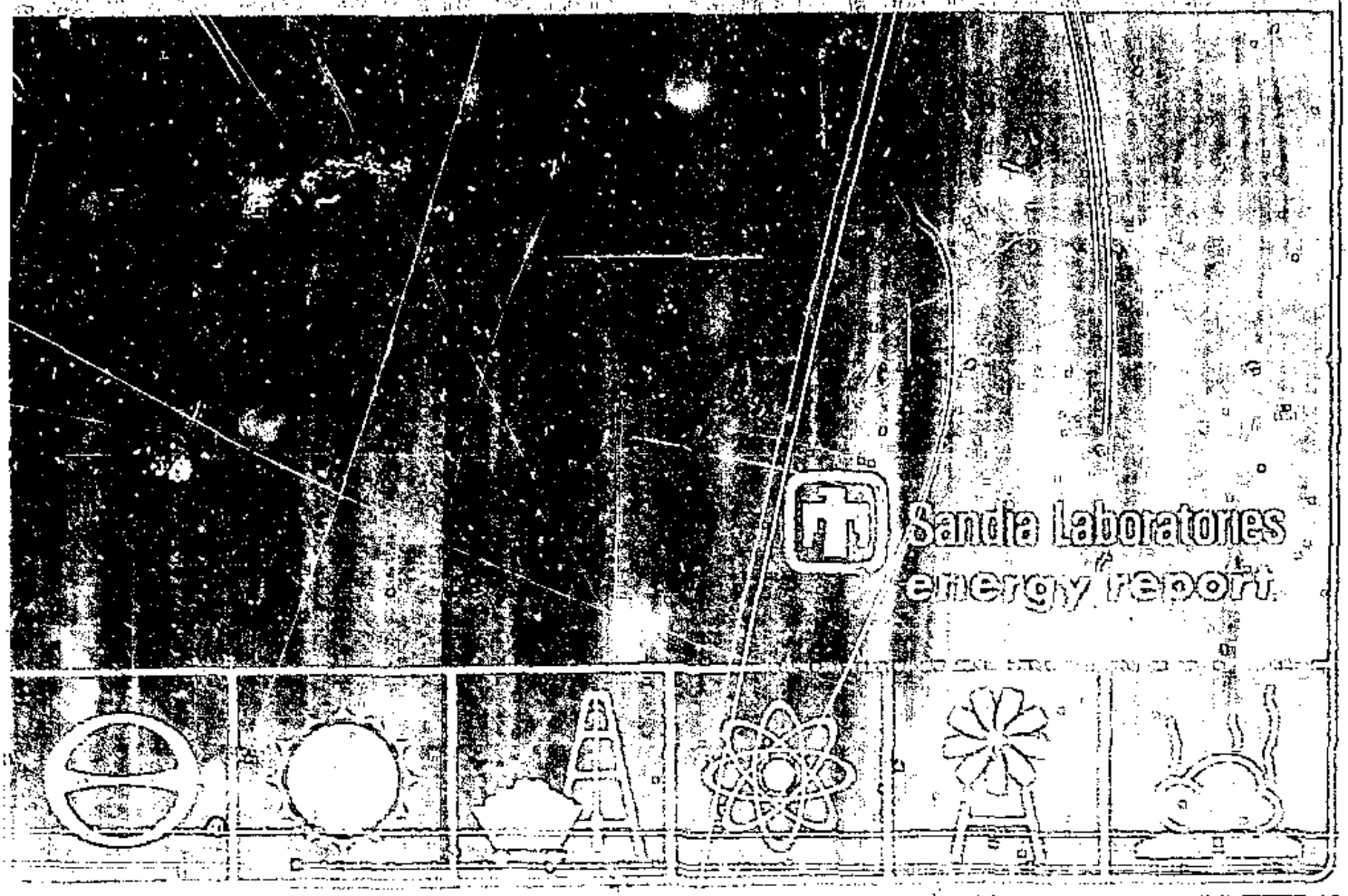

Sandia Laboratories
energy report

[redacted] Report for
the United States Atomic Energy Commission by Stearns Corporation

NOTICE

This report was prepared as an account of work sponsored by the United States Government. Neither the United States nor the United States Atomic Energy Commission, nor any of their employees, nor any of their contractors, subcontractors, or their employees, makes any warranty, express or implied, or assumes any legal liability or responsibility for the accuracy, completeness or usefulness of any information, apparatus, product or process disclosed, or represents that its use would not infringe privately owned rights.

Printed in the United States of America

Available from
National Technical Information Service
U. S. Department of Commerce
5285 Port Royal Road
Springfield, Virginia 22151
Price: Printed Copy $4.00; Microfiche $1.45

SAND74-0042
Unlimited Release
Printed September 1974

DEEP ROCK NUCLEAR WASTE DISPOSAL TEST: DESIGN AND OPERATION

Robert D. Klett
Systems Studies Division 4734
Sandia Laboratories
Albuquerque, New Mexico 87115

ABSTRACT

An electrically heated test of nuclear waste simulant in granitic rock was conducted to demonstrate the feasibility of the concept of deep rock nuclear waste disposal and to obtain design data. This report describes the deep rock disposal systems study and the design and operation of the first concept feasibility test.

NOTICE

This report was prepared as an account of work sponsored by the United States Government. Neither the United States nor the United States Atomic Energy Commission, nor any of their employees, nor any of their contractors, subcontractors, or their employees, makes any warranty, express or implied, or assumes any legal liability or responsibility for the accuracy, completeness or usefulness of any information, apparatus, product or process disclosed, or represents that its use would not infringe privately owned rights.

MASTER

DISTRIBUTION OF THIS DOCUMENT IS UNLIMITED

SUMMARY

A systems study was performed to compare various methods of permanent nuclear waste disposal. One of the most promising methods was found to be burial of solidified, uncontained high-level waste in holes drilled deep into bedrock. Heat generated by the waste would melt the surrounding rock, and the molten rock/waste mixture would later resolidify into a low solubility matrix when the heating rate decayed. A concept feasibility experiment was conducted to demonstrate this disposal method and to obtain substantial input data for analytical studies.

A testing method was developed by which nonradioactive waste simulants can be tested in representative bed rock without requiring expensive field tests with potentially hazardous radioactive waste. The waste simulant consisted of stable isotopes of representative waste or chemically similar elements and was heated electrically with a resistance heater. The simulant was in a cylindrical hole in the center of a 3 x 3 x 4.5 foot block of dolerite bedrock. The simulant and surrounding rock were heated to 2400° F so that the matrix became fluid and natural convection cells were set up in the melt. Instrumentation consisted of thermocouples in the melt and in the unmelted rock, strain gages, and sonic transducers. The operation of the test was successful, and all the desired data were obtained. Digital thermal stress and heat transfer codes gave good approximations to the actual temperatures and crack patterns observed in the experiment.

Even though the rock cracked, there was no loss of the melt because the cracks were self-sealing. Thermocouple data provided enough information to determine the size and effectiveness of the convection cells in augmenting heat transfer. The method of handling liquid expansion used in the experiment should also be effective in an operational configuration.

The dolerite test rock is being sectioned, and the posttest analyses will include (1) chemical analyses; (2) crystallography; (3) measurements of porosity, leachability, conductivity, and viscosity; and (4) mapping of convection cells. The test data and posttest analyses will be used (1) to determine the effects of convection, the mixing and stratification of the rock and waste, the degradation of the surrounding unmelted rock, and the integrity of the rock/waste matrix; (2) to evaluate the accuracy of analytical methods and laboratory experiments, and (3) to visually demonstrate the concept feasibility.

This report describes the initial systems study, the experiment design and operation, and the pretest analytical analyses. The final report will contain the test data, posttest analyses, and conclusions. All tests and analyses to date have indicated that this concept should be feasible even though some engineering problems were uncovered.

ACKNOWLEDGMENT

The author wishes to thank P. L. Nelson for his contributions to the test hardware design and the operation of the DRD-1 experiment. The assistance of the following Sandia personnel is also gratefully acknowledged.

J. A. Barber
A. G. Beattie
E. K. Beauchamp
B. M. Brake
F. J. Conrad
R. J. Eagan
J. H. Gieske
H. J. Gregory
K. L. Hankins
B. T. Kenna
R. H. Richards
J. T. Schatnaun
A. C. Zuppero

TABLE OF CONTENTS

TABLE OF CONTENTS (Cont.)

LIST OF ILLUSTRATIONS

LIST OF ILLUSTRATIONS (Cont.)

DEEP ROCK NUCLEAR WASTE DISPOSAL TEST: DESIGN AND OPERATION

Introduction

Nuclear reactors can supply a large part of our future energy needs, but to do so it will be necessary to manage radioactive wastes in a manner that poses no threat to people and environment. Of particular importance are the high-level wastes which remain biologically hazardous for an estimated half million years (Reference 1). Projected properties of the high-level waste inventory by the year 2000 are given in Table I from Reference 2. The last two groupings in the table give the quantities of air or water that would be needed to dilute the waste to a level acceptable for inhalation or ingestion. This convenient measure of toxicity is set by the U. S. Government's Radioactivity Concentration Guide.

TABLE I

Projected Properties of the High-Level Waste Inventory in the Year 2000
Based on an Accumulated Volume of 470,000 ft^3 of Solid Waste

Type of Waste	Total (for each property) Accumulated by Year 2000 Radioactivity (10^{-6} Ci)	Total (for each property) After Given Number of Years After the Year 2000			
		1000	10^4	10^5	10^6
All high-level waste	150 000	39.2	14.6	4.45	1.51
Total fission products	149 000	4.37	4.15	3.16	0.665
Sr^{90}	13 200[1,2]	-	-	-	-
Zr^{93}	0.392	0.392	0.390	0.374	0.247[1]
Tc^{99}	2.92	2.91[1,2]	2.83[1,2]	2.11[1,2]	0.111
Cs^{135}	0.0786	0.078	0.0784	0.0768	0.0624[2]
Cs^{137}	19 000	-	-	-	-
Total actinides	1650	34.8	10.4	1.27	0.218
Ra^{226}	-	0.0001	0.0058	0.0458[2]	0.0085[2]
Th^{229}	-	0.0011	0.0081	0.0346	0.0661[1]
Pu^{238}	214[1]	0.183	-	-	-
Pu^{239}	0.739	0.919	1.74[1]	0.241[1]	-
Am^{241}	4.9	14.6[1]	2.138	-	-
Cm^{244}	891[2]	-	-	-	-
Cm^{245}	0.318	0.292[2]	0.137[2]	-	-
	Thermal power (kW)				
Fission products	614 000	4.94	4.58	2.90	0.183
Actinides	50 700	937	242	30.9	15.4
	Inhalation hazard (m^3 air)				
Fission products	6.69×10^{20}	2.73×10^{15}	1.64×10^{15}	1.27×10^{15}	2.60×10^{14}
Actinides	6.62×10^{21}	2.18×10^{20}	8.34×10^{19}	7.38×10^{19}	4.09×10^{18}
	Ingestion hazard (m^3 water)				
Fission products	4.99×10^{16}	1.73×10^{10}	1.70×10^{10}	1.29×10^{10}	2.31×10^{9}
Actinides	2.17×10^{14}	1.81×10^{13}	5.91×10^{12}	2.31×10^{12}	6.83×10^{11}

[1] These nuclides control the inhalation hazard at the indicated time.

[2] These nuclides control the ingestion hazard at the indicated time.

As seen from Figure 1 (from Reference 1), fission products are the most toxic waste component for the first 500 years after the waste is removed from the reactor and the actinides and their daughter products are the most toxic thereafter.

Fission products are formed by the fission of uranium or plutonium. The most toxic are strontium-90, cesium-137, and krypton-85. Others which are less toxic include zirconium-93, technetium-99, iodine-129, cesium-135, and technetium-99. With the exception of iodine-129, which has a half life of 1.59×10^7 years, the half lives of the dominant fission products are generally less than 30 years; so after 700 years the fission products' activity is less than 10^{-7} the original level (Reference 2).

Actinides which include radium-225, thorium-229, plutonium-238 and -239, americium-241, and curium-244 and -245 are formed by neutron absorption of the uranium or thorium fuel. They are all very toxic and have half lives that range from 17.9 years for Cm^{244} to 24,390 years for Pu^{239}. It is the actinides that make high-level waste toxic for so many years.

In the case of permanent geologic disposal, the most likely hazard would be contamination of water. If this happened, the ingestion hazard would be primarily from Sr^{90} and Cs^{137} for the first 350 years. After 350 years, these fission products decay to a level that would make the actinides and Tc^{99}, Cs^{135}, and Zr^{93} the dominant potential hazard (Reference 1).

Light water reactors consume 20 tons of fuel rods for each gigawatt year of electricity they generate. When this amount of spent fuel is processed, about 25 m^3 of liquid high level waste or 2 m^3 of solid high level waste is produced. In 1970 the annual production of solidified high-level waste was only 4.8 m^3/year. By the year 2000 the predicted nuclear electric power capacity is expected to be as high as 1.2×10^{12} watts. Depending on the predicted power capacity and the solid waste form, estimates of the solid high-level waste production in the year 2000 range from 1300 m^3/year (Table II from References 2 and 3) to 1950 m^3/year (Table III from Reference 4). The accumulated volume of high-level waste could be as high as 25,500 m^3 by 2000 and have a radioactivity level of 320 gigacuries. Containing or disposing of this quantity of waste in a manner that is technically feasible and politically and socially acceptable is a serious problem.

Currently, government high-level waste is being stored as a liquid or slurry in tanks at Savannah River, South Carolina, and Hanford, Washington, and as a calcined solid in steel bins inside concrete vaults at the National Reactor Testing Station in Idaho. Commercial high-level wastes are being stored in an acidic aqueous form in stainless steel tanks at the processing plants. Federal regulations (Reference 5) require these wastes to be solidified within 5 years after they are generated and the stable solids to be shipped to a federal repository within 10 years. There are four basic processes for converting liquid high-level wastes to solids. The characteristic of each solid are given in Table IV from Reference 6. A borosilicate glass solid is also formed by a process similar to that by which phosphate glass is formed (Reference 7). It has a higher melt temperature, thermal conductivity, density, and fission product capacity and a lower leach rate than does phosphate glass.

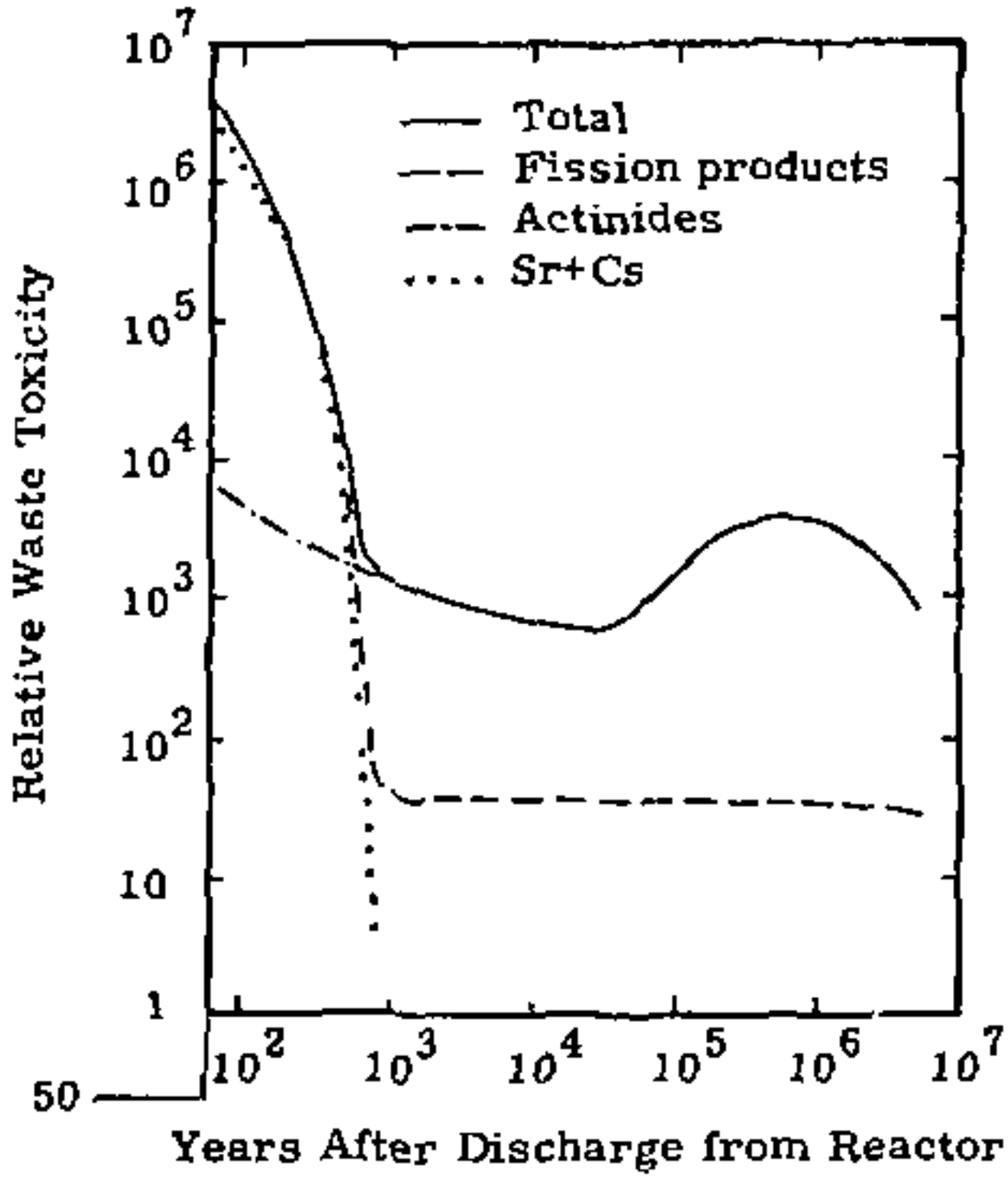

Figure 1. Toxicity of wastes from light water reactors with 99.5 percent removal of uranium and plutonium. The upturn at 10^6 years is caused by the growth of daughter products not present in the original material.

TABLE II

Full Cycle Waste Projections for the Year 2000

Category of Waste	Annual Generation		Total Accumulated		
	Volume (10^3 ft^3)	*Activity* (MCi)	Volume (10^3 ft^3)	*Activity* (MCi)	*Power* (kW)
High-level solidified	46	100	340	16,000	72,000
Alpha-beta-gamma					
Cladding hulls	70	1.4*	750	35*	24,000
Misc. solids	870	2.8*	5,300	20*	-
Alpha solids	2,500	75*	25,000	420*	650
Beta-gamma					
Tritiated water	1,500	0.2	36,000	4	-
Tritiated solids	4.5	14	30	95	3.4
Noble gas	2.1**	210	25	1,700	2,800
Iodine (KI)	0.01	0.001	1	0.01	0.008
Misc. solids	14,500	0.1	150,000	0.8	-
Ore tailings	860,000	0.3	15,000,000	4.5	-

*Activity of only the actinides are included.
**At 2200 psi.

TABLE III

Estimated High-Level Commercial Waste

	1980	2000
Installed capacity, 10^3 MW(E)	150	1 100
Spent fuel processed, metric tons/yr	3,000	21,000
Volume of high-level liquid waste		
Annual production, 10^6 gal/yr	1.0	6.9
Accumulated, 10^6 gal (if not solidified)	4.4	90
Volume of high-level waste, if solidified		
Annual production, 10^3 ft^3/yr	0.7	89
Accumulated, 10^3 ft^3	44	900

All of these solids are stable as long as their temperatures remain below their process temperatures. However, if the process temperatures are exceeded, volitization of some of the constituents has been observed and divitrification takes place, with a resulting increase in the leach rate. At or above 1200° C, boron and phosphate volitize from the glasses. These solid forms were designed for engineered storage and may not be the best forms for permanent disposal. Engineered storage is a temporary method of waste management which is to be used until a safe method of permanent disposal or elimination can be developed.

At this time engineered storage is the safest and most logical method of handling high-level waste. However, it cannot be used indefinitely. Aside from the moral aspect of burdening future generations with our waste, there are also practical reasons for developing a permanent method of disposal. Storage requires surveillance and maintenance, and in the half million years that the waste is toxic many changes in government, social structure, and territorial boundaries will take

place. Since storage facilities must be accessible, they are vulnerable to natural phenomena such as earthquakes, floods, and glaciers and to man-made destruction including wars and sabotage. Any of these occurrences could disrupt surveillance. It is possible that a disposal site could be lost. The expense of perpetual maintenance and rebuilding would be prohibitive.

TABLE IV

Characteristics of Solidified High-Level Purex Wastes

	Pot Calcine	Spray Melt	Phosphate Glass	Fluid Bed Calcine
Form Description	Calcine cake Scale	Monolithic Micro-crystalline	Monolithic Glass	Granular Amorphous
Fission-product oxides, mole %	Up to 60	Up to 20	Up to 25	Up to 50
Bulk density, g/ml	1.1 to 1.5	2.7 to 3.5	2.7 to 3.0	1.0 to 1.7
Thermal conductivity, Btu/(hr)(ft)(°C)	0.15 to 0.25	0.5 to 1.0	0.4 to 1.0	0.10 to 0.25
Maximum heat, W/liter of solid	65	220	190	70
Leachability in cold water, g/(cm^2)(day)	1.0 to 10^{-1}	10^{-3} to 10^{-6}	10^{-4} to 10^{-7}	1.0 to 10^{-11}
Hardness	Soft	Hard	Very hard	Moderate
Friability	Crumbly	Tough	Brittle	Moderate
Residual nitrate, wt. %	≤0.05	≤0.005	≤0.005	≤4.0
Volume, liters/1000 MWd(t)	1 to 2.5	1.2 to 3	1.5 to 5	1.5 to 5
Maximum stable temperature, °C	~900	Phase separation at ~900	Devitrifies at ~500	~600
Container material	Stainless steel	Mild steel or stainless steel	Mild steel or stainless steel	Mild steel or stainless steel

The ideal solution would be to eliminate the wastes by conversion to a useful or at least a safe material. If this is not possible, the next best solution would be to permanently dispose of the waste. A disposal concept must meet the following criteria to be acceptable.

1. Waste must be isolated from present and future areas of habitation or visitation. Some areas that are isolated today may be centers of population in the future.
2. Waste must not be placed in any potentially useful mineral deposits.
3. Waste can not be allowed to enter the food chain, water supply, or air supply. This can be accomplished either by isolation, containment, or negligible leach rates.
4. The waste should not be placed in natural hazard areas where there are frequent natural disturbances such as earthquakes or floods.
5. The waste should be safe from geologic or climatic changes (i.e., the media must be stable).
6. The waste form should be radioactively and thermally stable. The disposal method should accept stored waste which has partially decayed as well as fresh waste.

7. *The waste must be immobile unless it can only move to a more desirable location.*

8. *Costs must not prohibit the use of nuclear fuel.*

9. The disposal method must be maintenance free and not be dependent on political or social stability.

Recoverability has often been mentioned as a desirable feature for a disposal concept in case a use can be found for the waste or a better disposal or elimination method can be found. However, if the waste can be recovered intentionally, it is also susceptible to natural or accidential exposure. Recovered waste could also be used for destructive purposes or blackmail.

Alternate Methods of Disposal

There have been numerous systems studies to determine which method or methods of nuclear waste disposal meet requirements similar to those set down in the Introduction (References 1, 2, 4, 8, 9, and 10). The newest and probably the most complete study is the one being conducted at Battelle Northwest. The following is a synopsis of the proposed methods of elimination or disposal of high-level nuclear waste.

Separation

Extraction of the actinides and long-lived fission products from the high-level waste could simplify the disposal of at least part of the waste. As shown in Figure 2 from Reference 2, the radiation from the remaining short lived waste falls within the range of natural radiation in about 600 years.

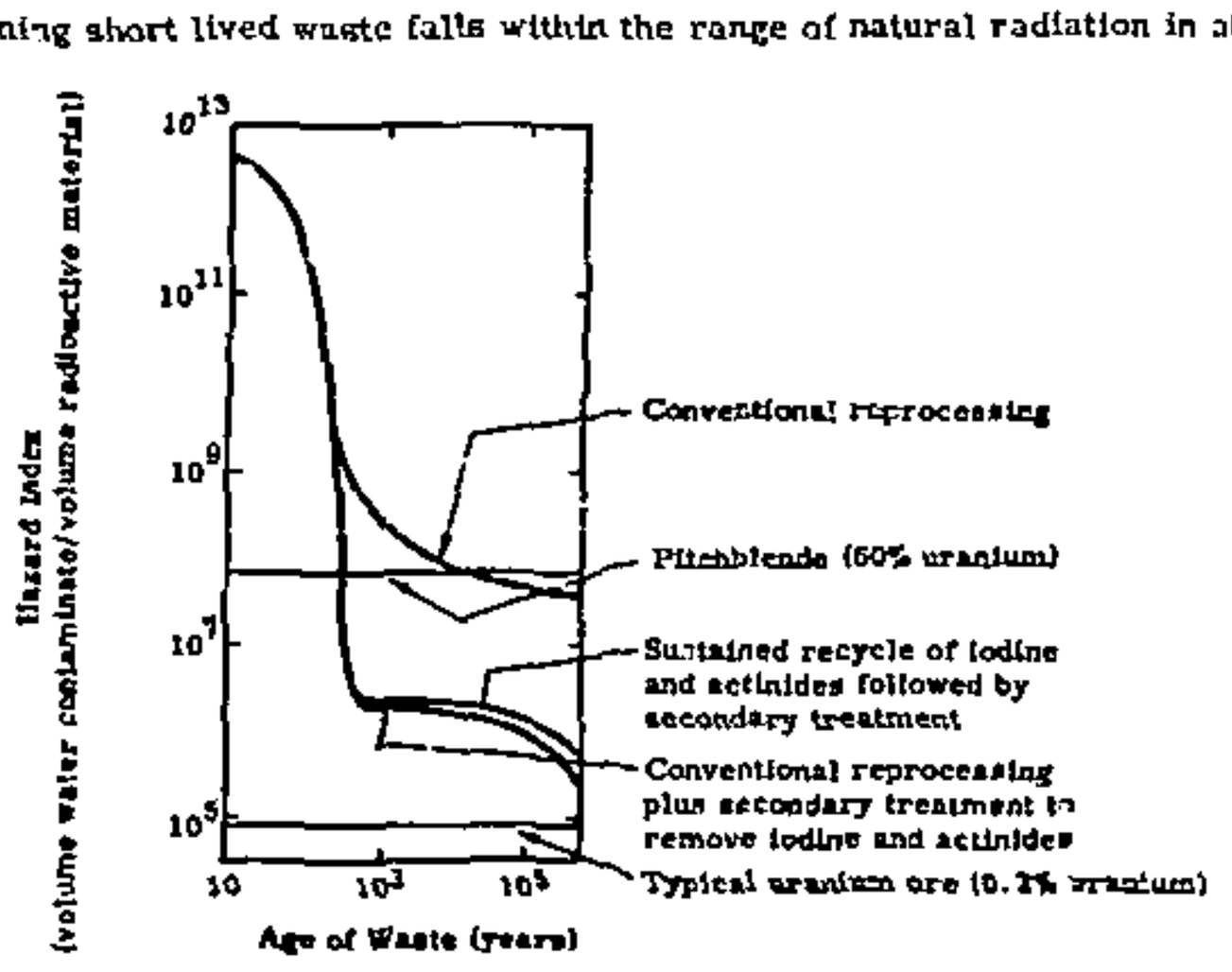

Figure 2. Effects of separating short and long-lived high-level waste

Transmutation

This method would use the nuclear process to change long-lived radioactive waste to short-lived waste or stable isotopes by the absorption of radiation. Used in conjunction with separation, all waste could potentially be converted to short-lived isotopes. The indications are that actinides

can be transmuted in fission reactors, but it appears that fission products will require the use of a fusion reactor (Reference 8). Most products of transmutation will still require some means of permanent disposal, but the hazard times would be shorter.

Extended Storage

Perpetual use of engineered storage has been mentioned as a disposal technique. The waste would be contained in vaults, mined cavities, or in shielded containers on the surface of the earth. Cooling would be by conduction or convection. The waste would be recoverable, but the costs would be high, surveillance difficult, and long-term safety questionable.

Antarctic Rock and Ice Sheets

The advantages of these locations are that all ground water is frozen, and hence immobile, and the ice would cool the waste. Presently, only people with scientific backgrounds visit these areas, and presumably they would take proper precautions. The difficulties are that permafrost or Antarctic rock is only frozen to a depth of about 300 metres and the temperatures are not much below freezing. This means that the waste would have to be spread over a large area to prevent melting. The waste would also have to be spread over a large part of the continental ice sheets to prevent melting of the ground-ice interface which could increase ice flow. Compared to the half-million years that the waste is dangerous, the ice flows are not permanent geologic formations. Transportation to these areas could pose a safety problem, and logistics at the disposal site would be difficult. Currently, both of these locations are excluded by international treaty.

Seabed

Ocean trenches, ocean tectonic subduction zones, deep ocean abyssal plains, and ocean floor sediments have all been proposed as repositories for high-level waste. Possible advantages given for seabed disposal are: (1) remoteness from normal human activity, (2) good heat dissipation, (3) large dilution and dispersion capacity in the event of a failure, (4) low cost, and (5) possibility of mineral buildup to provide additional containment. General arguments against seabed disposal include the difficulty of containment because of the corrosive environment and the possibility of radioactivity entering the food chain if there is a leak.

Convection cooling is lost when waste is buried in sediment or tectonic subduction zones, and the waste must be treated similarly to waste buried on the continents. In Reference 11 it is shown that vertical upward diffusion of uncontained radionuclides through the water is the dominant transport process where sedimentation rates are low. Deep ocean trenches are remote, but solid and liquid transport rates are high. The same currents that cause high sedimentation rates to cover waste now could also uncover them within the next 500,000 years. Little is known about tectonic subduction and stable deep ocean seabeds. Some seabeds may have little or no life and may be free of currents, but much oceanographic research is needed before any definite conclusions can be drawn. United States and international policies do not permit the disposal of high-level wastes in international waters. As more information becomes available, these policies may change.

Extraterrestial

NASA has been investigating the possibility of using the space shuttle vehicle to place high-level waste in an earth orbit. The waste could be either left in earth orbit or additional rocket stages could be used to fire the waste into a solar orbit, into the sun, or into deep space. Direct sun impact is not possible with today's vehicles (Reference 8). Cost estimates vary, but this is probably one of the most expensive concepts that has been proposed. In the event of an aborted launch or short-lived orbit, the waste could impact either in the ocean or on the continents. The container would, therefore, have to survive the environments of all types of seabed disposal and also be shielded in case of a terrestial landing. In addition, it would have to be able to survive a launch pad abort fire, reentry heating, and earth impact. Waste successfully launched into the sun or into deep space would be permanently eliminated.

Salt

Disposal of high-level waste in bedded salt is being investigated by Oak Ridge National Laboratory. Germany is working on disposal in salt domes. Bedded salt has the advantage of being the older and more stable of the two formations. Salt beds have remained free of circulating ground water since they were formed. However, there is no guarantee that there will be no circulating water in the future and flowing water can dissolve a salt formation. Salt is capable of plastic deformation. Any fractures in the salt would be self-healing, and filled entrances to the storage areas will eventually be self sealing. The salt will also flow when heated by the waste. The extent and consequences of the thermal flow are not as yet fully known. Other advantages of salt are high thermal conductivity, abundance and wide distribution in the U. S., ease of mining, and usual occurrence in seismically stable regions. Other disadvantages of salt are that it is highly corrosive and is normally associated with other valuable minerals. Salt deposits are considered to be deep enough (150 to 600 metres) by some investigators but too close to the surface by others. The salt bed proposal has been developed further than any other disposal concept, but there are still questions to be answered. The technical work so far has been with contained waste, but stainless steel and ceramic containers could fail in six months to three years (Reference 12). The melt temperature of the salt (1472° F) surrounding the waste could be exceeded, and the waste could mix with the molten salt. The behavior of this matrix is not completely known.

Self Burial

References 13 and 14 describe a concept by which containers of high-level waste would melt their way toward the center of the earth. It is proposed that high-level waste be placed in a refractory container and ballasted if necessary to give the container a higher density than the rock it penetrates. The container would be placed at the bottom of a hole drilled into bedrock 0.5 to 2 km deep. The heat generated by waste would melt the surrounding rock. As the container settles, the molten rock wake would resolidify, forming a permanent seal. The same hole could be used for subsequent containers which would melt their way downward in series. Analyses performed by Logan (Reference 14) for 1 and 2 m. diameter spheres with various waste loadings in basalt and granite rock indicated

that the containers would penetrate between 0.5 and 50 km before the heat generation level decayed to a level that could be accommodated by conduction. It was predicted that some waste/container combinations would penetrate the crust and enter the mantle. Although this is an attractive concept, the analytical work must be verified experimentally and heat transfer predictions of the interior of the container must be made. The most serious problem is finding a container that would survive in contact with the waste and all types of rock above the rock melt temperatures (2200-2800° F) for the life of the decent, which was predicted to range from 5.6 to 500 years depending on the depth of penetration.

Deep Rock Burial

In this category of nuclear waste disposal techniques, waste is isolated by placing it deep into bedrock well below mineral resources and water (References 4, 15, 16, and 17). Types of rock being considered are shales, limestones, and silicates. The waste would be aged to reduce the heat generation rate and/or dispersed in the rock sufficiently to prevent melting of the waste and rock. The waste could be a contained solid which would be placed in a drill hole or in mined shafts and tunnels. The entrances would be sealed with a material such as cement which is similar to the rock. It may be possible to retrieve waste disposed of in this manner. An alternate proposal is to hydraulically fracture the lower end of a drill shaft using liquid waste. The waste mixed with cement would then fill the fractures in the bedrock and harden in place. The advantage of deep rock burial are that the media is insoluble, has low porosity, is accessible in most of the U. S., and is usually not associated with valuable mineral resources. The disadvantages are that the rock is brittle and, if cracked, will not seal itself at low temperatures. It may be possible that ground water could reach the waste.

Deep Rock In Situ Melt

These deep rock in situ melt concepts place the nuclear waste in deep bedrock similar to the Deep Rock Burial concepts but differ in the following respects.

1. The waste is not encapsuled, and, therefore, success does not depend on the survival of a container at high temperatures for long periods of time.
2. Younger and/or larger quantities of waste are placed in each location so the heat generated by the waste is sufficient to melt the waste and surrounding rock. The diffusion and convection currents cause the molten rock and waste to mix. After the heating rates decay to a level lower than conduction losses, the mixture will resolidify into a low solubility matrix.

All of the in situ melt concepts have the advantages of low cost, high temperatures during the time of high radioactivity which will keep ground water away from the waste, dilution of the waste by the molten rock, and final solidification into a glassy matrix with a low leach rate. Safety increases as the burial depth increases. Disadvantages include possible mobility during the melt phase. Some configurations are more prone to migrations than others. Other disadvantages are

the possibility of the high temperatures, which may cause gases to evolve from the matrix, and thermal expansion problems.

The in situ melt concepts differ in (1) the size and shape of the cavity in the bedrock, (2) the waste form, and (3) the method of filling the cavity. The Lawrence Livermore Laboratory proposal (Reference 18) consists of placing liquid wastes in a large spherical cavity. The cavity is a deep underground chimney formed by a nuclear explosion and partically filled with rubble. Cavities would be located underneath processing plants and filled with liquid waste and water. Heat generated by the waste would be removed during the fill period by boiling the water. After about 25 years, the cavity would be full and the liquid waste would be allowed to boil dry. The heat would then begin to melt the surrounding rock. After 90 years, the conduction losses into the rock would exceed the heat generated and the waste/rock matrix would gradually cool. Resolidification would take hundreds of years. The advantages of this method are: waste would not have to be transported from the processing plant; some low level waste could be left in the high-level waste, thus reducing the amount of separation needed; and the waste would not have to be solidified. Most of the disadvantages stem from the large cavity size (see Appendix A). The concentration of such a large amount of heat in one location might cause high cavity pressures and extensive cracking or upheaval because of thermal expansion of the heated rock. The large size also means a long fill period when the waste is mobile and the cavity is nonplastic, more possibilities of failure in the fill mechanism, and a longer period when the matrix is molten. A spherical or short cylindrical geometry is more likely to migrate when molten than are other geometries.

Another configuration described in Reference 10 is a large flat disc-shaped cavity formed by hydraulic fracturing of the bedrock. The waste is then pumped into the fracture in the form of a self-curing slurry. The melt would then proceed perpendicular to the fracture. Because of the extended surface and smaller volume, the melt period would be the shortest for this configuration. Control of the fracture and assuring melt over the entire volume would be difficult.

The third configuration utilizes a cylindrical configuration (Appendix A and Reference 10). Holes ranging from about 1 to 4 feet in diameter, depending on the age and concentration of the waste, are drilled deep into bedrock. The bottom part of the holes are filled with solid high-level waste. The hole is then sealed and the upper part of the hole is filled with cement or similar material. After the waste and rock melt, numerous convection cells will form or turbulent flow will develop in the long column which will cause melting to proceed primarily in the radial direction. The time the matrix remains molten would be longer than the hydrafraced configuration but substantially shorter than the large spherical configuration. The waste form would have to be either a solid or a self-curing slurry and consist primarily of high-level waste to assure sufficient melting.

The waste disposal methods described above are not mutually exclusive. Combinations such as in situ melt in the rock below deep ocean seabeds, partial transmutation followed by deep rock burial, and extraterrestial disposal of some components of the waste after separation are also possible. Most seabed and geologic disposal concepts can be used either in a central repository or with distributed disposal sites.

None of these disposal methods are developed sufficiently to use at this time; feasibility studies have not even been completed on most. Many studies have been based on assumptions and include many simplifications because of the lack of good input data. It is, therefore, not advisable to completely develop one of the concepts until more is known about the more promising alternatives.

Deep Rock Disposal (DRD)

The criteria for selection of an attractive means for high-level radioactive waste disposal are safety, reliability, flexibility, logistics, and cost. Preliminary analyses have indicated that Deep Rock In Situ Melt disposal meets these requirements. The particular design which appears to be the most promising is the one in which uncontained solidified waste is place in long drill holes deep in bedrock. Since work on this concept is consistent with Sandia Laboratories capabilities and it has not been developed through the feasibility stage, it was selected for further analyses and tests. The configuration shown in Figure 3 includes modifications made as a result of these tests and analysis and represents the basic disposal system now under consideration.

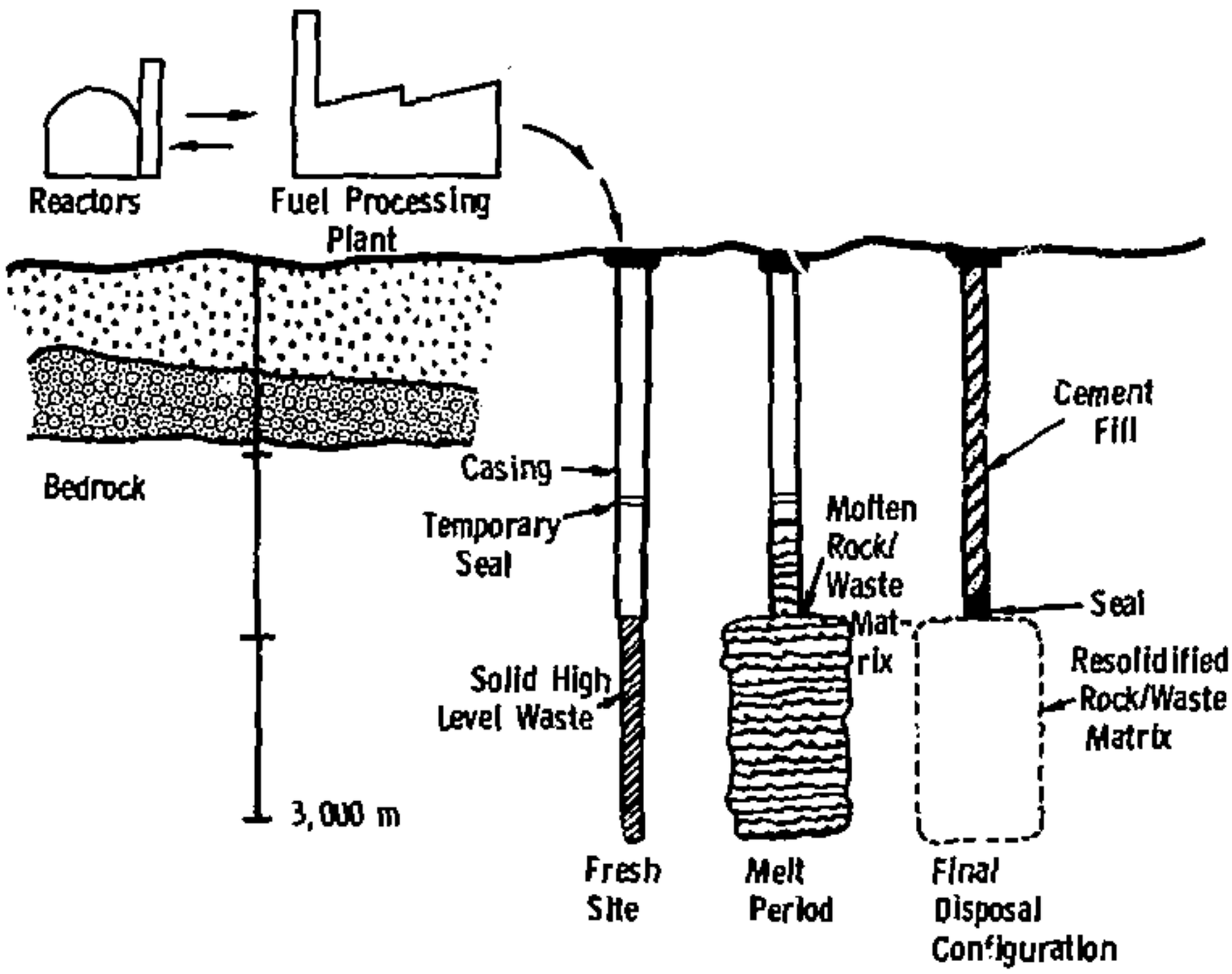

Figure 3. Deep rock nuclear waste disposal with in-place melt

Thermal Analysis

The initial thermal analysis of deep rock disposal utilized parametric solutions of constant spherical, line, and plane heat sources in an infinite media to determine the approximate concentration of waste that would be needed to melt the desired amount of rock. It was then determined if these cavity sizes were practical relative to excavating in deep bedrock for each configuration. Digital computer program DELT was used to conduct the parametric study. This program used Equations (1-5) which were derived from the instantaneous point source equation (Reference 19), heat generation rates at one year ranging from 80 to 150 kW/m^3 decaying as shown in Figure 4, and material property data from Appendix B. Since it was necessary to average the heating rates and property data, these solutions are only approximations.

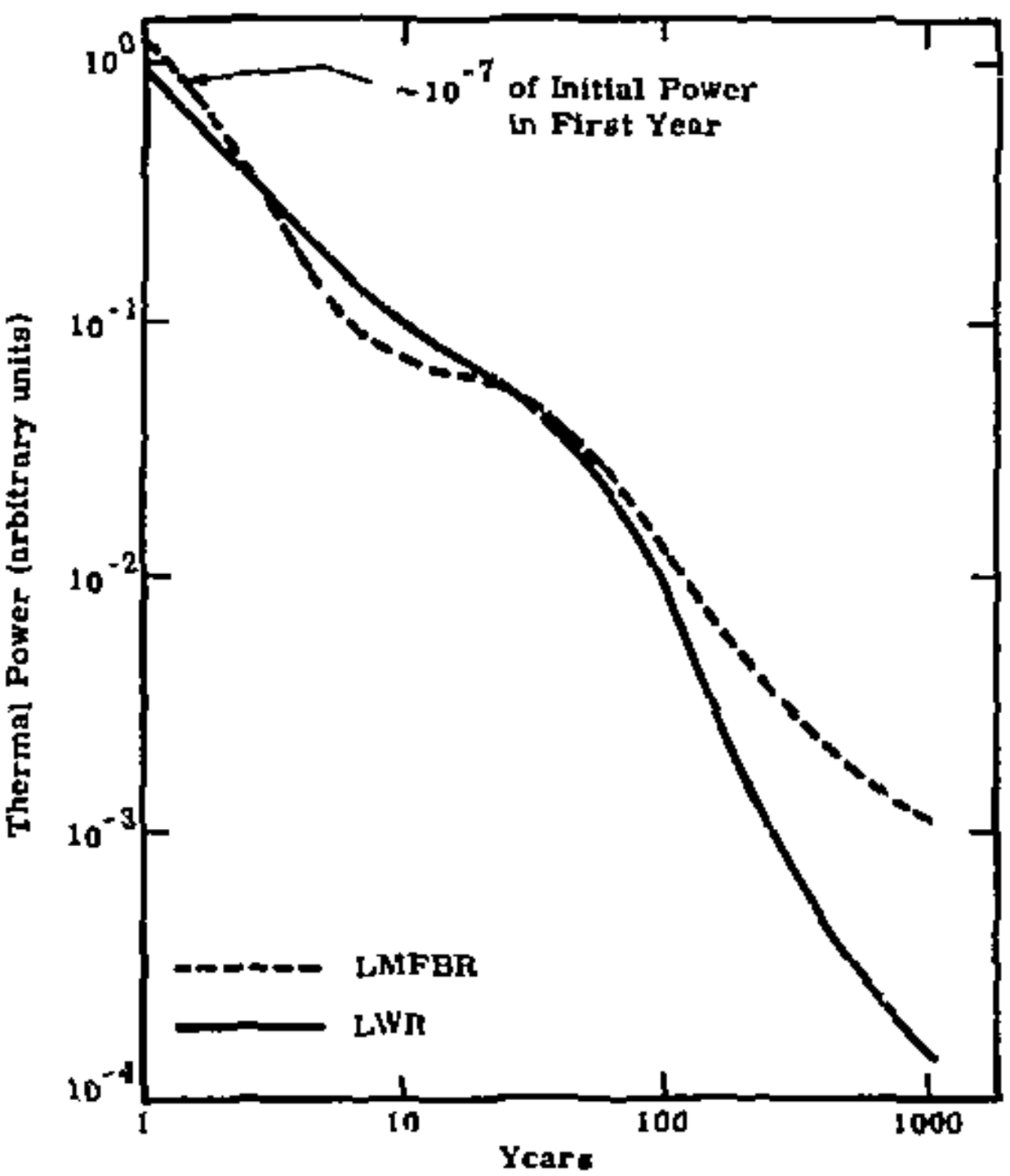

Figure 4. Normalized heat generation rate decay for light water reactor and high temperature gas-cooled reactor wastes (derived from Reference 20).

The approximate temperature rise of the rock surrounding a spherical waste cavity as a function of time and radius is given by

$$\Delta T = \frac{q}{8\pi Kra}\left\{2\left(\frac{\alpha\tau}{\pi}\right)^{1/2}\left[\exp-\frac{(r-a)^2}{4\tau\alpha}-\exp-\frac{(r+a)^2}{4\tau a}\right]-(r-a)\,\mathrm{erfc}\left(\frac{r-a}{2\sqrt{\alpha\tau}}\right)+(r+a)\,\mathrm{erfc}\left(\frac{r+a}{2\sqrt{\alpha\tau}}\right)\right\} . \quad (1)$$

The temperature rise around a line source is

$$\Delta T = \frac{-q'}{4K\pi} \, \mathrm{El}\left(-\frac{r^2}{4\alpha\tau}\right) \quad . \tag{2}$$

For small values of z

$$\mathrm{El}(-z) = \gamma + \ln z - z + \frac{1}{4} z^2 \ldots \quad . \tag{3}$$

Therefore, for the large values of time that are of interest in this case

$$\Delta T = \frac{q'}{4\rho c_p \pi\alpha} \ln\left(\frac{4\alpha\tau}{r^2}\right) - \frac{\gamma q'}{4\rho c_p \pi\alpha} \quad . \tag{4}$$

For a uniform plane source the equation is

$$\Delta T = \frac{q''}{\rho C_p}\left(\frac{\tau}{\pi\alpha}\right)^{1/2} \exp\left(-\frac{x^2}{4\alpha\tau}\right) - \frac{q''x}{2K} \operatorname{erfc}\left(\frac{x}{2\sqrt{\alpha\tau}}\right) \tag{5}$$

where

- a = radius of the spherical surface
- C_p = specific heat
- El = the exponential integral
- K = thermal conductivity
- q = total heat generation rate from a spherical surface
- q' = heat generation rate per unit length
- q'' = heat generation rate per unit area (includes both sides of the fracture)
- r = radius
- ΔT = temperature rise
- x = distance perpendicular to a flat source
- α = thermal diffusivity ($K/\rho C_p$)
- γ = the Euler - Mascheroni constant
- ρ = density
- τ = time

It was found that both spherical and cylindrical cavities could be formed in deep bedrock that would result in substantial rock melt. Not enough was known about the geometry of a hydraulic fracture to assure melt in that configuration. The diameter of the drill holes for the cylindrical configuration using solidified high-level waste could range from about 0.3 to 1.5 metres depending on the age and concentration of the waste. Very old waste or a very fluid rock/waste mixture could increase the allowable diameter. A low viscosity melt would enhance convection and hence keep peak temperatures to an acceptable level in a large cylinder.

The next step was to ascertain the relative heat-up and cool-down times and the length of time the matrix remained hot after resolidification using an actual decay curve with temperature

dependent material properties and convection in the melt zone. The CINDA digital computer program was used to make these computations. A one-dimensional version of the cylindrical thermal model described in Appendix C was used. Material properties were obtained from Appendix B, and convection was computed using the methods described in Appendix D. In the interest of conserving computational time, a typical case was selected and the results were normalized. Figure 5 shows that the resolidification time is about 5.5 times as long as the melting time when the waste is one year old when it is buried. Melting periods can range from several weeks for young high-level waste in very small diameter holes to tens of years for aged waste in large holes. Figure 6 shows that the centerline temperature remains fairly constant during the melt period because of convection and heat of fusion. The long period of time that the resolidified rock/waste matrix would be at elevated temperature is illustrated in Figure 7. The exponential temperature decrease from the 2200° F melt temperature would keep the matrix dry for many years. The exact cool-down time for each set of initial conditions is yet to be determined.

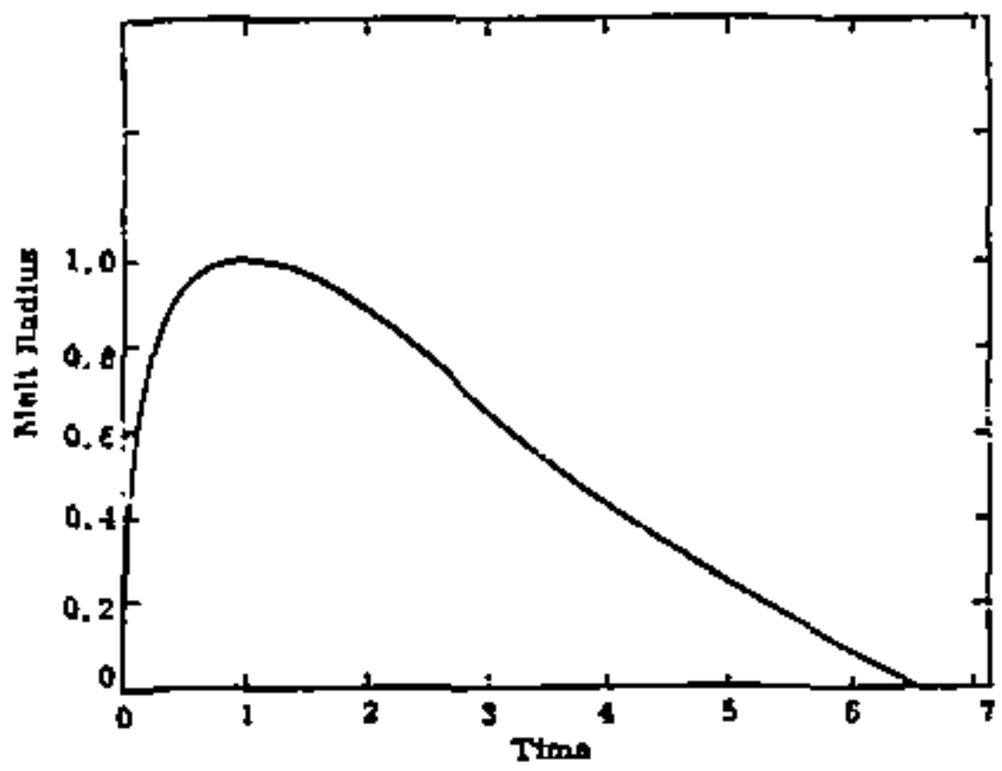

Figure 5. Normalized melt radius

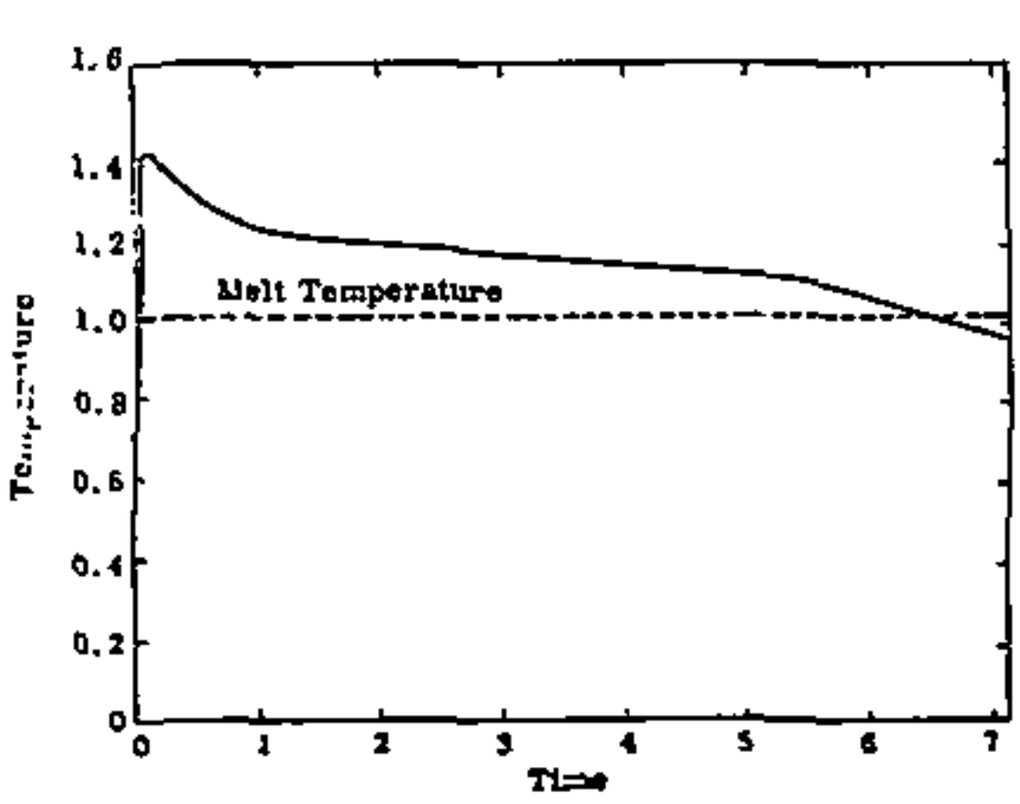

Figure 6. Normalized centerline temperatures

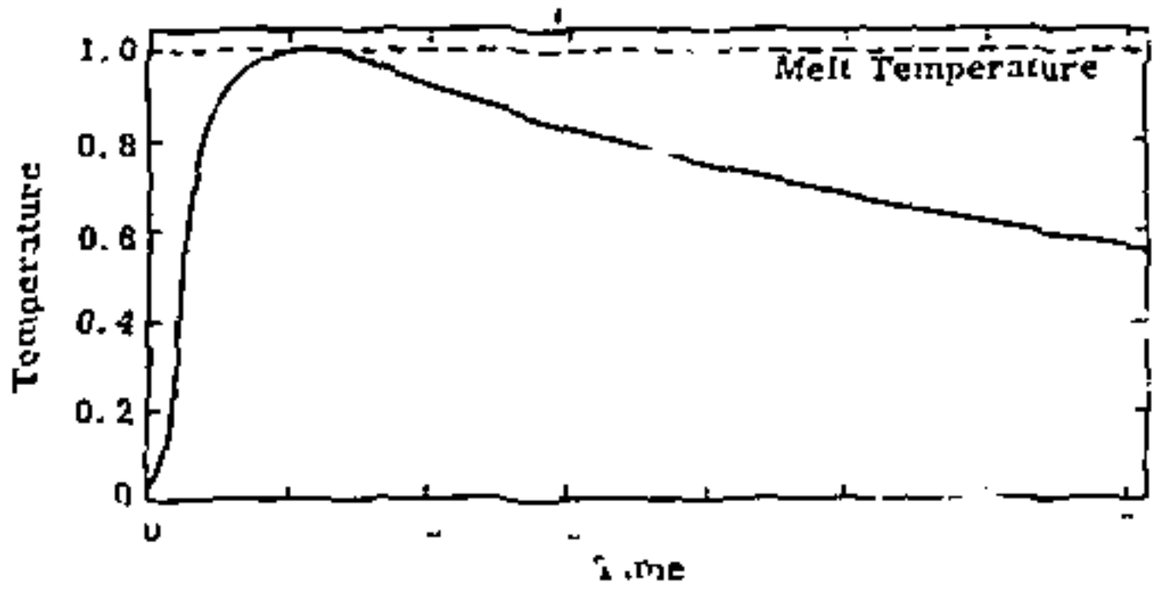

Figure 7. Normalized temperatures at maximum melt radius

It has been suggested in Reference 1 that the actinides be removed from the rest of the high-level waste to reduce the hazard time. Figure 8 shows that the heating duration of the remaining fission products plus Sr and Cs is long enough to melt the rock in all the proposed in situ melt configurations. If the extracted actinides cannot be transformed to a short-lived isotope by transmutation, they could be buried separately, possibly in a central location, and/or at a greater depth. Although the heating rates per unit volume of the actinides is initially lower than that of the other waste products, Logan showed that the heating rates are high enough to melt rock (Reference 14).

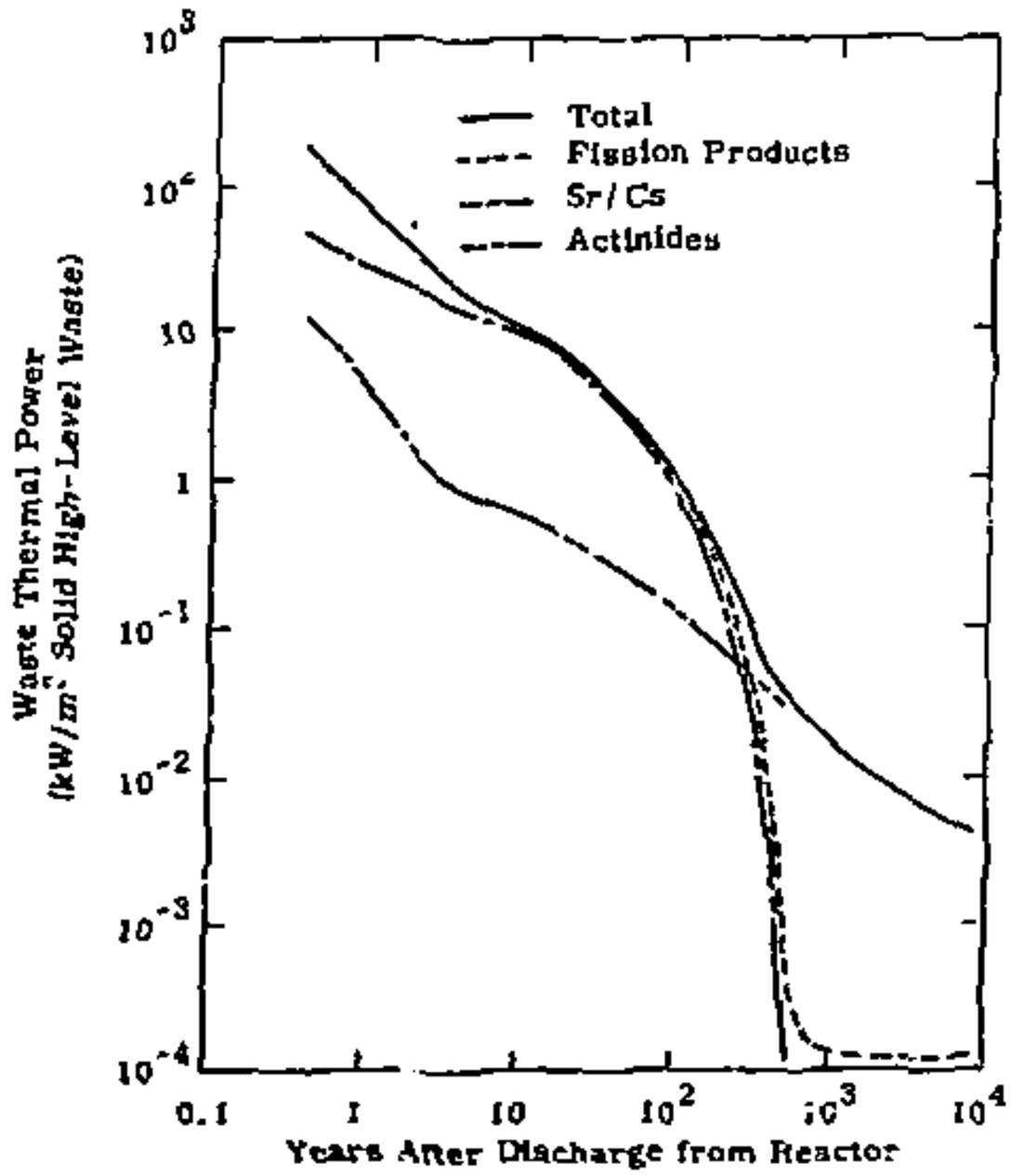

Figure 6. Thermal power for light water reactor high-level waste. Derived from Reference 1.

Disposal Location and Cost

Reference 21 shows the locations, depths, and categories of basement rock in the continental United States. Approximately three fourths of the U. S. has Precambrian silicate bedrock, about half of which is within 2,000 metres of the surface. This very old and stable bedrock exists in almost all geographical locations of the U. S. which means the waste could be disposed of at or near processing plants if desired. Another alternative is to use a central repository for all the high-level waste. *A study was conducted by the USGS (Reference 22) to determine if the Nevada Test Site would* be a suitable central repository. Preliminary results are not conclusive but do indicate that locations at NTS may meet the requirements of deep rock disposal.

To date, the deepest drill hole is 9160 m and the deepest cased 14-inch diameter hole is 4330 m. The reference depth selected for costing and capacity studies was 3000 m; which is well within the limits of existing drilling technology. It was also assumed that only the bottom 1000 m of the hole would be filled with waste so the site selection would not be restricted and all the waste would be remotely located. Table V lists capacities and initial thermal output for a range of hole diameters.

TABLE V

High-Level Waste Capacities and Initial Power Levels Based on 1000 m of Fill

	Hole Diameter (m)			
	0.3	0.5	1.0	1.5
Volume (m^3)	70.7	196	785	1,767
Power plant capacity per hole (GWe - yr)	35	98	394	885
Holes per year (1980)	4.3	1.5	0.38	0.17
Holes per year (2000)	31.4	11.2	2.8	1.2
Average initial power (kW/m)	8.1	22.5	90.3	203.2

The number of holes per year and the power level of holes in the one meter diameter range are acceptable for deep rock disposal. However, a few large diameter holes may be needed to dispose of the aged waste that has been in storage and has a lower thermal output.

Cost estimates are based on References 23, and 24 adjusted to 1973 prices. It is assumed the holes are drilled in remote locations in very hard rock to a depth of 3000 metres. The upper 2000 metres of the holes are assumed to be cased to prevent water from leaking into the bedrock. Table VI is a summary of the cost estimates. Waste transportation and filling costs are not included. The cost of uncased holes is included only as a reference.

The 1 metre diameter holes are the least expensive, but compared to the 10-11 mill/kWH production cost of electricity, the DRD disposal costs of high-level wastes are negligible. Costs are also low compared to the estimated 100 year engineering storage cost of $35,000/$m^3$.

TABLE VI

Costs of 3000 m Deep Rock Disposal Drill Holes

	Hole Diameter (m)			
	0.3	0.5	1.0	1.5
Uncased hole ($1,000)	900	1,280	2,550	5,360
2/3 Cased hole ($1,000)	1,280	1,960	4,080	14,700
Sealing and filling top 2/3 ($1,000)	7	21	82	185
Cost/m^3 waste ($1,000)	18.2	10.2	5.3	8.4
Disposal cost/kWH electric (mills)	0.004	0.002	0.001	0.002

Conceptually, the cylindrical deep rock in situ melt disposal method is attractive, and preliminary system analyses are encouraging. However, before this method could be selected for development and operation the following general categories must be addressed:

1. The chemistry and physics of the melting and mixing of waste and rock must be thoroughly understood,
2. Analytical models must be developed or modified that will predict DRD phenomena,
3. Accurate and complete input data for the analytical models are needed,
4. All possible safety and environmental problems must be investigated, and
5. Preliminary hardware design and operational procedures must be completed to assure feasibility.

Specifically, the unknowns and potential problem areas are listed in Table VII.

TABLE VII

Deep Rock Disposal Unknowns and Engineering Problems

1. Circulation in the melt including convective heat transfer and flow patterns.
2. The amount of diffusion, mixing, stratification, solubility, and chemical reactions of the rock and waste.
3. Shape and migration of melt zone.
4. Chemical compatibility of waste, containers, and rock.
5. Optimum waste form for each type of bedrock.
6. Integrity, solubility, and erosion of the rock/waste matrix.
7. Optimum size and shape of the disposal cavity.
8. Optimum age and concentration of waste.
9. High temperature chemical, mechanical and thermophysical properties of rocks.
10. Thermal expansion causing cracks, upheaval, or extrusion.
11. Gas generation, pressure buildup, and diffusion mechanisms.
12. Possibility of water seepage and effects.
13. Site selection and burial depth.
14. Filling procedures and scheduling.

Table VIII contains an outline of the steps in the development of the DRD concept of high-level waste disposal. The intent is to employ analytical studies along with scaled experimental programs in order to obtain the maximum indication of concept feasibility prior to commitment to very expensive full scale tests or experiments. Functional design and concept proof testings are dependent on the results of concept feasibility studies and hence Steps III and IV of Table VIII are only tentative. The development program could also be terminated if a better solution to the nuclear waste problem is found or if unacceptable safety hazards are uncovered relative to the DRD concept.

TABLE VIII

Deep Rock Disposal Development Program

I. System Scoping

- A. Quantities of high-level waste to be disposed of.
- B. Availability of basement rock.
  1. Types, locations
  2. Depth below surface
- C. Drilling technology
  1. Cost
  2. Capability
- D. Potential environmental problems

II. Concept Feasibility

- A. DRD experiment series
  1. Convection effects on heat flow.
  2. Shape and migration of melt zone.
  3. Amount of diffusion, mixing, stratification, solubility, and chemical reactions of the rock and waste.
  4. Chemical compatibility of waste, containers, and rock.
  5. Integrity, solubility, leachability, and erosion of the rock/waste matrix.
  6. High temperature chemical, mechanical, and thermophysical properties of rocks and waste.
  7. Degradation and cracking of rock outside melt.
  8. Method rock enters melt (chemical, melting, or mechanical).
  9. Check of analytical and numerical models.
  10. Check on experimental models.
  11. Develop test methods at high temperatures in a reactive environment.
  12. Visual demonstration of concept feasibility.
- B. Lab convection experiments
  1. Indications of melt geometries.
  2. Indications of melt migration.
  3. Indications of convection.

III. Functional Design

- A. Correct size and shape of the disposal cavity.
- B. Correct waste form for each type of bedrock.
- C. Optimum age and concentration of waste form.
- D. Control of thermal expansion causing cracks, upheaval, or extrusion.
- E. Gas generation, pressure buildup, and diffusion mechanisms.

TABLE VII (Cont.)

F. Potential for water seepage and effects.

G. Potential site selections and burial depth.

H. Filling procedures.

I. Scheduling relative to reactor locations.

J. Detailed economic analyses.

K. Development of analytical convection and geological stress models.

IV. Concept Proof Testing

A. Determine which phases can be done analytically, with scaled experiments or need full scale tests.

B. Conduct a scaled hot cell test with actual waste at NRDS.

C. Conduct full scale test at NTS.

Systems scoping has been completed, and concept feasibility studies are underway. The DRD experiment series consists of nonnuclear melting of waste simulants in several types of bedrock and the laboratory tests necessary to support these experiments. Analytical models are being developed or modified and are being checked against data from the experiments. The laboratory tests are also providing input data for the analytical analyses. The design and operation of the first simulation experiment (DRD-1) is the subject of the remainder of this report.

Laboratory convection tests consisted of electrically melting short cylinders of low melt temperature materials such as ice and paraffin to determine the size, shape, and migration of the melt in these materials. The data were used to verify analytical modes of convection around spherical and short cylindrical heat sources. The results of the convection tests are given in References 25 and 26.

The DRD-1 Experiment

DRD-1 is the first in a series of experiments designed to evaluate the feasibility of disposing of high-level uncontained solid radioactive waste in deep bedrock using the in place melt concept. The tests will also provide input data for analysis and a physical example to check the accuracy of analytical methods. The specific goals of the test series are listed in Table VIII, Part II-A. Simulation models can be used to investigate some of the specific phenomena associated with DRD, but representative bedrock and nuclear waste or a waste simulant must be used in meaningful feasibility tests. The material combination of bedrock and nuclear waste is unique in the following respects:

1. Mechanical response as a function of temperature,

2. Thermal degradation of the granular rock,

3. Diffusion of the melt into the rock,

4. Chemical reactions and compatibility,
5. Pronounced temperature and concentration dependence of the matrix Rayleigh number and the resulting effects on convection,
6. Mixing and stratification of the components of the matrix, and
7. Properties of the solidified matrix.

Experimental Description

A preliminary analysis using the DELT computer program indicated that granite rock could be melted around a cylindrical heater with about a 1.9 kW/ft thermal input. This meant that a relatively inexpensive test could be conducted using an electric resistance heater surrounded by an annular column of nonradioactive waste simulant in a block of bedrock. The conceptual design of the experiment is shown schematically in Figure 9. Silicon carbide was found to be the best material for a resistance heater in the DRD-1 environment. A 2.125-inch diameter bayonet type heater would produce the heat flux required for the test. A 3-inch diameter, electrically nonconducting, refractory tube was required to protect the heater from the molten rock and waste simulant. With this diameter, the heating length should be a minimum of 2-feet long to minimize end effects. A 4- to 5-inch radius melt zone was desired to assure convection, to obtain the desired rock to simulant ratio, and to allow for a concentration gradient in the melt. Allowing for a rock degradation zone around the melt and sufficient virgin rock to hold the experiment together, the required rock size was found to be 3- x 9- x 4.5-feet high. The rock was buried in granitic sand for a thermal impedance match and for support if thermal stresses cracked the rock. A ceramic tube provided access to the rock from the surface.

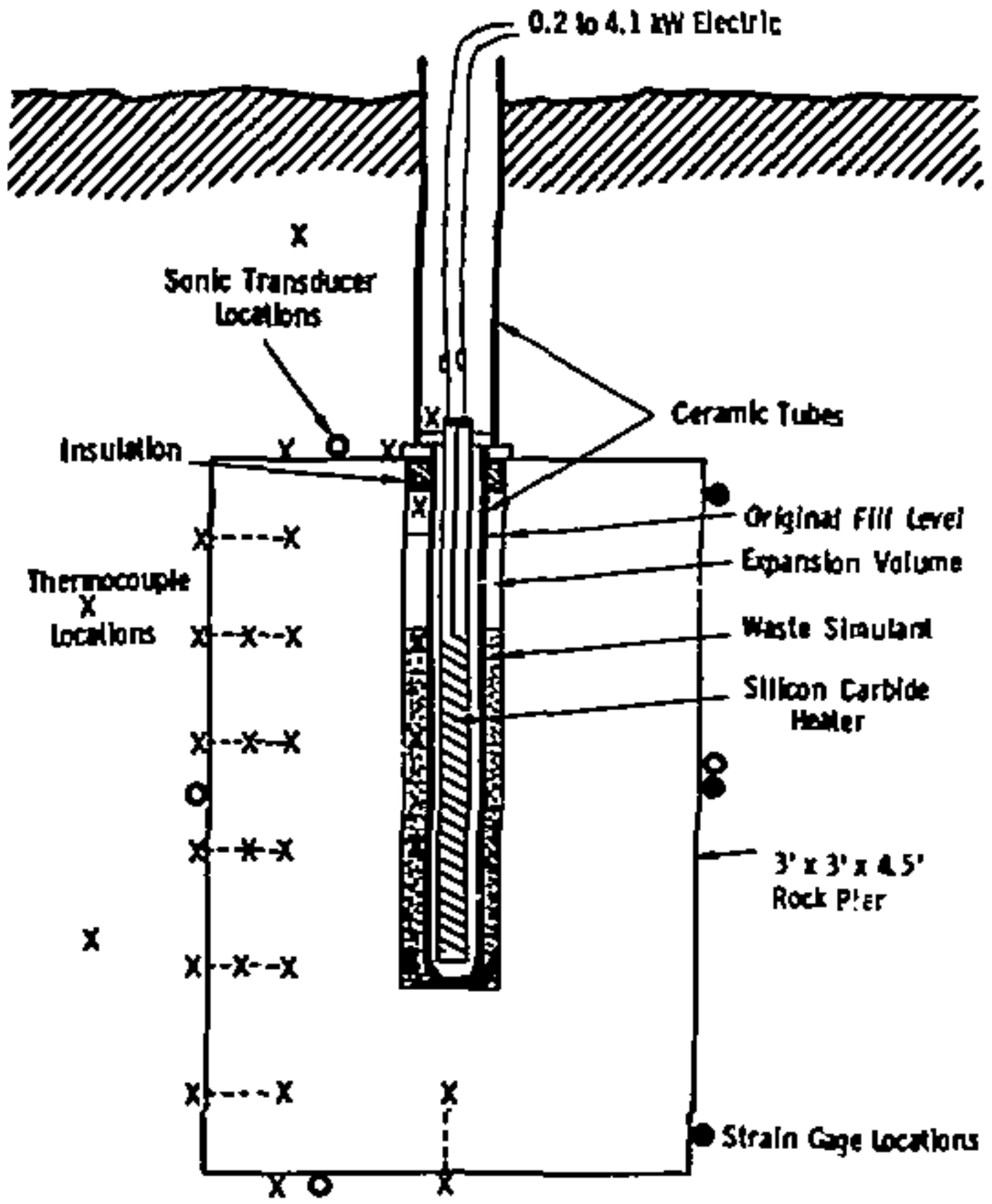

Figure 9. Deep rock disposal experiment 1

Data Acquisition

Data acquisition during the test was accomplished with thermocouples, strain gages, sonic transducers, and a melt sampling pipet. There were 29 fixed thermocouples located in a radial and vertical array for ease in correlating with temperature gradients predicted analytically and to determine the effect of convection, as illustrated in Figure 10. There was also a probe thermocouple that could be moved vertically in the melt which was used to obtain a continuous vertical temperature profile next to the heater tube and to locate the top of the liquid in the expansion volume. The top of the convection cell was located by the inflection point in the vertical temperature profile. Three strain gages were located on the sides of the rock to check the surface strain predicted by the thermal stress analyses. Strain gage data were only good until the surface temperatures reached 350° F. Six ultrasonic $LiNO_3$ transducers were attached to the faces of the rock to locate any cracks that occured during the test by using acoustic emission and triangulation techniques. A quartz transducer was placed next to one of the side transducers. This pair was used for pulse echo in an attempt to locate the edge of the melt zone and the beginning of rock degradation. Through transmission was used to measured delay times through the rock as the temperature changed. These data were used to calibrate pulse echo and acoustic emission data. An attempt to correlate through transmission diffraction measurements and thermocouple data may provide a method of measuring temperatures in areas where thermocouples can not be used. Details of the acoustic instrumentation are given in Appendix E.

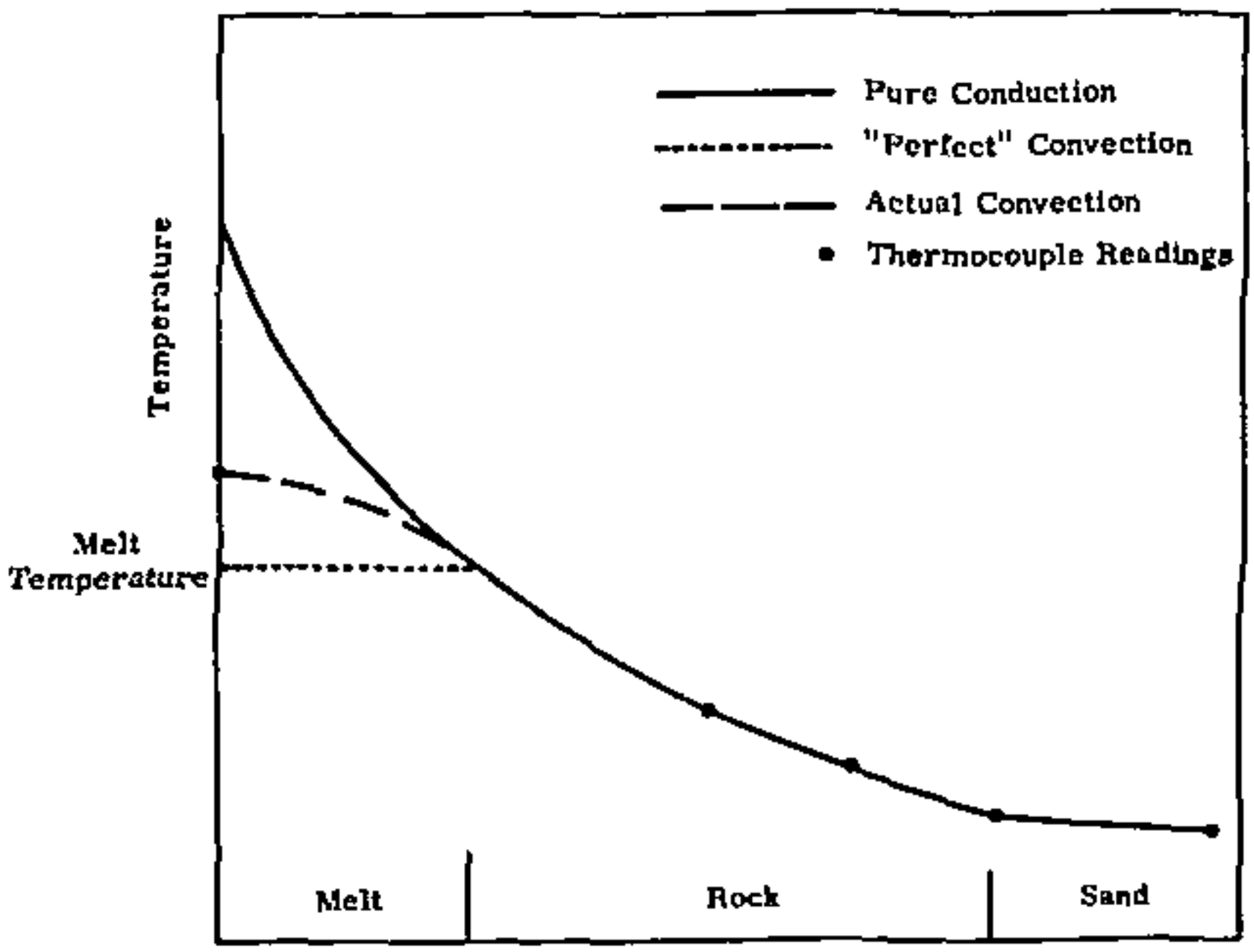

Figure 10. Use of radial thermocouple data

The sampling pipet was used to extract samples of the melt near the end of the test to measure the amount of rock that had melted. The composition of the sample, and hence the ratio of rock to waste simulant, was determined using X-ray fluorescence spectroscopy.

Bedrock Selection

The rock types selected for the DRD series not only had to be representative of bedrock but also had to have properties that would facilitate testing. The desired properties were good tensile strength to reduce cracking, high degradation temperature to insure integrity after the test, and good sonic transmission. Felsic and mafic granular igneous rocks were collected from various parts of the United States and subjected to thermal, mechanical and sonic tests. The results of these tests are given in Table IX with the rocks listed from the most acidic to the most basic. Composition and texture of the various types of bedrocks are given in Appendices B and C of Reference 27 and Section I of Reference 28. The slump tests were used to determine the degradation temperatures and relative high temperature viscosities. Sample bars of each rock were supported at each end as shown in Figure 11 and were placed in an oven for approximately one hour at temperatures of 800, 900, 1000, 1100, and 1200°C. Posttest inspections indicated the amount of flow and degradation at each temperature. A hot stage microscope was used to determine the temperatures when the first component of the rocks melted and the temperatures at which the rocks flowed. Convection could be expected to begin at about the flow temperature. Details of the thermal tests are given in Appendix F.

TABLE IX

Rocks Tested for DRD Experiments

	Density $\left(\frac{lb}{ft^3}\right)$	Compressive Strength (psi)	Tensile Strength (psi)	Sonic Attenuation 1 MHz (dB/cm)	Slump Temperature (°F)	First Liquid (°F)	Flow Temperature (°F)
California Potash Granite	165	31,600	2,050	22	1,650*	2,210	>2,370
Georgia Potash Granite	164	28,400	1,890	22	2,010*	2,100	>2,370
Virginia High Quartz Granite	163	30,500	2,570	3	2,190	2,250	>2,370
Texas Granodiorite	165	32,300	2,150	2	2,010	2,140	2,320
New York Granodiorite	174	33,400	2,760	2	2,100	2,100	>2,370
Minnesota Monzonite	171	31,700	2,010	1	2,010	2,190	2,280
California Diorite	179	31,900	2,120	1	>2,010	2,140	2,320
North Carolina Dolerite	191	39,400	3,000	1	>2,190	2,100	2,280

*Fractured

All rocks except the potash granites could have been used in the DRD test series. Two rocks which bracketed igneous bedrocks in composition and thermophysical properties were selected for further testing. These were: (1) dolerite, which was the least refractory, the most fluid, and consisted of calcium rich plagioclase feldspar, pyroxene, and olivine; and (2) high quartz granite, which was the most refractory, the most viscous, and consisted of quartz, orthoclase feldspar, sodium

rich plagioclase feldspar, and biotite. Differential thermal analysis (DTA) was used to measure the melting range of these rocks. The dolerite had a well defined melting point, but the various components of granite melted over a 315°F temperature range (Appendix F). Data in Reference 28 indicate that granular silicate rocks expand 8 to 10 percent during the melting process. Expansion of this magnitude required an expansion volume in the experiments. Tests of the dolerite showed the expansion in going from a granular to a glassy structure increased the volume by 13 percent.

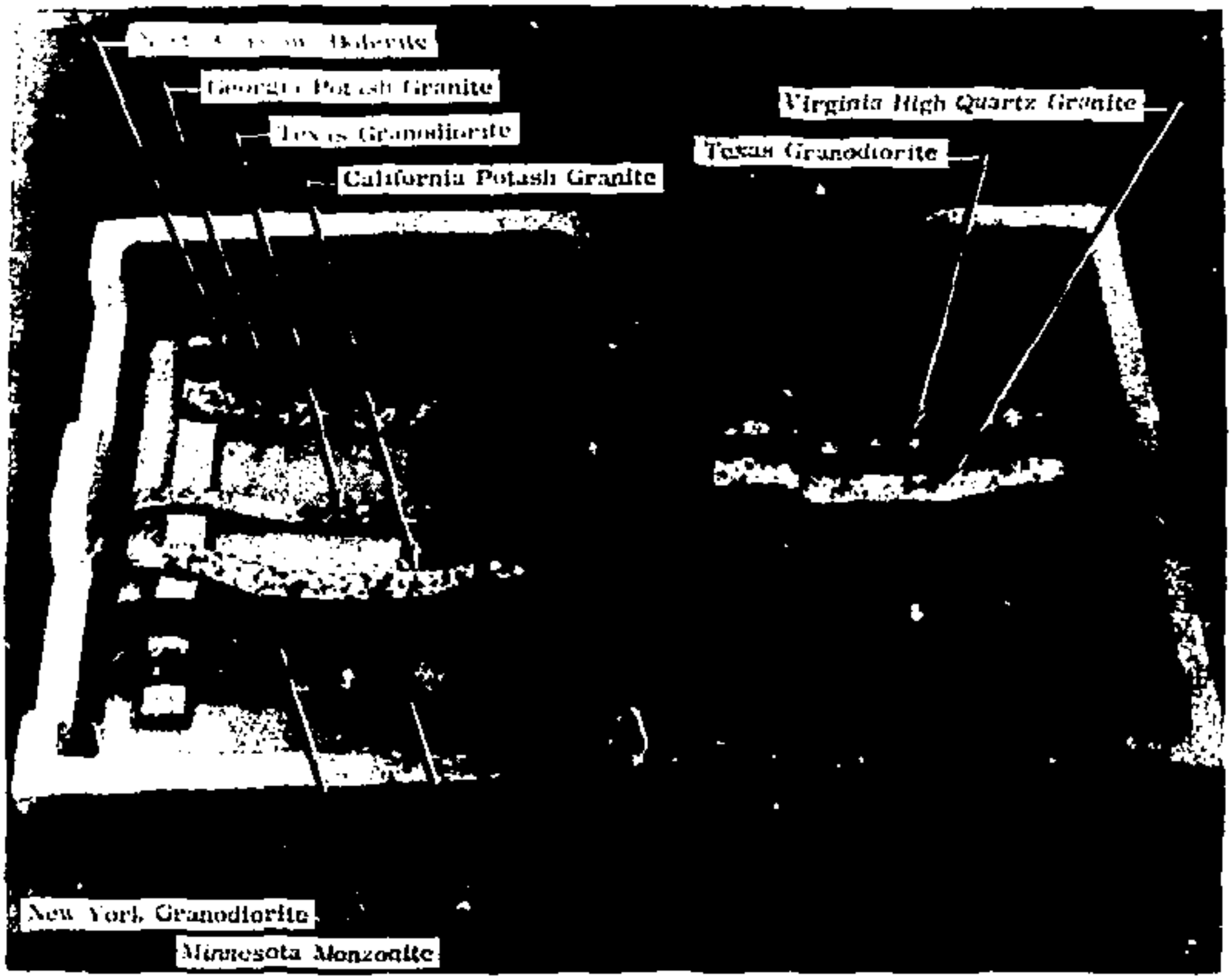

Figure 11. Results of the 1200°C slump test

Thermal conductivities of bedrock vary greatly even within a given classification, with grain structure having as large an effect as composition (Reference 29). Figure 12 gives the conductivities of several mafic rocks with chemical compositions similar to the North Carolina dolerite. Gabbro is course grained, dolerite is fine grained, and crystalline basalt is aphanitic. The range of thermal conductivities of high quartz granitic rock is equally as large. Viscosity data for these rocks were not available when the DRD-1 test was designed. Viscosities of similar rocks were used for bracketing studies. These and other thermophysical data for the rocks are given in Appendix B. Dolerite was selected for the first test because the lower melt temperature would facilitate developing the new testing techniques needed for the DRD test series. It is also similar to the manzonite and diorite found at Nevada Test Site.

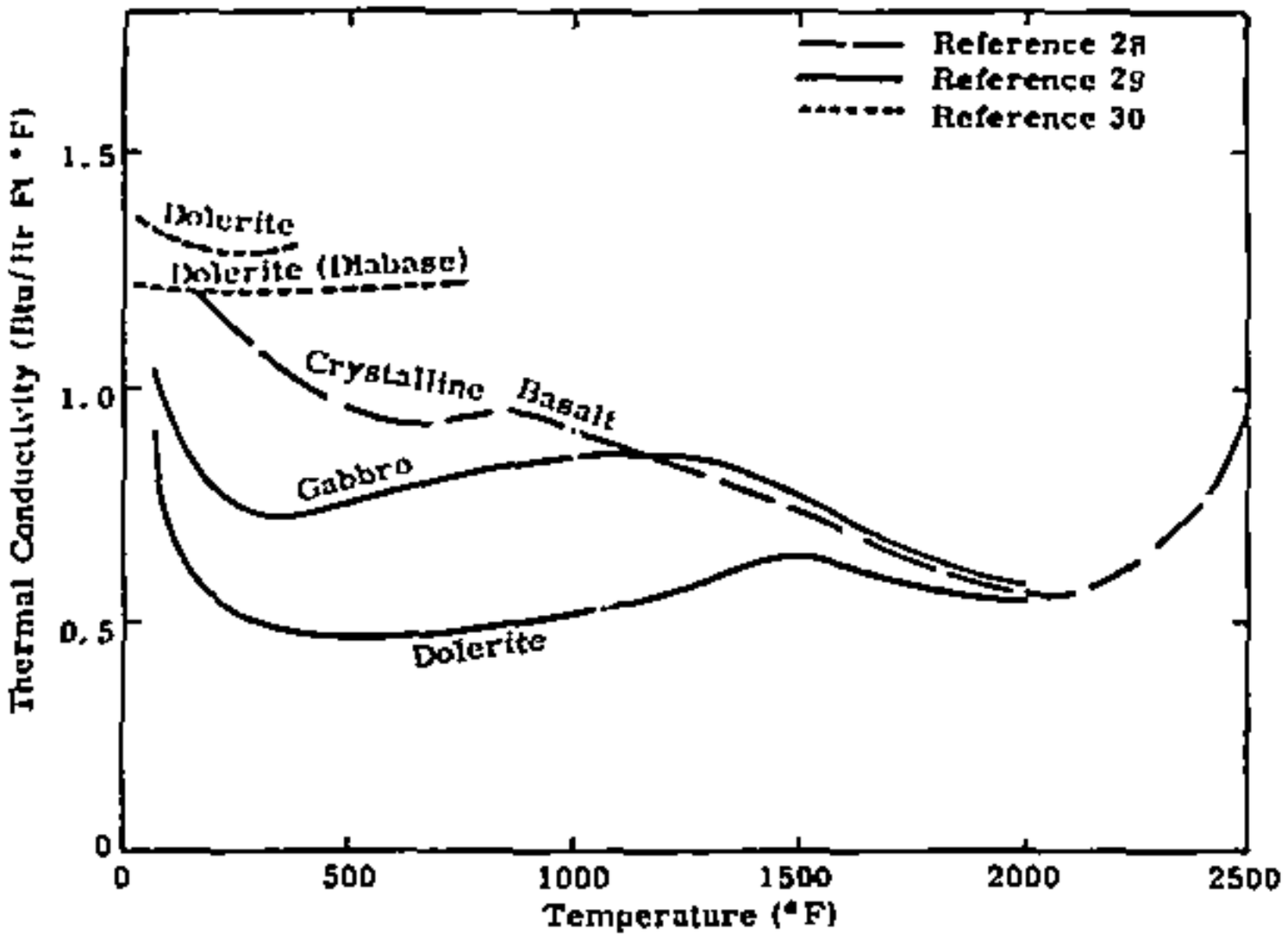

Figure 12. Thermal conductivity of mafic rocks

Waste Simulant Design

Current forms of high level waste have been designed for storage and may or may not be well suited for DRD. However, it was not possible to develope a new waste form for DRD-1, and the waste simulant was selected from the existing forms. The primary considerations in selecting a waste form for the DRD-1 experiment were a low viscosity to promote good convection and chemical compatibility with the rock and test hardware. The phosphate and borosilicate glass forms of waste were selected for testing based on their thermophysical properties. The phosphate glass was the most fluid, but it reacted with the oxide refractories it came in contact with, and the P_2O_5 vapors attacked the furnace heating elements at the melt temperatures of the rocks. The phosphate glass is also more soluable in water than borosilicate glass. The ternary eutectic of borosilicate glass is nearly as fluid as the phosphate glass and is less reactive. The quality of borosilicate glass samples was good, and it was selected for the DRD-1 test. The composition of the simulant is given in Appendix G along with details of the tests and manufacturing. The simulant is made up of stable isotopes of high-level waste plus boron and silica. Elements that have no stable isotopes were replaced with elements which are chemically similar. Thermophysical properties of the simulant are given in Appendices B and G.

The limited volume in the annulus around the heater made it necessary to have a simulant packing density of at least 65 percent. This density could not be obtained with a granular form, so the simulant was pressed into semi-annular rings which were stacked around the heater tube (Figure 13). A small amount of frit was used at the bottom of the hole to fill the volume under the heating tube and bring the quantity of waste to the exact amount needed to fill the annulus to the top of the heater when it melted. Figure 14 shows the 34.250 lbs. of solid simulant and the 1.094 lbs. of loose frit used in the experiment.

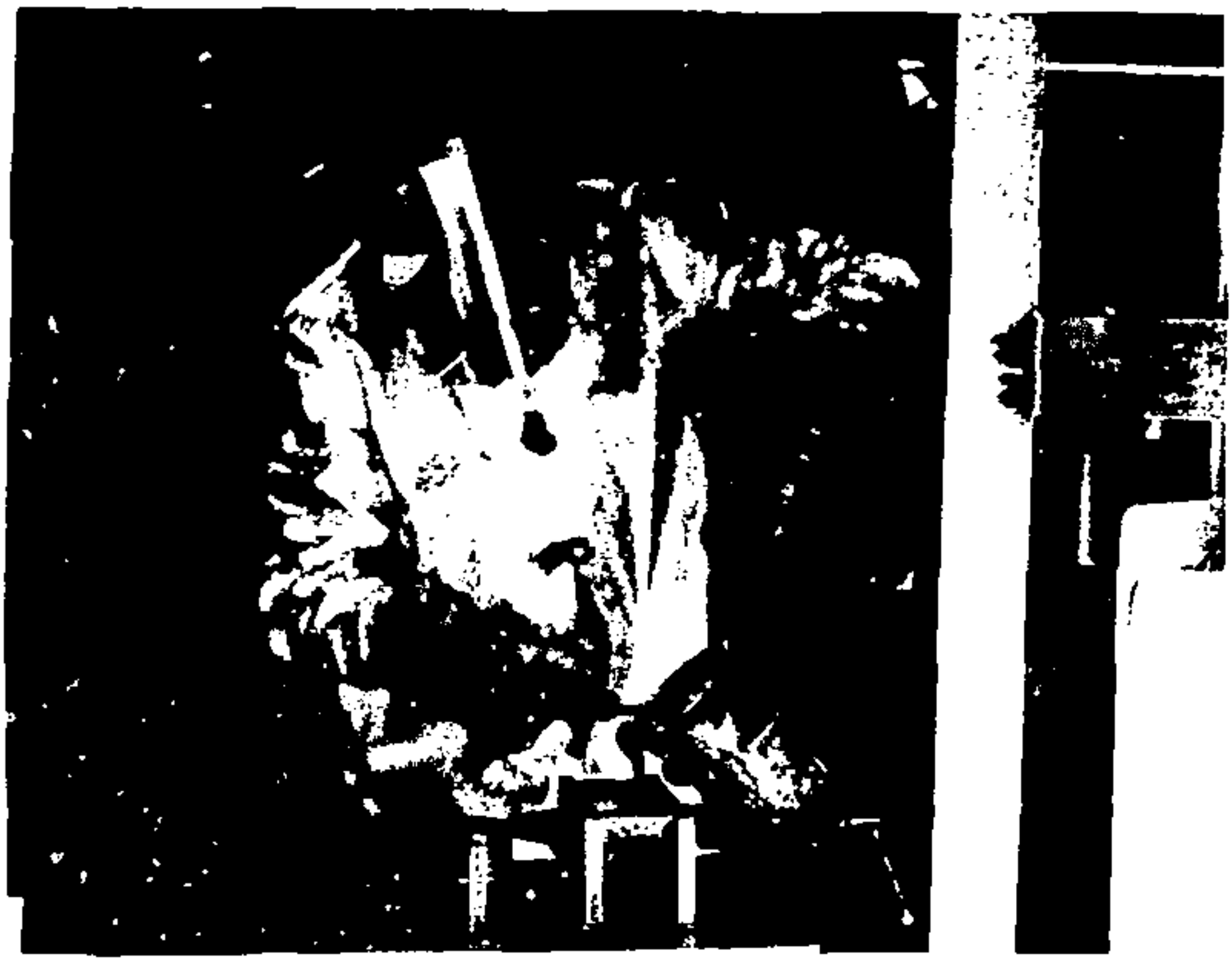

Figure 13. Pouring waste simulant into a mold at approximately 1800° F

Material compatibility data for the borosilicate form of high level waste were available at the melt temperature of the waste (1500° F), but none was available at the melt temperature of rock (2200° F). The heater tube and thermocouple sheaths would be in contact with molten simulant at 2200° F and with mixtures of simulant and rock up to approximately 2400° F. Material selection for these two components was based on tests in which candidate materials were immersed in molten simulant or simulant/rock mixtures for up to 24 hours to observe the erosion. The materials tested included metals, oxides, carbides, silicides, and nitrides. All materials disolved at the higher temperatures except tin oxide and platinum which showed no signs of attack. Platinum sheathed thermocouples were selected, and a recoverable platinum protective sheath was placed over an alumina heater tube. The alumina was used as a structural support and as an electrical insulator. Tin oxide was not available in tube form.

The borosilicate simulant reacted chemically with both the dolerite and high quartz granite. The effects were that rock entered the melt below the rock melt temperature, and the viscosity of the melted mixture was lower than that of pure rock. Rock does not enter the molten mixture by

pure melting until there is a large rock concentrati - in the m'xture. Even then, diffusion and mechanical failure of the rock surrounding the melt zone can affect the rate at which rock enters the melt. This leads to the possibility of tailoring the waste form for a given bedrock to make the most fluid molten mixture. For instance, a waste form without silica should absorb some of the excess silica in high quartz bedrocks to reduce the effective rock melt temperature to that of the remaining rock components.

Figure 14. Waste simulant hot pressed semiannular rings and frit used in the DRD-1 experiment

Experiment Design and Pretest Analyses

The limited input data and unknowns that created a need for the DRD-1 experiment also made it impossible to accurately predict the functional requirements of the test hardware or the environments to which it would be subjected. The test philosophy was to monitor all critical parameters and to design the hardware with several options. The test procedure could then be altered during the test if a change was indicated by the instrumentation.

Test Equipment Installation

The test was conducted in Sandia Test Area III, Albuquerque, New Mexico. This site was selected because the granitic soil had nearly the same thermal diffusivity as the rock, and power supplies and recording equipment were readily available. An elevation view of the test installation is shown in Figure 15. The rock was buried 3 feet below the surface to assure uniform heat loss from the rock during a 45-day test. This depth was sufficient because of the low diffusivity of the rock and sand. Several inches of free flowing, water washed, Ottawa type sand were placed around the rock to protect the instrumentation and lead wires and to minimize any surface discontinuities. A 6-inch diameter Mullite tube provided access to the top of the rock during the test. A portable shelter which contained the amplifier and protected the access tube and electronic equipment from the elements was placed over the rock. The test was conduced next to the environmental facility building which housed the power supply, air compressor, and recording equipment. Strip chart recorders provided a visual readout during the test. Data were also recorded on magnetic tape for digital data reduction after the test.

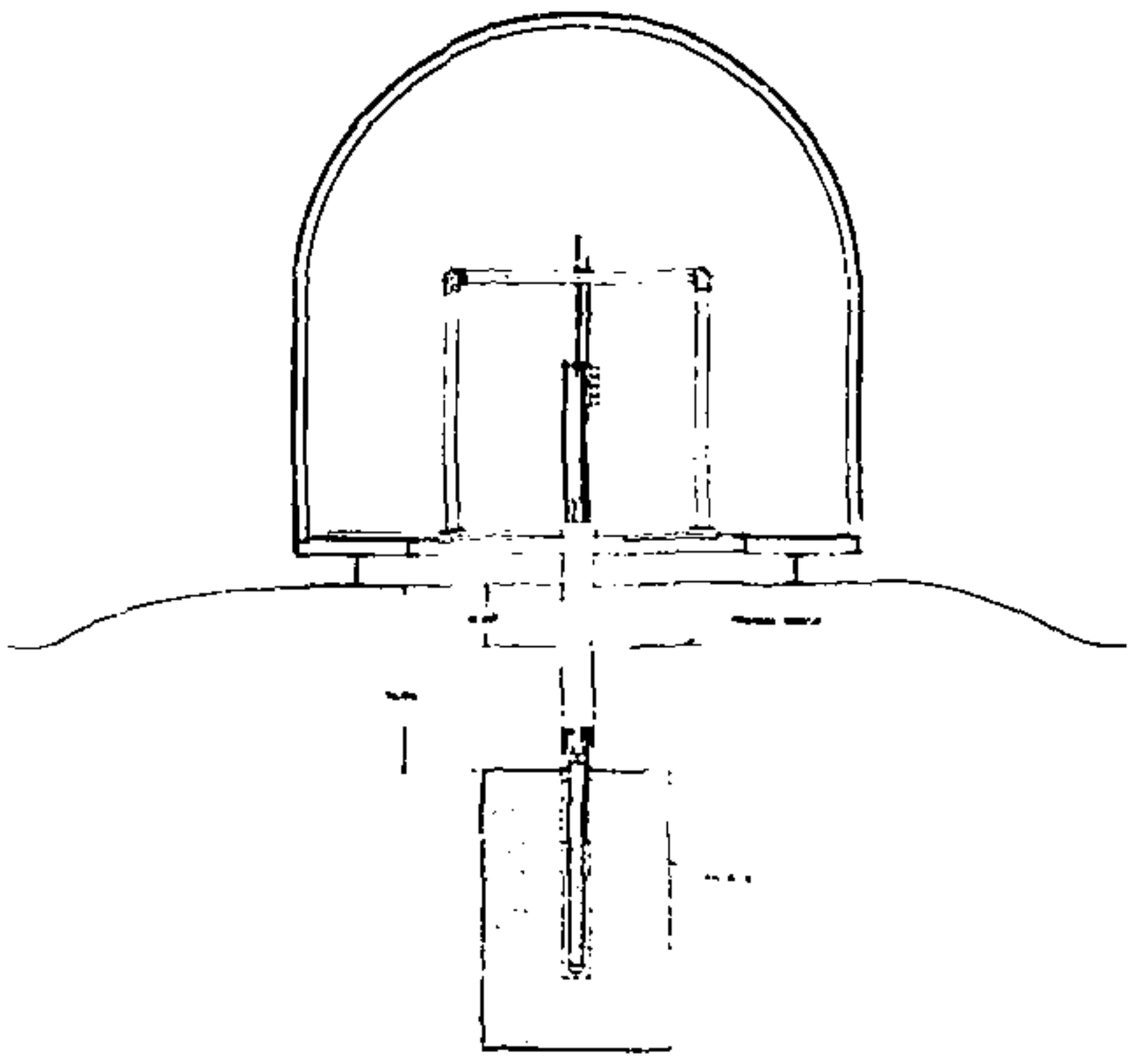

Figure 15. DRD-1 installation drawing

The largest bayonet type 2.125-inch diameter silicon carbide heater that was commercially available had a 24-inch heated section and a 17-inch stem. This component limited the size of the experiment and was a dominant constraint in the design of the rest of the hardware. The maximum voltage output of the variable power supply which was readily available was 130 volts, and the heater resistance at the desired peak temperature was about 4.2 ohms. This meant that the maximum power that could be delivered to the rock would be about 4 kW, 3 percent of which would be generated in the stem of the heater. The design of the heat pulse was based on a 3.88 kW maximum heating rate.

Thermal Analysis and Design

The 344 node CINDA digital heat transfer program described in Appendix C was used to design the heat pulse and predict temperatures in the simulant, rock, and sand. The thermal model was two-dimensional (radial and vertical) in cylindrical coordinates and included only the bottom half of the rock. A uniform heat source experiment with a molten core such as DRD-1 has vertical mass transfer and a vertical temperature gradient which results in more radial heat transfer and melting at the top of the heated section than at the bottom. However, the current version of CINDA is restricted to isotropic conduction and has no mass transport option. This problem was circumvented by analytically computing the vertically averaged radial heat transfer by convection and converting to an equivalent radial thermal conductivity. This resulted in the CINDA program predicting temperature distributions symmetric about the vertical midpoint. This error was not large enough to interfere with the test design. The procedures used to compute convection, effective conductivities, and average velocities in the melt are defined in Appendix D. The negligible amount of heat input that went into the melt as sensible heat above the melt temperature (0.064 percent) and the slowly increasing heat rate made it possible to obtain closed form solutions for the effective conductivity. Nusselt numbers, or the ratio of conduction to convection temperature gradients, were computed to be as high as 2.95 for a 50/50 rock/simulant mix at an average temperature of 2360° F, an annular width of 1.8 inches, and low viscosity rock. In the DRD-1 experiment with a slowly increasing heat pulse, the average inner temperature of the melt was never expected to exceed 2500° F with low viscosity dolerite or 2600° F with high viscosity dolerite because the increase in melt radius and hence the increase in Rayleigh number and effective conductivity of the melt nearly compensates for the increase in heat flow.

The actual fluid flow in the annulus can be approximated by the use of analytical techniques and experimental data from J. W. Elder, E. R. S. Eckert, W. C. Carlson, and G. K. Batchelor (see references in Appendix D). Figure 2 in Appendix D shows the types of laminar cellular flow that can be expected in the annular as a function of Rayleigh number which is a measure of (1) bouyancy, (2) inertial and viscous forces, and (3) momentum and thermal diffusivities. The maximum Rayleigh number predicted for the DRD-1 experiment is between 10^5 and 4×10^5 depending on the viscosity of the rock. Therefore, there was probably only one or possibly two convection cells. Ice melting tests conducted by H. C. Hardee and W. N. Sullivan (Reference 25) showed the effect of convection on the shape of the melt zone when heated by a fixed cylindrical heating rod. The heating

ratio was too low to initiate convection in the ice melt test shown in Figure 16. The melt, seen as the dark area in the center, expanded uniformly in the radial direction with heat being conducted through the liquid. The ice in the test shown in Figure 17 was heated at a higher rate, and heat transfer in the liquid was by convection. The liquid moving upward along the heater established a positive vertical temperature gradient. This gradient and the fixed melt temperature caused more heat to be transferred to the ice at the top of the annulus than at the bottom, which resulted in the inverted conical shaped melt. A conically shaped melt zone was expected in the 1 TD-1 experiment, but it was not expected to be as pronounced as that in Figure 17.

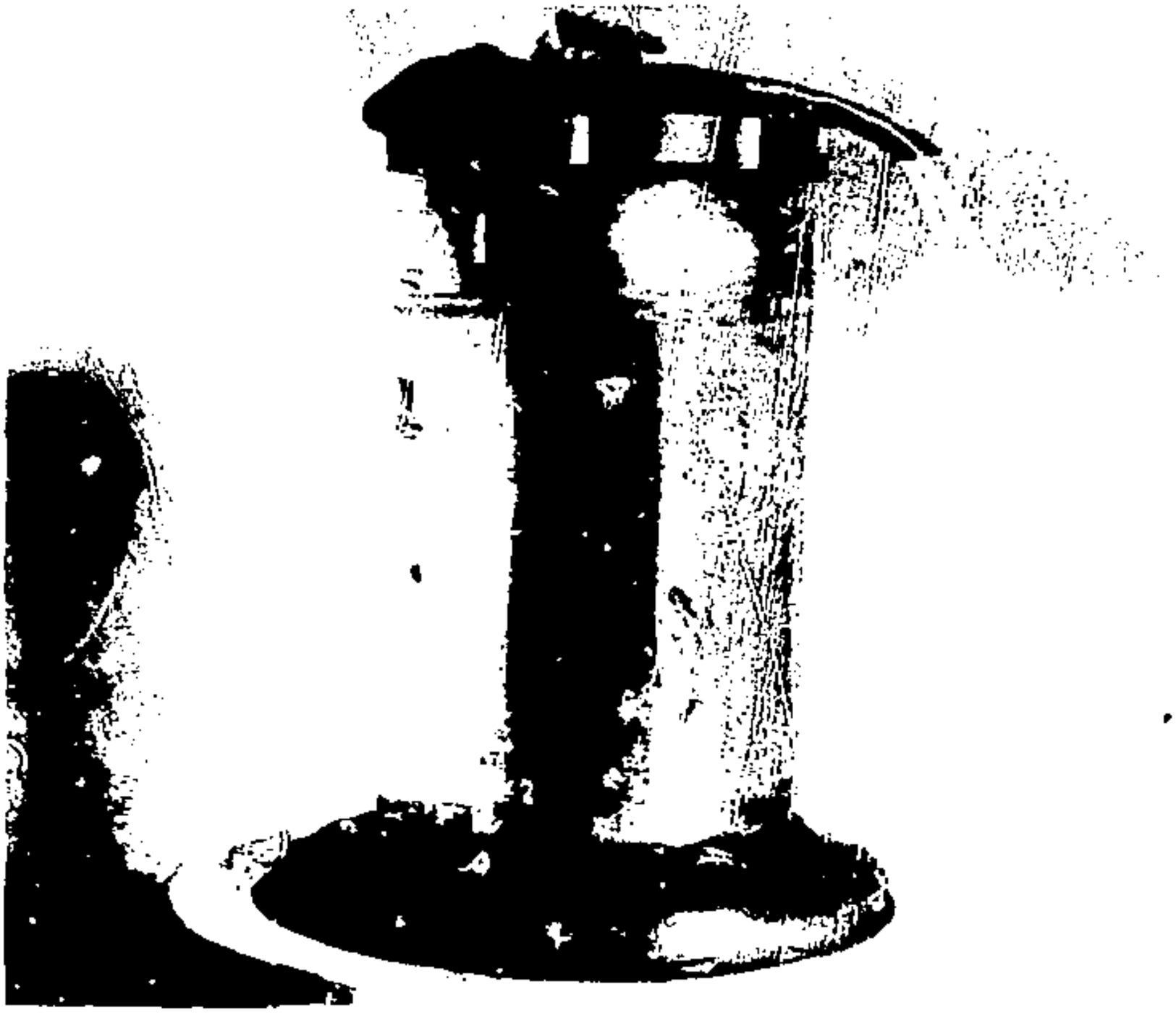

Figure 16. Ice melted by a central heater with pure conduction. Low Rayleigh number.

Preliminary stress analyses indicated a ramp heat pulse would minimize the thermal stresses in the rock during the heatup phase of the test. Thermal gradients would be lowest when the rock is cool and brittle and highest when the rock is hot and more plastic. A parametric study was conducted using the 2-D CINDA program with simulated convection to determine the effects of viscosity on the peak temperature and the effects of thermal conductivity on the melt radius. The maximum

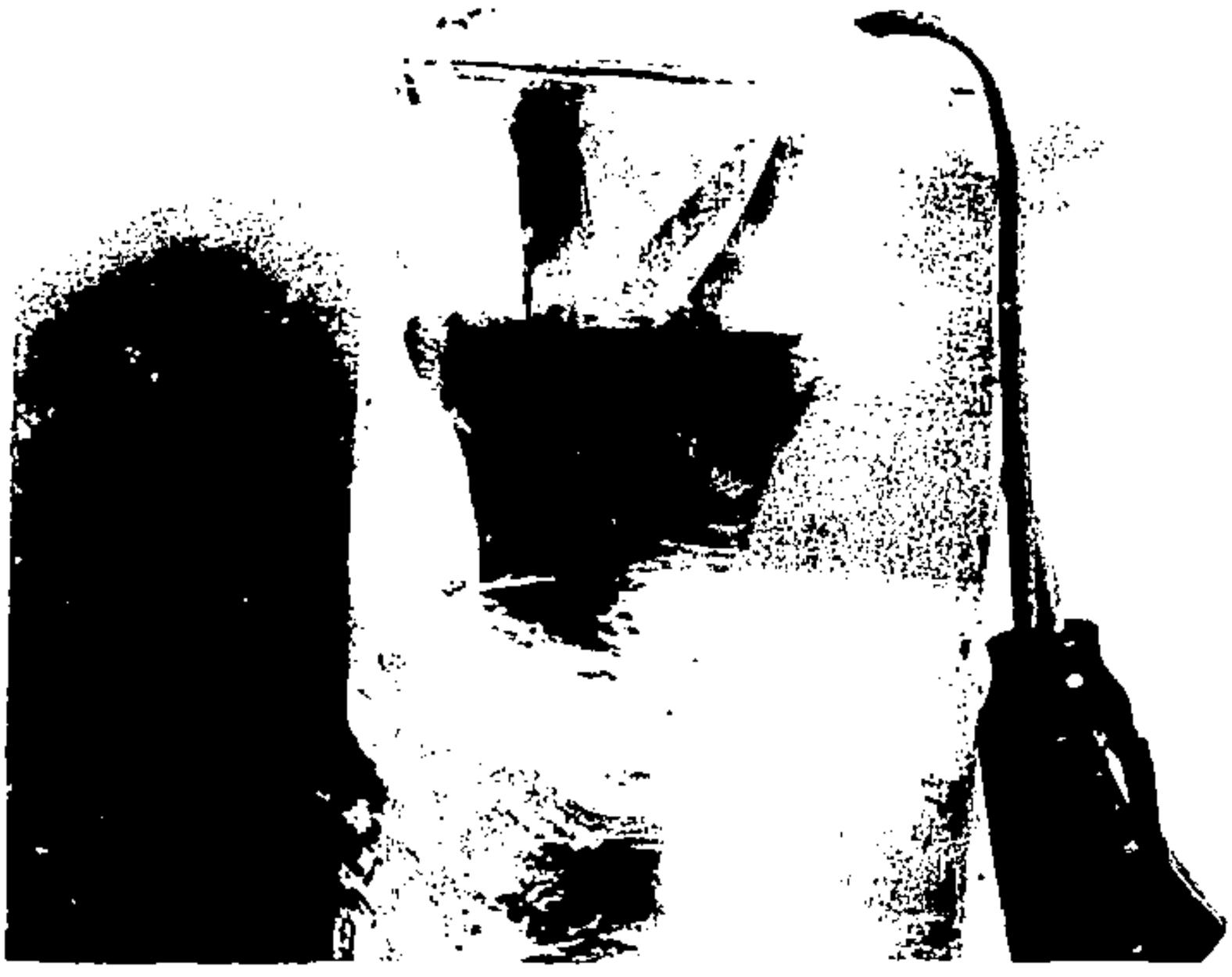

Figure 17. Ice melted by a central heater with convection. High Rayleigh number.

and minimum rock conductivity curves bracketed the data shown in Figure 12. The two viscosity curves are shown in Figure B-1 in Appendix B. The rest of the material properties are given in Appendix B. A 25-day ramp heat pulse going from 0 to 3.88 kW followed by a 5-day hold at 3.88 kW was used in the parametric study. Figures 18, 19, and 20 show the results of this study. Radial temperature profiles are plotted at 5-day intervals. At the end of the 25-day ramp, only 0.7-inch of rock was predicted to melt with high conductivity dolerite, but 2.5 inches would melt with the low conductivity dolerite. The extremes in viscosity of the melt would make less than 100° F difference in the maximum temperature at the surface of the heater tube. Visual and comparative tests of the conductivity and viscosity indicated that the rock viscosity was fairly low and the conductivity very high. Therefore, the melt radius might be less than desired, but the allowable heater temperature would not be exceeded. The small change in the temperature slope at 1.5 ft in Figure 20 shows the good impedance match between the rock and sand.

The thermal stress analysis of the DRD-1 rock was hampered by an absence of high temperature tensile strength and creep properties. The two dimensional analysis discussed in Appendix H

indicated that the rock would probably crack vertically in tension even with a ramp heat pulse. When the simulant melts and convection begins, additional heat will suddenly be transferred to the top part of the rock which increases the thermal stresses in that area. Tensile cracks formed after convection begins would propagate from the top edges downward and inward. Not enough was known about the thermal expansion of the rock/waste matrix or the degraded rock to predict contraction cracks during cool down.

During the cool down phase of the test, the power was gradually reduced for 4 days until all of the matrix was below 800° F to allow time for the glass to anneal. The power was then held at 200 watts for 10 days to assure the radial temperature gradient remained negative the same as it would with actual waste.

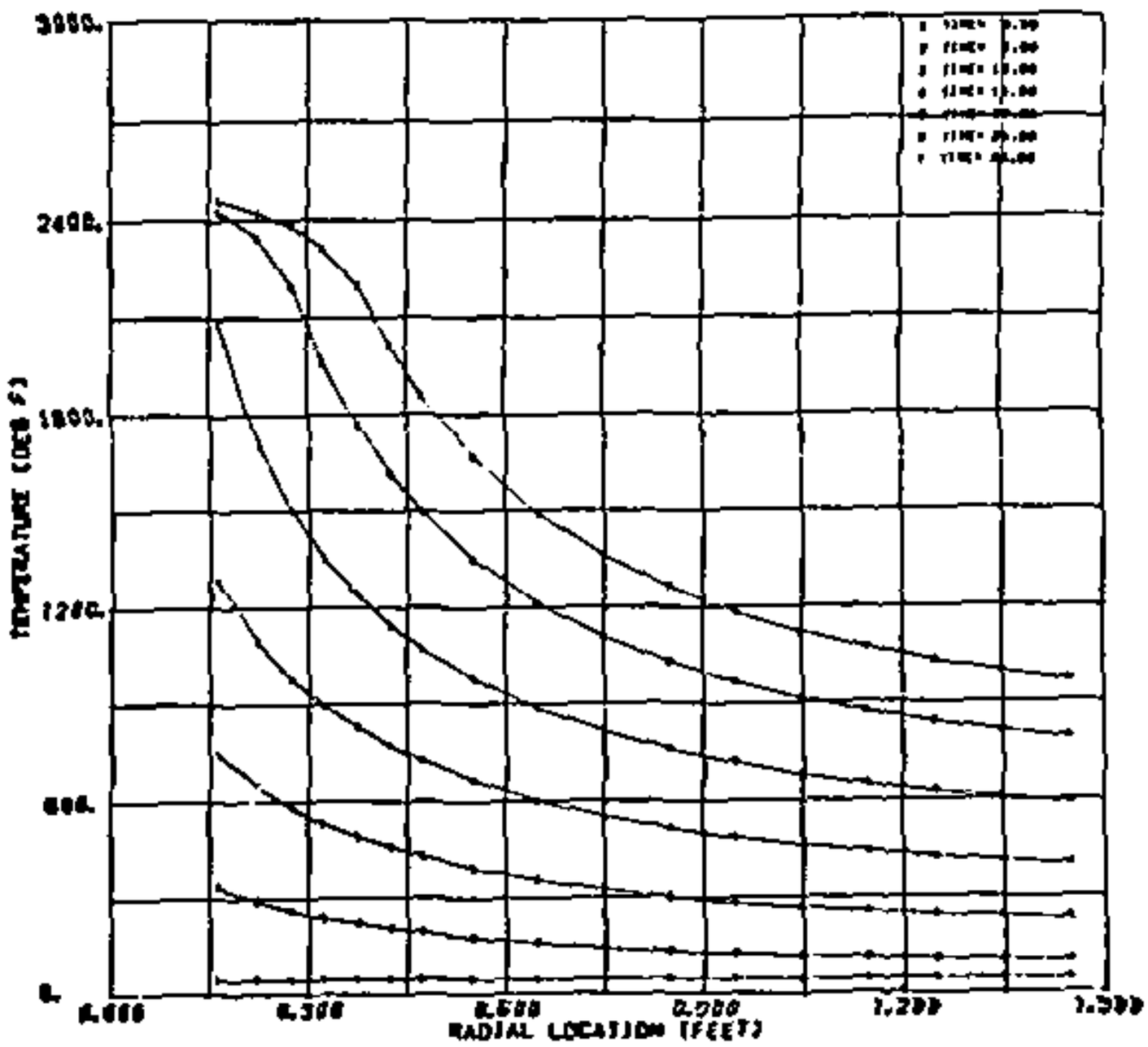

Figure 18. Dolerite, high K, low μ simulant and rock

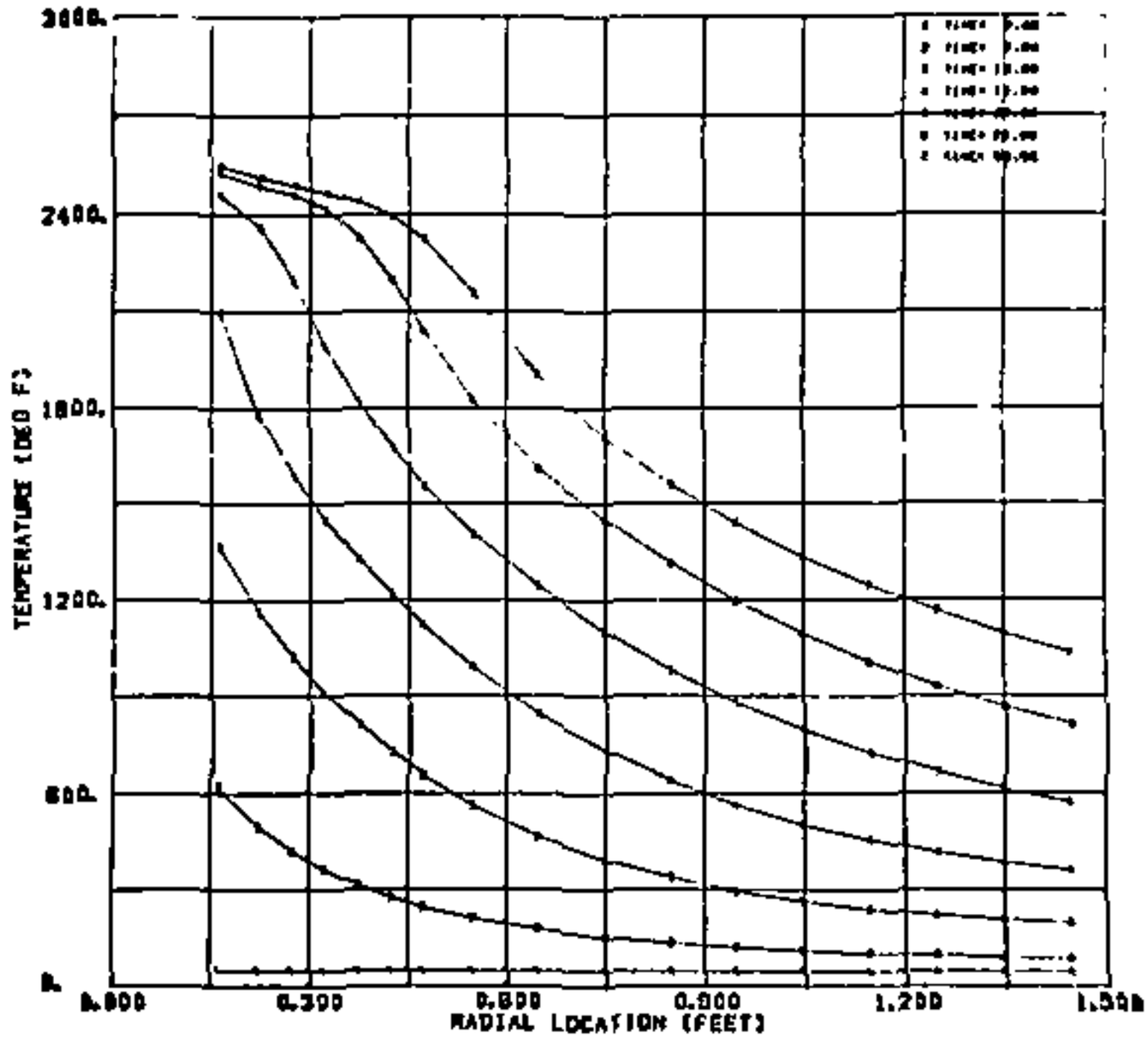

Figure 19. Dolerite, low K, high μ simulant and rock

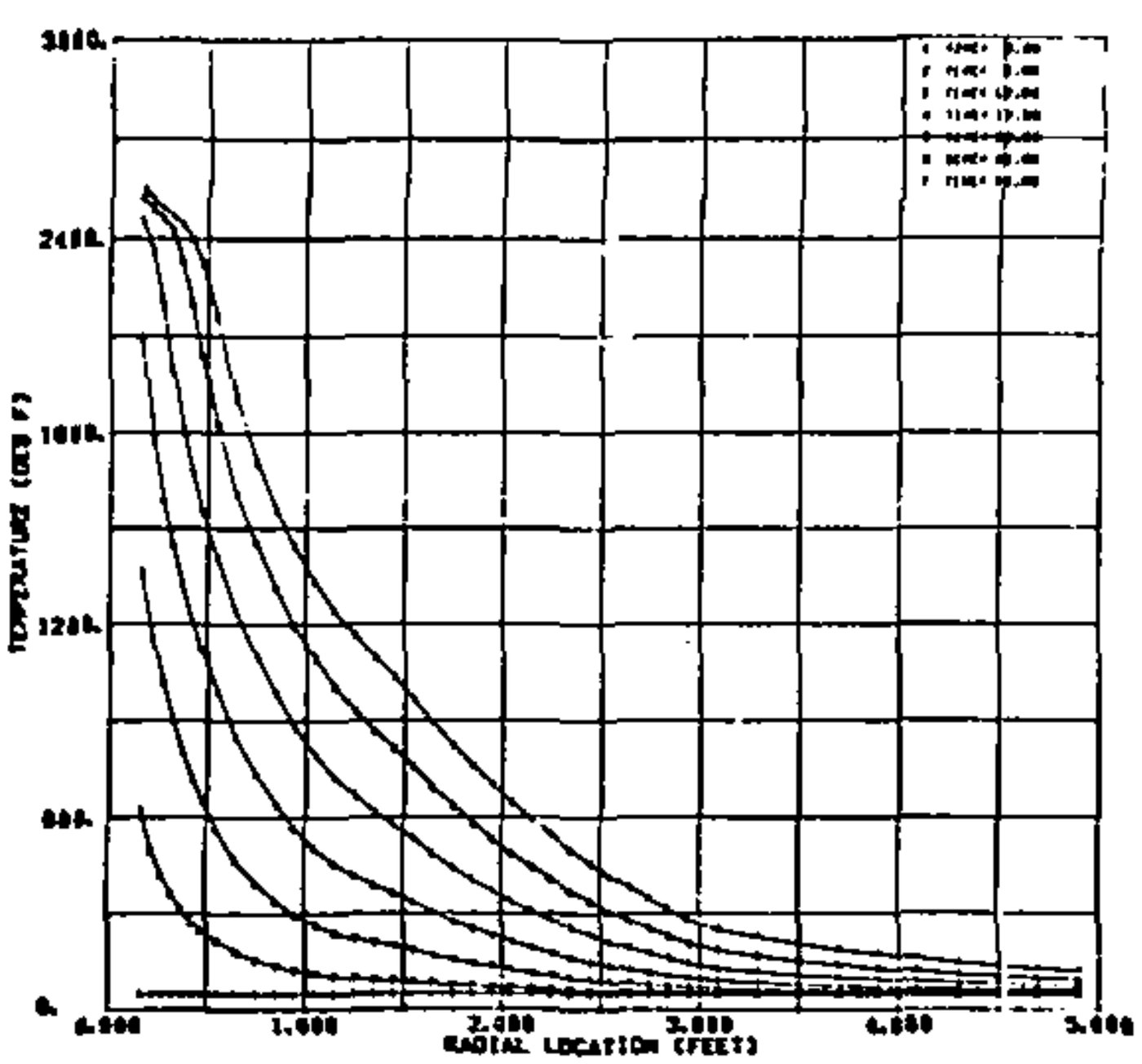

Figure 20. Dolerite, low K, high μ simulant, rock and sand

Test Hardware Design and Fabrication

Several m chining operations were required on the dolerite block including boring the central 5-inch diameter ole for the heater and simulant, 3-inch and 6-inch deep holes for thermocouples, and seats for th sonic transducer covers. Figure 21 shows one of these coring operations being conducted on the 700 lb. block. The section of the annulus around the heater tube above the heating element was use as the expansion volume for the molten rock and simulant. It was also used to stack the extra gs of simulant needed to fill the annulus to the top of the heater when the simulant elted. No othe expansion allowances were made on the rock. For the rest of the test hardware, thermal expansi was a prime consideration. Thermal gradients between pieces of hardware were large, and some omponents had to operate over ranges as large as 2600° F.

Figure 21. Machining operations on the dolerite block

The modified bayonet silicon carbide heater and the platinum sheathed alumina heater tube are shown in Figure 2. A subassembly of these components is shown in Figure 23. A zirconium oxide ring was molded o the bottom of the heater to center the heater in the tube. The heater support and

electrical lead attachment was redesigned to take higher temperatures, center the top end of the heater in the tube, and shorten the amount of stem used for the connector. Nickel was flame sprayed on the top of the heater for better electrical contact. Gold flashed copper connector plates were clamped to the heater with a segmented alumina support bracket and a stainless steel hose clamp. The aluminum lead cables were replaced with copper. The heater could have been lifted out of the tube during the test and replaced if it had been necessary. Also shown in Figure 23 is the tube support. The heater tube was grooved near the top and was held by a stainless steel hose clamp with 4 brackets which were attached to the upper base plate. The upper base plate could have been moved by the control rods during the test if more expansion volume were needed. A 2-inch thick fiberfrax insulation block centered the tube in the annulus and reduced heat losses from the annulus. Cooling air was injected parallel to the base plate to remove the heat generated by the upper part of the heater stem and the heat that entered the access tube via the lower base plate from the top of the rock. The temperature of the hardware in the access tube was measured with a thermocouple, and the air flow rate was adjusted to keep the temperatures below 500° F.

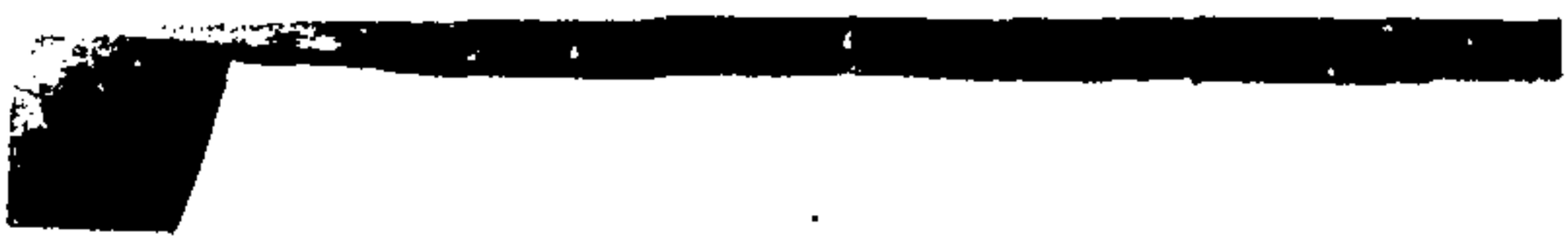

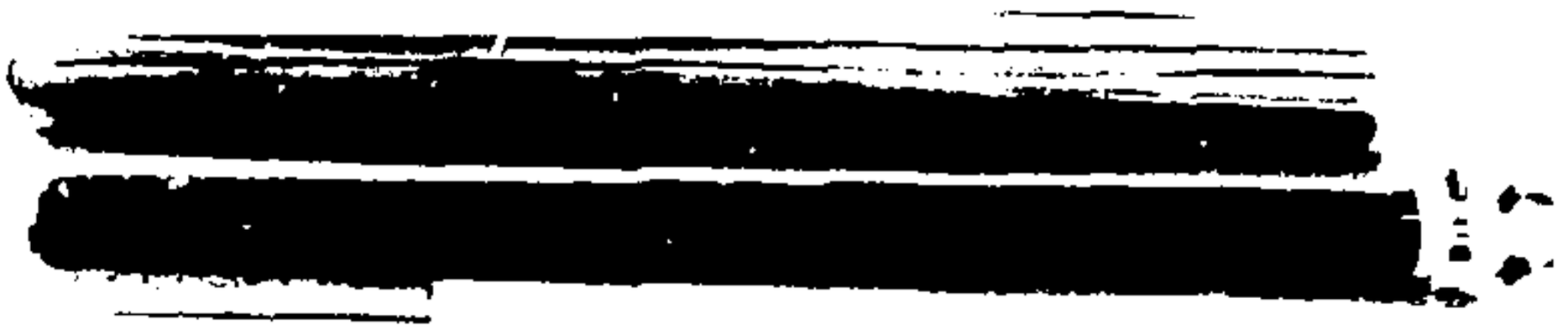

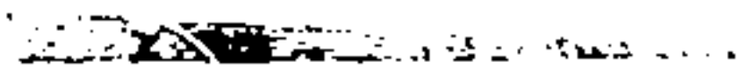

Figure 22. Heater tube with PT-Rh thermocouples and silicon carbide heater

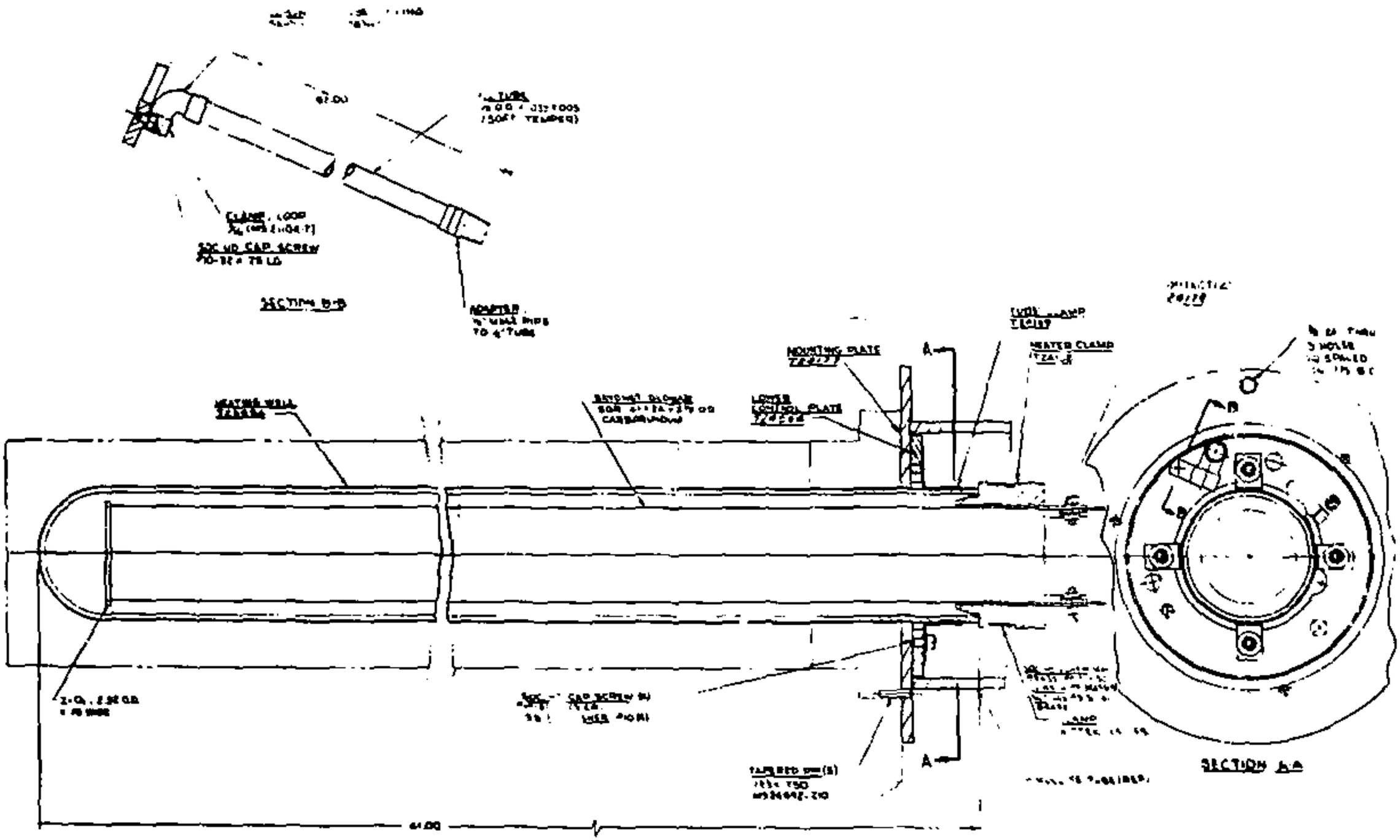

Figure 23a. Heater subassembly

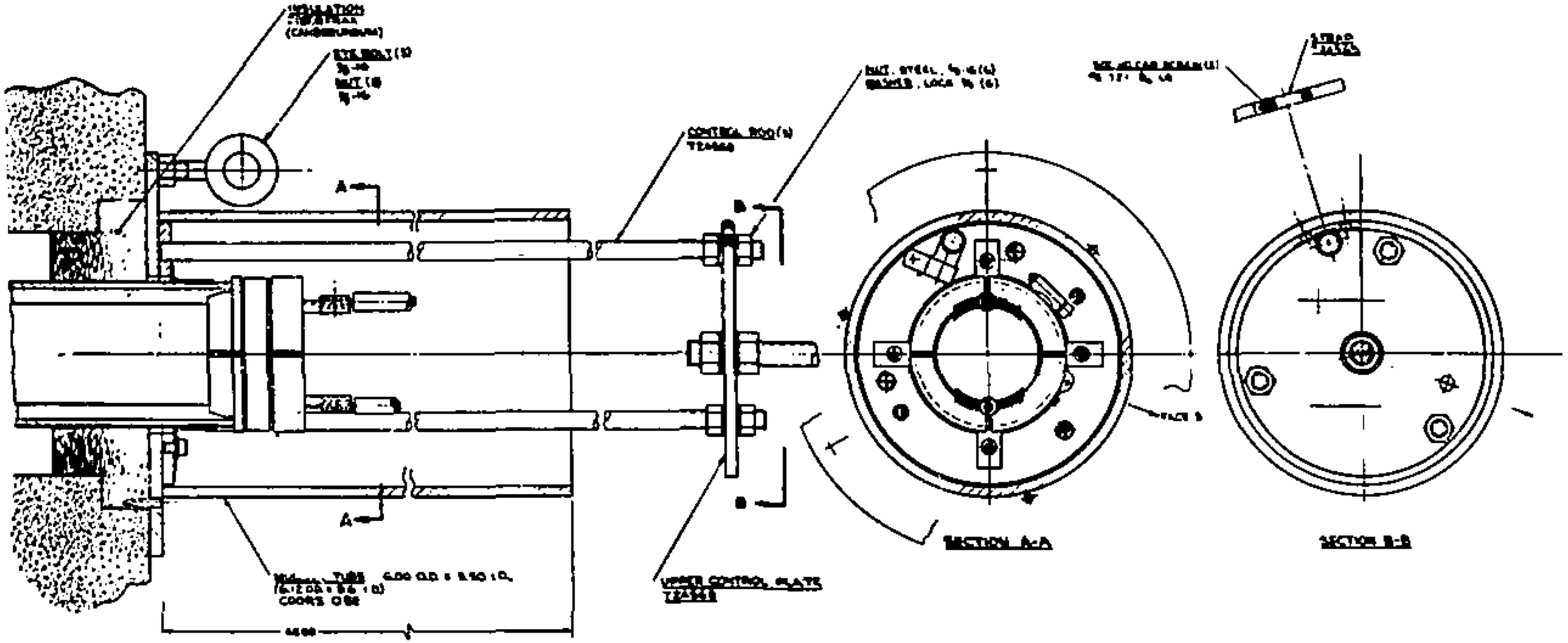

Figure 23b. Heater subassembly

The Pt-Rh probe thermocouple was attached to a calibrated steel rod and was inserted through holes in the insulation and base plates. The same holes were used for the melt sampling pipet. Four other Pt-Rh thermocouples were attached to the outer surface of the Pt sheath with Pt wire, as shown in Figures 22 and 24. They were equally spaced (8-inches apart) along the heating element. The remainder of the thermocouples placed in and on the rock, in the sand, and in the access tube were Chromel P-Alumel sheathed with Inconel 600. Sauereisen cement was used to fill the 3-inch and 6-inch deep thermocouple holes in the rock and to secure the thermocouples. Surface thermocouples were held in place with glass tape backed up by sand. Figure 25 shows the locations of the strain gages (SG) and sonic tranducers (SX). SX7 was the location of the quartz sonic transducer. One of the $LiNO_3$ sonic transducers and its spring loaded mount and coax lead wire is shown in Figure 26. A mixture of gallium and indium was used to couple the transducers with the rock. Strain gages were bonded to the rock in 6 locations (Figures 25 and 27) and covered with a waterproofing compound.

Periodic samples of the air coming out of the access tube were made, and cooling air flow rates were measured in an attempt to determine types and quantities of gases coming from the rock and simulant. The air was analyzed using a quadra-pole mass spectrometer. The temperature of the air coming from the access tube was measured continuously, and hydrometer readings were taken at intervals to determine if and when water liberated from the rock entered the access tube.

Continuous recordings of voltage, current, and wattage were made. Heater temperatures could be approximated using the computed resistance and the temperature dependent resistance curves for the silicon carbide heater.

Pretest Analytical Studies

Pretest analytical studies based on the design described above included rock/simulant expansion, temperature versus power limitations, and final temperature predications. Volumetric expansion of the solid rock during the heating phase of the test could have one of two effects on the volume available for the melt. If the inner hot rock did not yield or creep, verticle tensile cracks would propagate inward from the flat surfaces. If this were the case, the effective expansion volume for the melt would increase by approximately 3.2 percent (the volumetric expansion of rock up to the melt temperature). This volume would have to accommodate approximately a 4.1 percent increase in simulant expansion up to 2400° F and an 18 percent expansion of the melted rock. Assuming 1 inch of rock would melt and that there would be no outward motion of the cracked rock sements, only 86 percent of the expansion volume would be used. However, if the inner hot rock did yield or crumble and the outer part of the rock did not crack, there would be an inward motion of the solid rock which would decrease the available expansion volume. In this case, the rock and simulant expansion would exceed the available volume by about 90 cubic inches. If this had occurred, the heater tube would have been partially withdrawn and/or the test would have been terminated early.

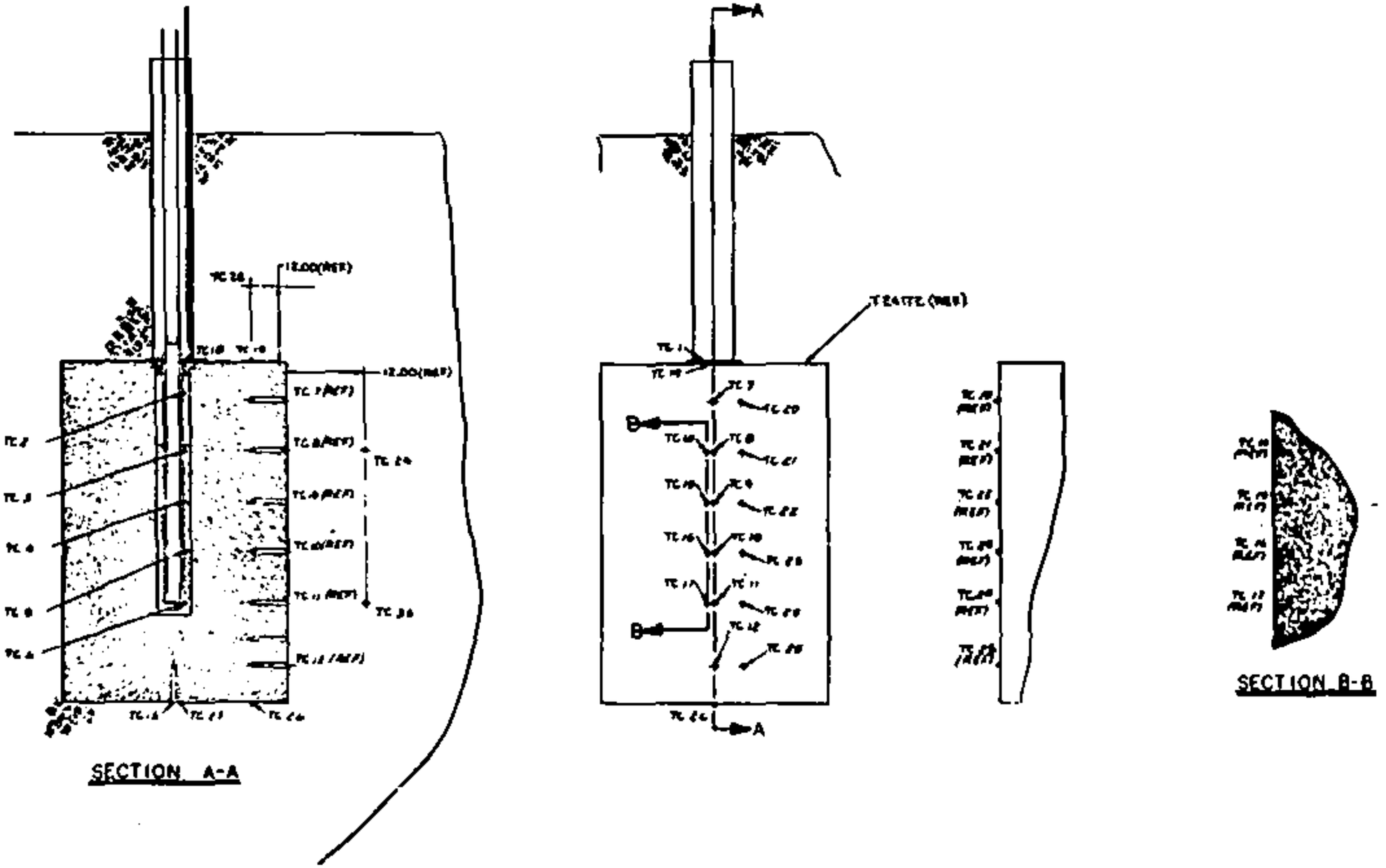

Figure 24a. Thermocouple locations

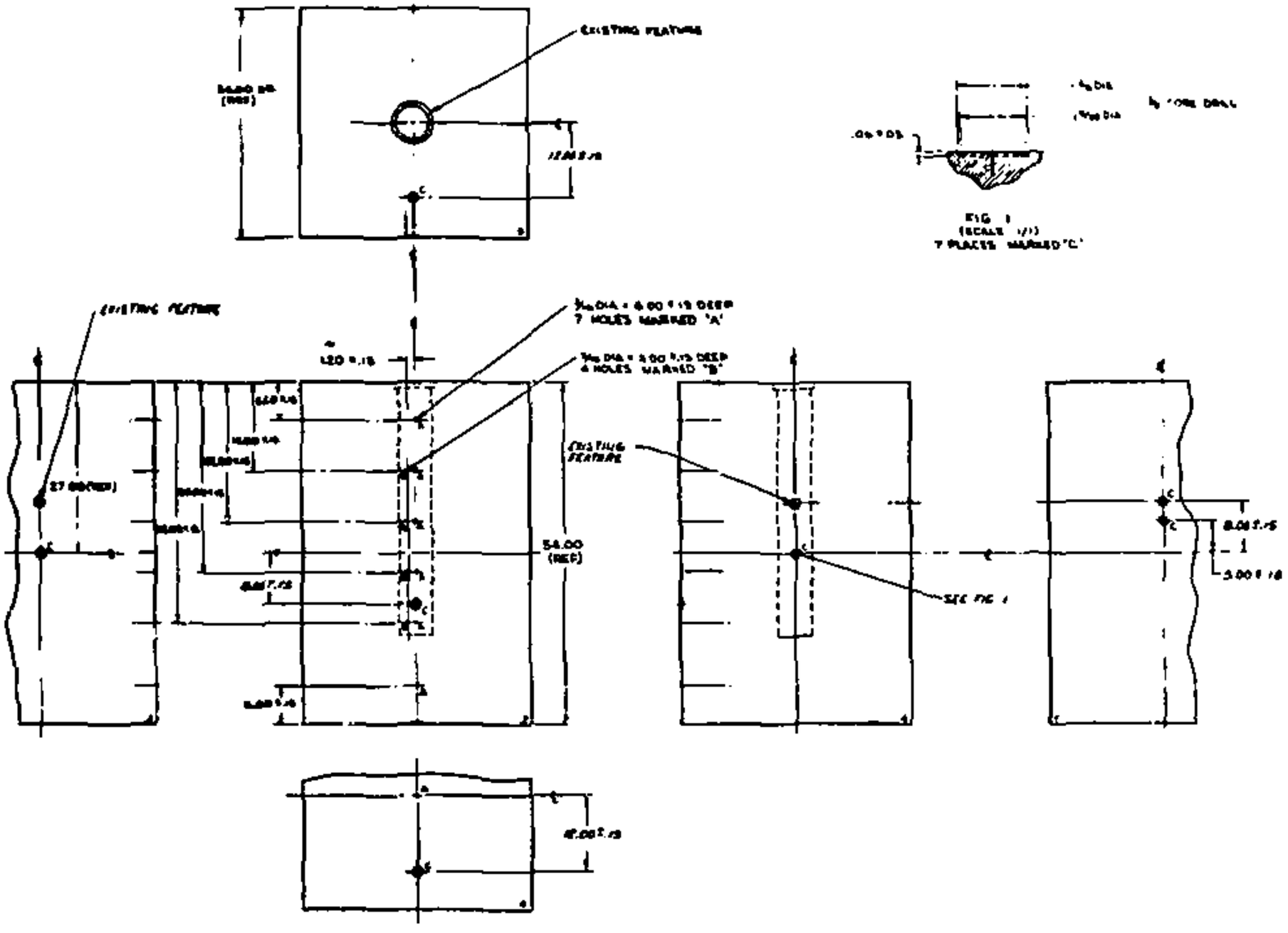

FIG 1
(SCALE 1/1)
7 PLACES MARKED "C"

Figure 24b. Block machining drawing

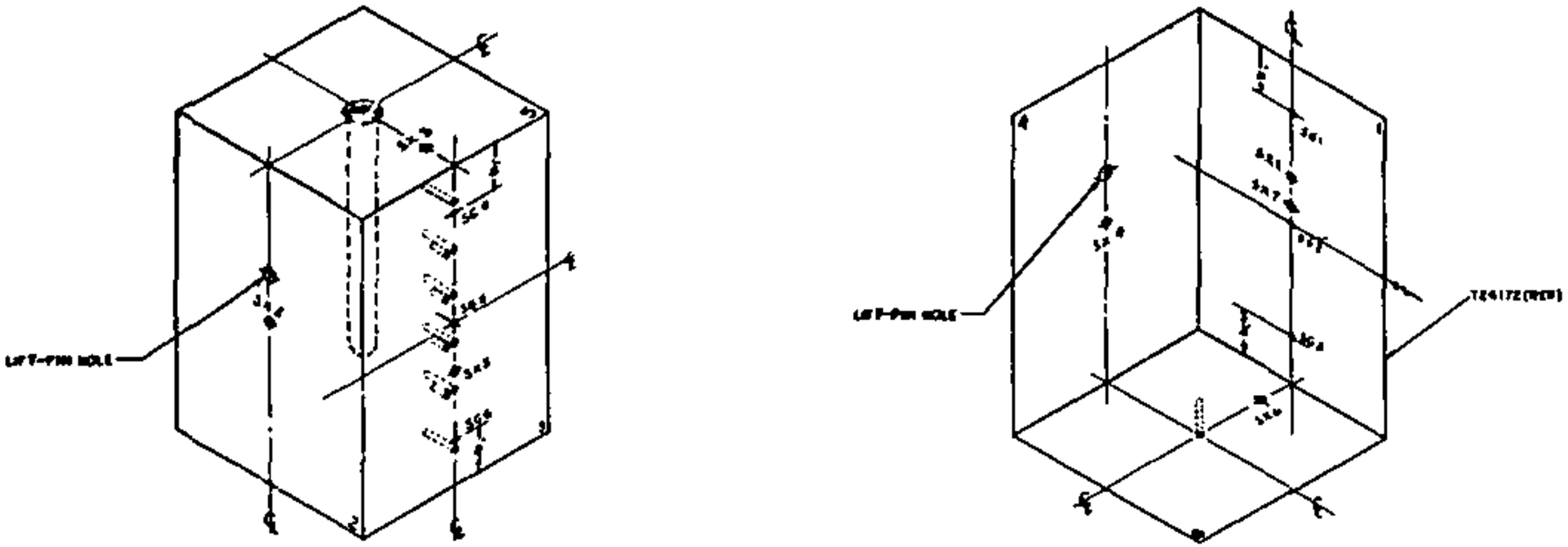

Figure 25. Strain gage and sonic transducer locations

Figure 26. $LiNO_3$ sonic transducer and spring loaded mount

The heating element, power supply, and alumina heater tube placed power versus temperature limitations on the test. Since it was only possible to monitor the temperatures of the outer surface of the platinum sheath, temperatures and surface gradients of the alumina tube and the heater had to be found analytically. This was accomplished using the T2SLT computer program which predicts temperature drops across multiple radiating and conducting gaps and multiple solid layers for a given heat flux. Figure 28 shows the heater temperatures as a function of the thermocouple temperatures on the platinum surface (TC 2, 3, 4, and 5) for several power levels. This curve, the heater resistance as a function of temperature, and the power supply maximum voltage were used to generate the power supply limit shown in Figure 29. Figure 28 and maximum allowable power versus temperature for the silicon carbide heater were used to generate the heater limit line in Figure 29. The gap between the platinum and alumina varied from 0.0325 to 0.0350 inch. Since the platinum temperature is uniform around the circumference and the heat flow is constant, the variation in thermal resistance in the gap would cause a variation in the temperature of the alumina. These circumferential surface gradients, the vertical surface gradient, and the radial gradient cause thermal stress in the alumina tube. The alumina surface gradient limit line in Figure 29 was based on these stresses with a safety factor of 2 and results of the T2SLT predictions. With a ramp heat pulse, the only predicted limiting factor was the power supply.

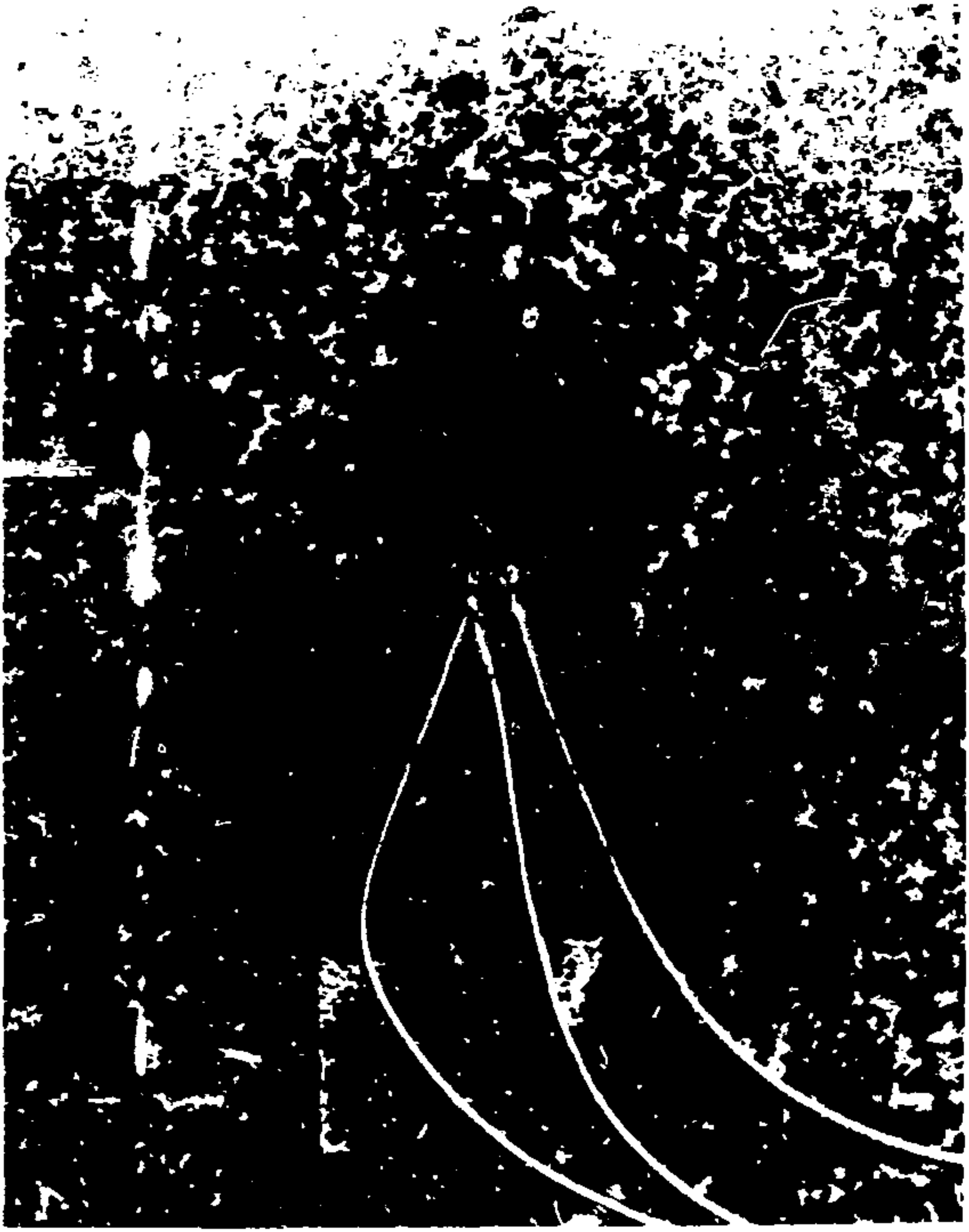

Figure 27. Mounted strain gage without protective coating

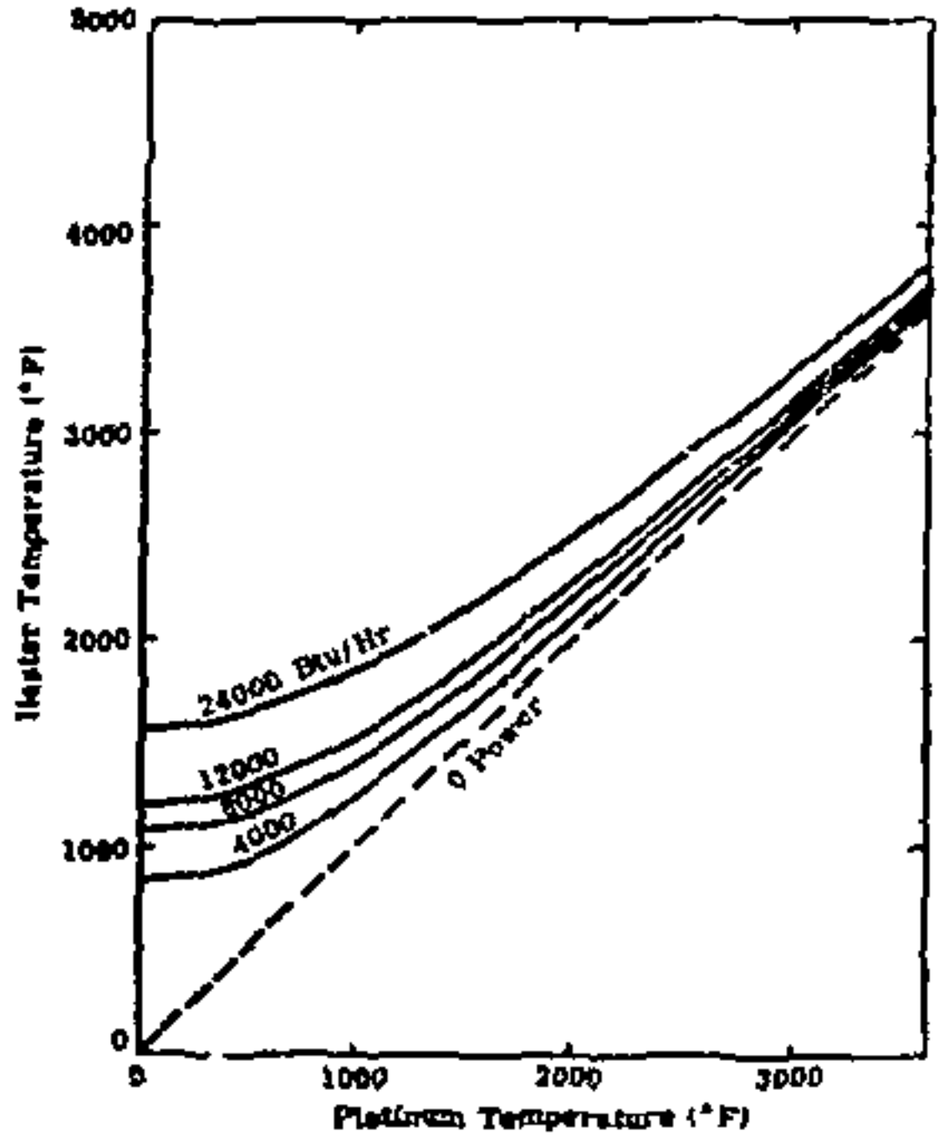

Figure 28. Heater temperature versus platinum temperature

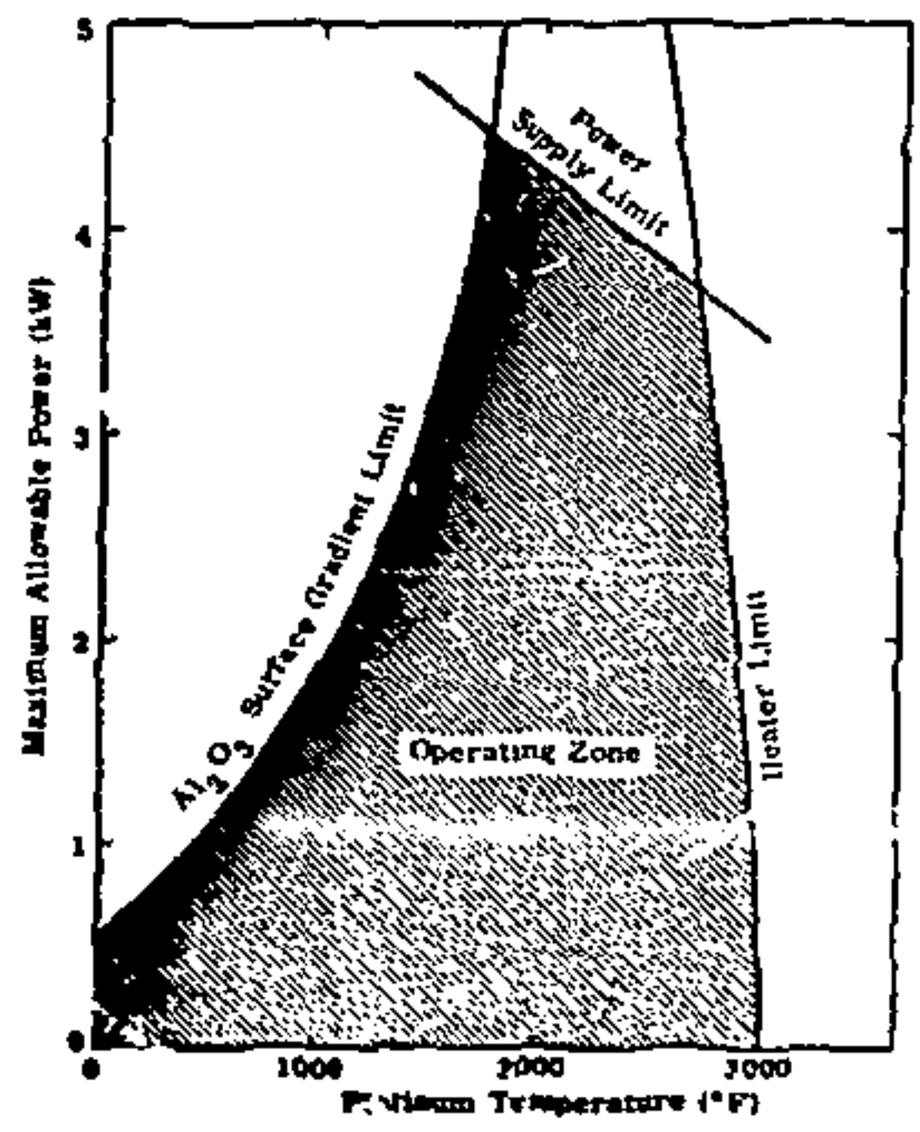

Figure 29. Power/temperature limitations on DRD-1

At the beginning of the test, the heating rate increase was not fixed but could be changed to obtain the desired temperature gradients. Twenty days into the test, it was decided to continue the increase at 100 W/day until the maximum level of about 4.1 kW was reached and to hold at that level for 4 days before starting to decrease power. The CYNDA program was then run using the design heat pulse shown in Figure 30 and the material properties given in Appendix B. Low viscosity and a high conductivity were selected for the dolerite. These predictions would be used in conjunction with thermocouple data to check the accuracy of the analytical methods. The program was also run assuming pure conduction in the melt. Figures 29 and 31 show that if there is no convection, the maximum temperature of the heater would be exceeded. Figures 32 and 33 show the predicted radial and vertical temperature profiles with convection. At the end of the heating phase of the test, the sand temperatures 3 feet above or below the rock was expected to increase less than 150°F. Figure 34 shows the predicted, vertically averaged temperature of the melt next to the heater tube. The slope of the curve decreases when convection begins. Temperature predictions late in the cool down would be high because the thermal model would become saturated. Figure 35 gives the predicted temperatures at the surface of the rock.

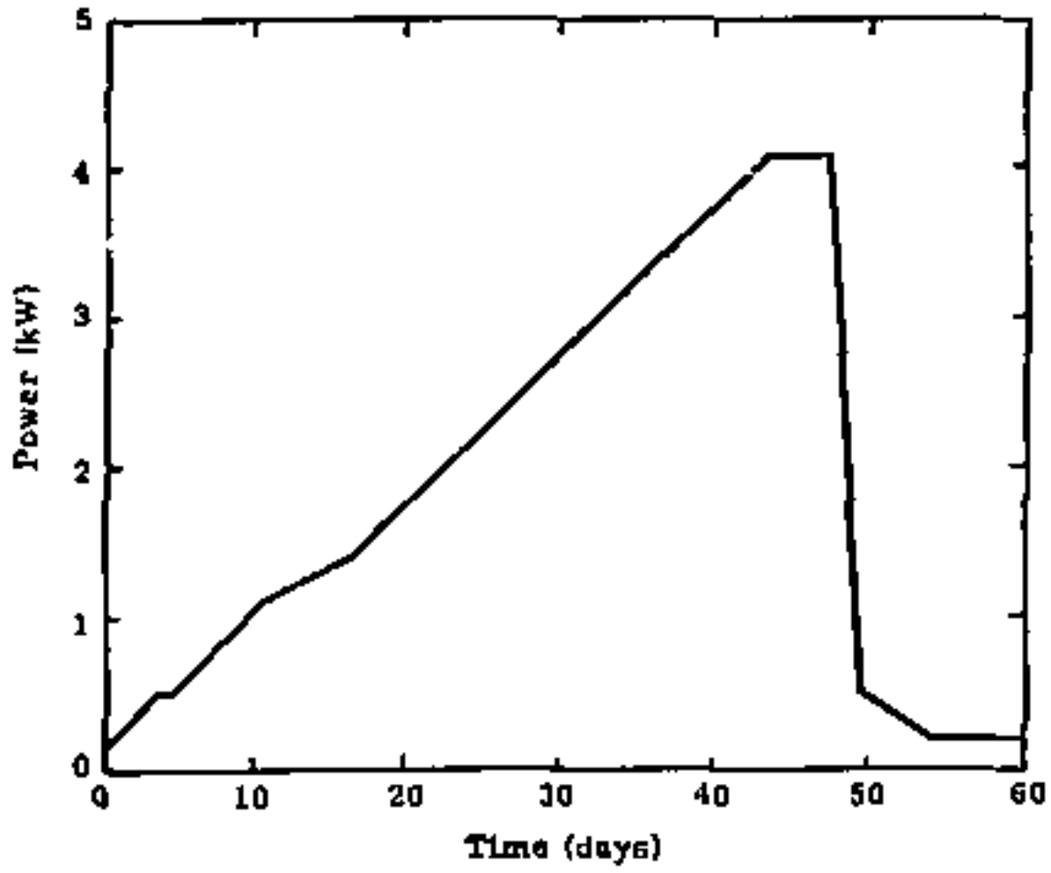

Figure 30. DRD-1 design power input

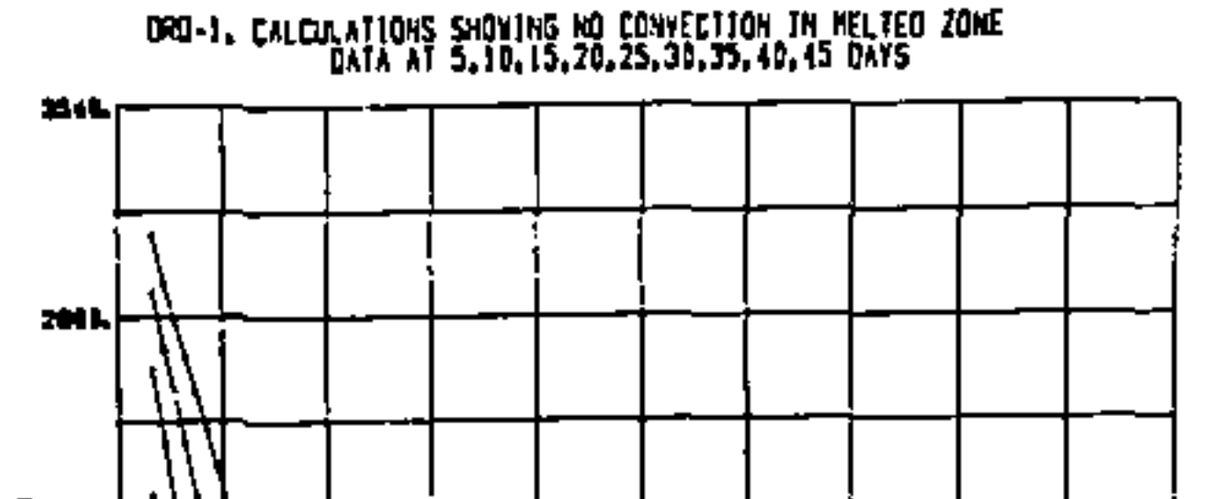

Figure 31. Predicted radial temperature distributions *in rock and sand assuming no convection*

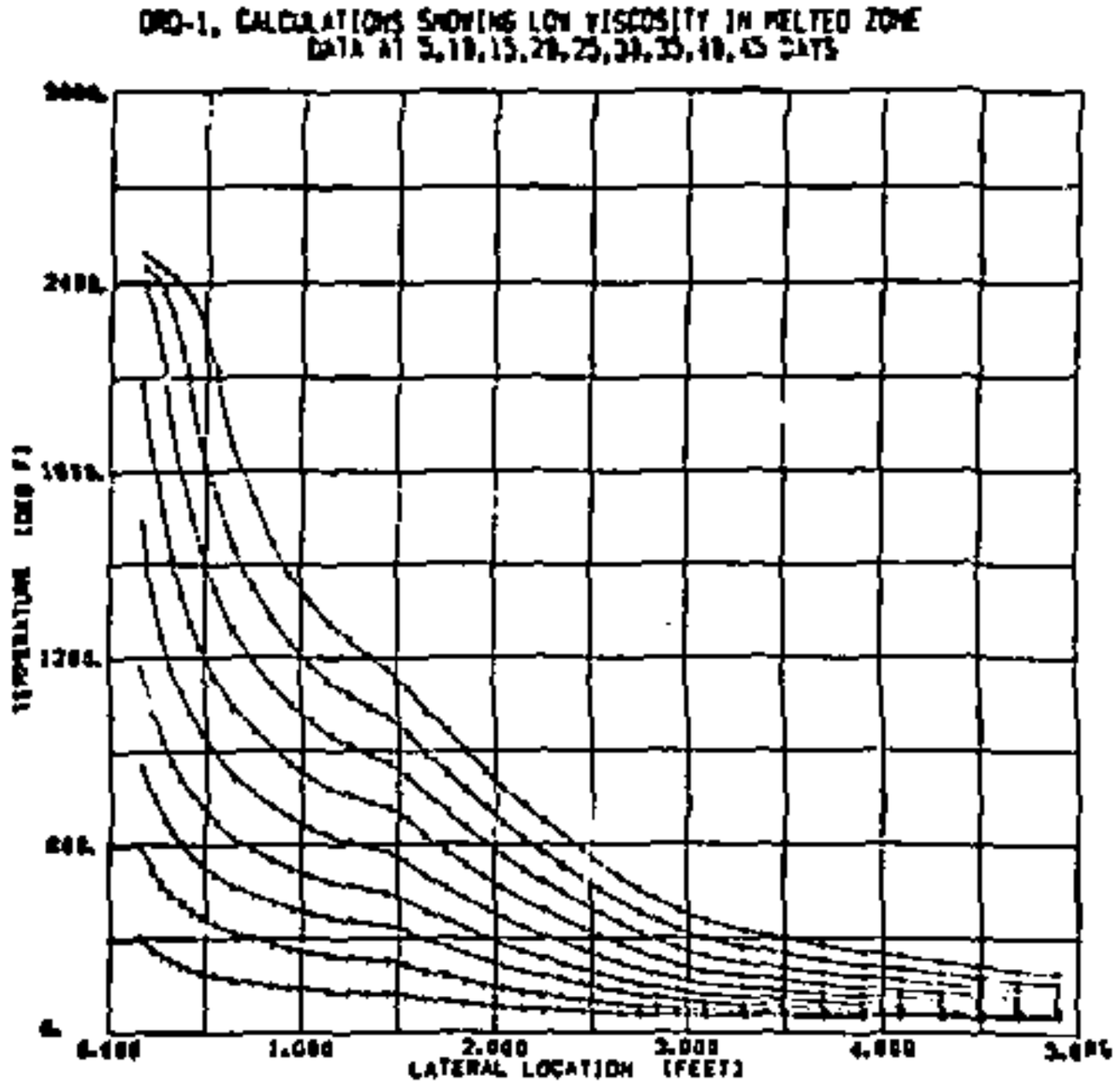

Figure 32. Predicted radial temperature gradients in the rock and sand with averaged convection

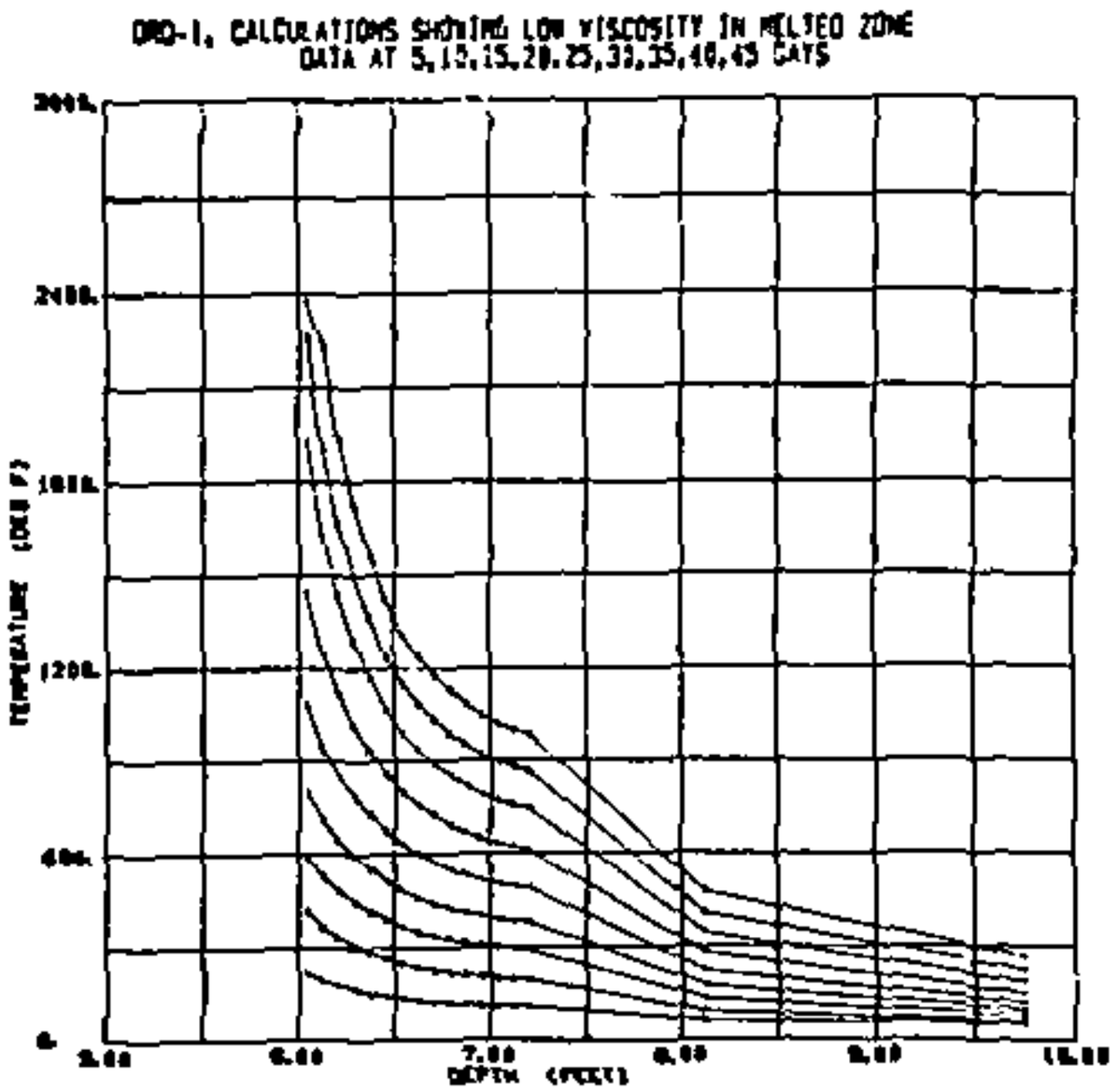

Figure 33. Predicted vertical temperature gradients measured downward from the bottom of the heater

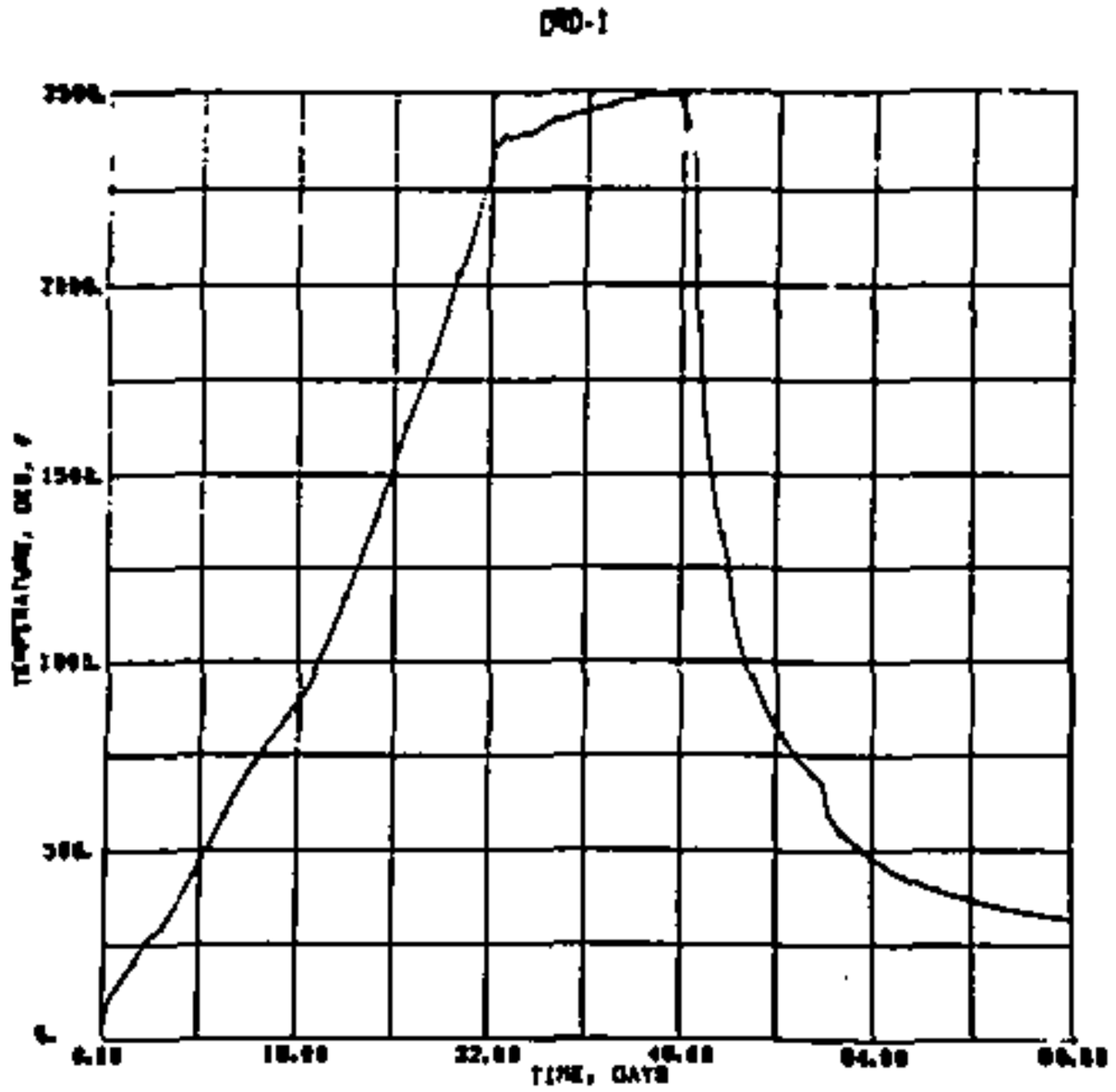

Figure 34. Predicted average temperature-time plot of the melt next to the heater tube during heat up and cool down

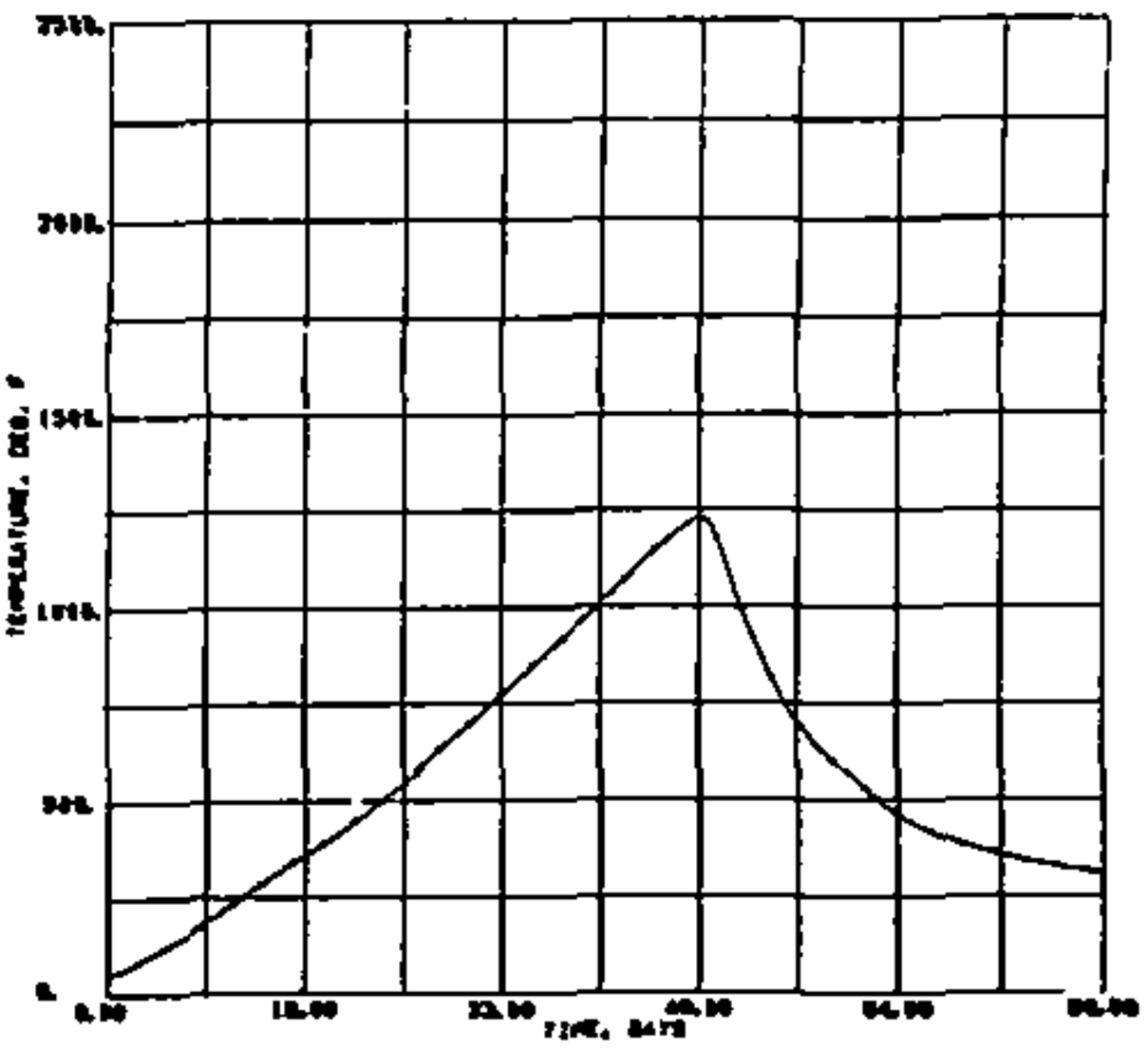

Figure 35. Predicted temperature-time plot of the outer surface of the rock averaged over the length of the heater

Operation and Preliminary Results

After the instrumentation was installed, the simulant was loaded and the heater tube and base plates were assembled. The effective packing density of the semi-annular simulant rings in the annulus around the heater tube was 70 percent, which made it necessary to stack the rings to within 6.75 inches of the top of the rock, as shown in Figure 36. Also shown in this figure is the heater tube, platinum sheath, and the thermocouples which were attached to the tube. The final part of the assembly prior to burial consisted of installing the insulation and attaching the base plates to the heater tube (Figure 37). The port for the probe thermocouple and sampling pipet is shown in front of the thermocouple bundle. The entire assembly was then lowered into a 6.5-feet deep hole (Figure 38). The wooden framework was used to support the lead wires and was removed when the rock was in place. Figure 39 shows the rock partially covered with sand, just prior to the installation of the Mullite access tube. The heater, air line, and control rods have been added. The complete above ground assembly is shown in Figure 40. The hole is filled and mounded and the shelter is over the access tube (Figure 15). Thermocouple junctions are above the flooring and on the control rods.

Figure 36. Simulant and heater tube

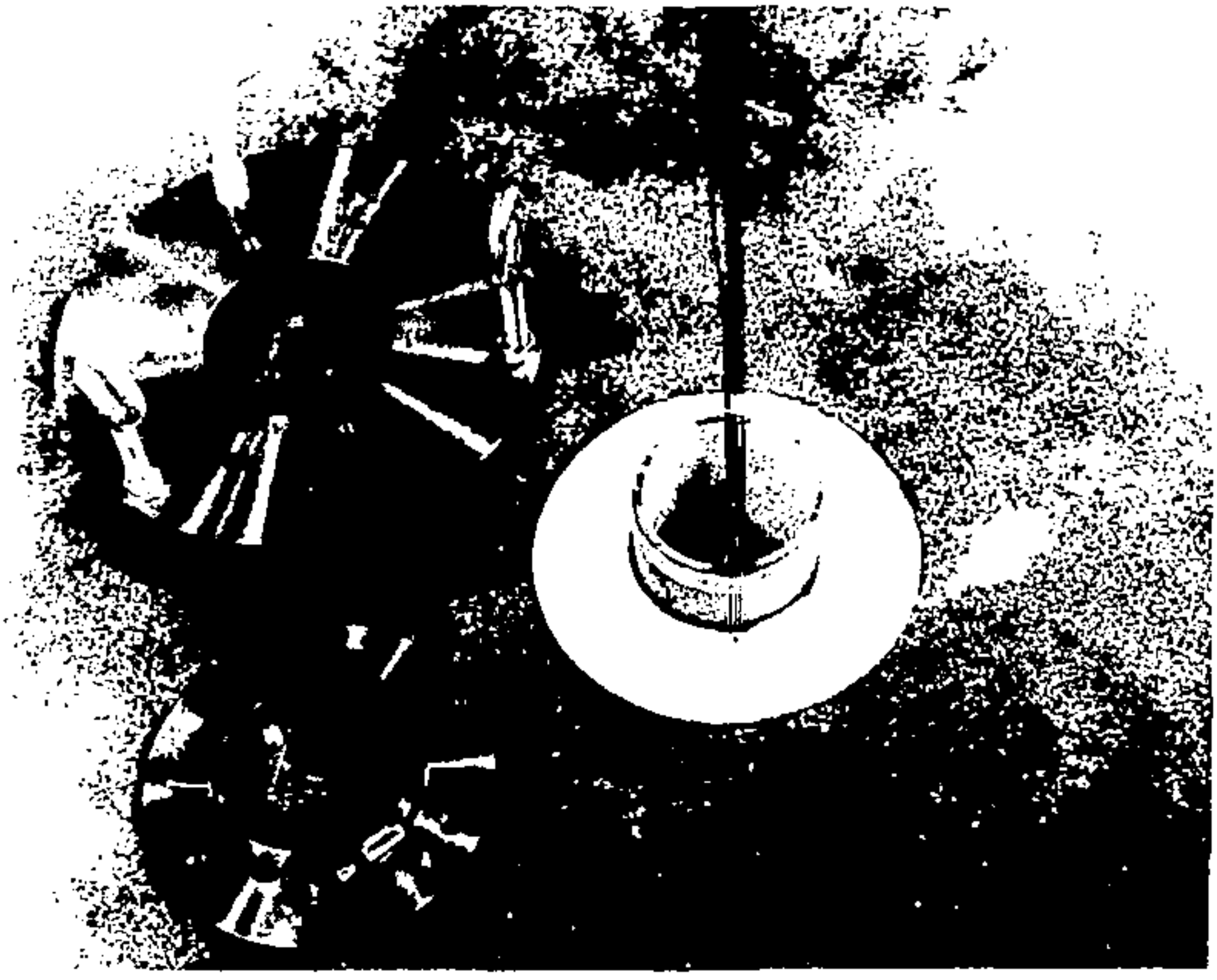

Figure 37. Base plate and insulation

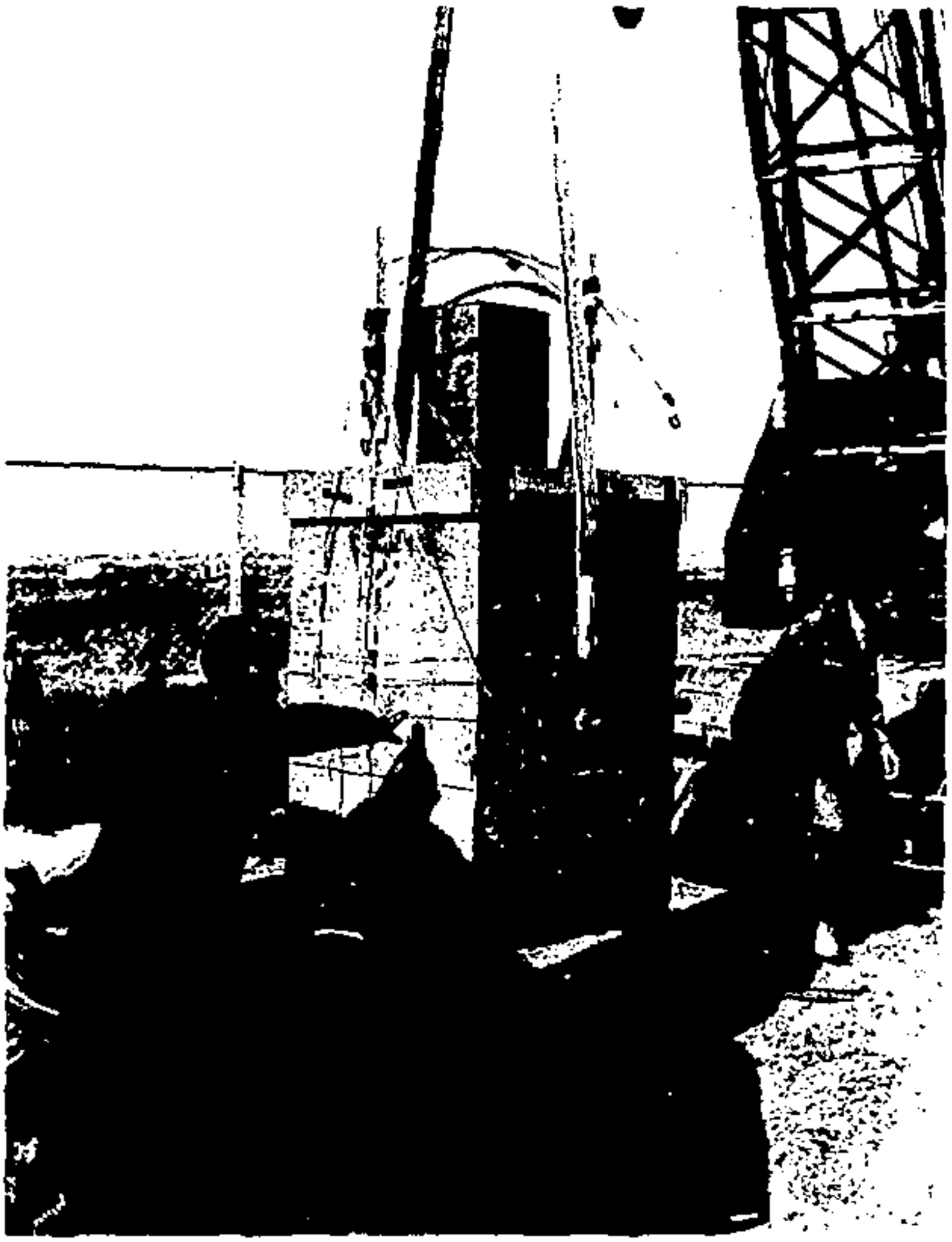

Figure 36. Lowering ORD-1 into the ground

Figure 39. DRD-1 with heater and control rods installed and partially covered with sand

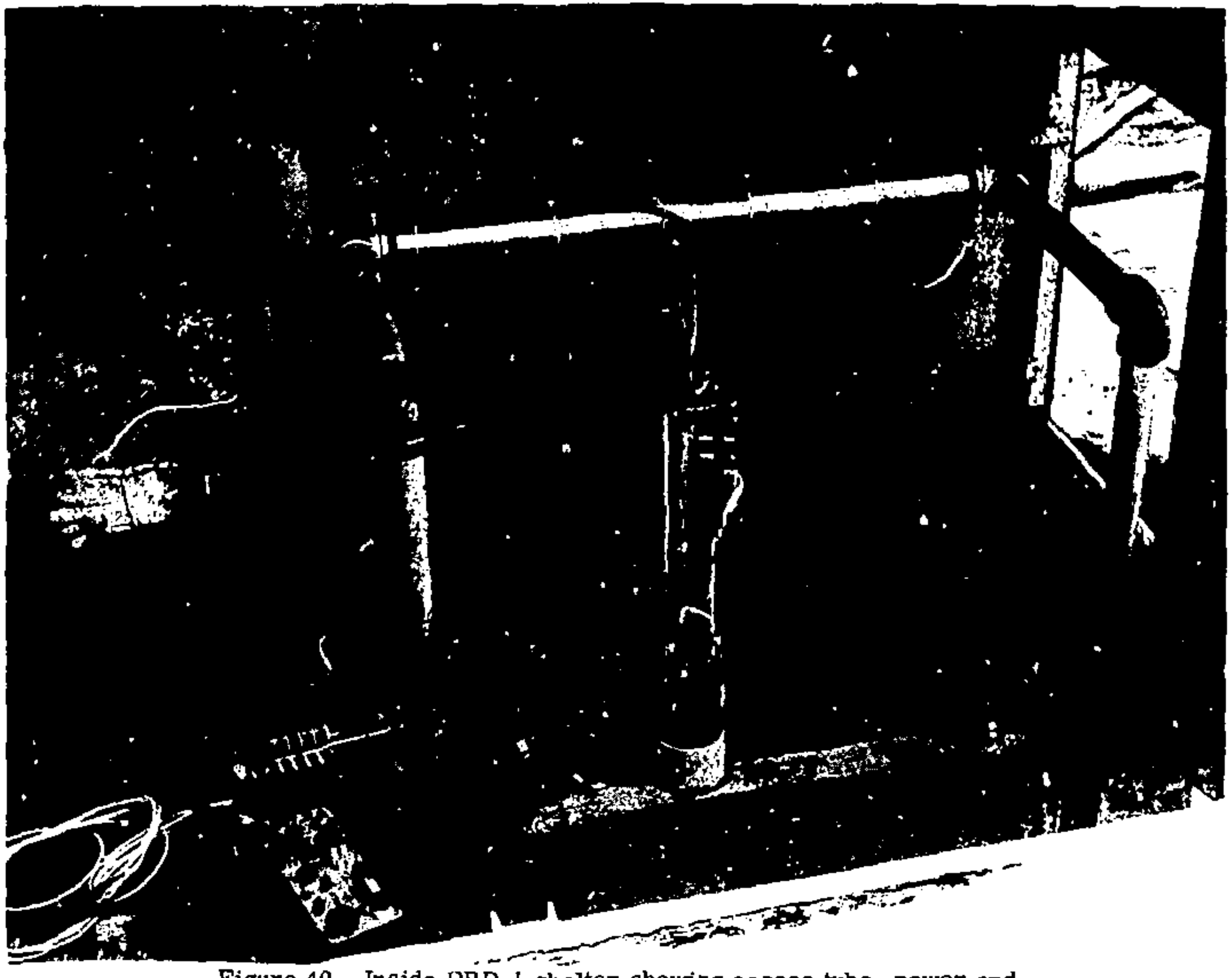

Figure 40. Inside DRD-1 shelter showing access tube, power and cooling lines, instrumentation and control mechanism

The actual power input measured at the power supply is given in Figure 41. The power delivered to the 24-inch heating section of the silicon carbide heater was 93 percent of the values shown. During the last 5 days of the test, the power supply was operating at its maximum output. Variation in line voltage accounted for the varying power during the five day hold at maximum power. At no time during the test were the heater temperature limits or the heater tube surface gradients exceeded (Figure 29). All the test hardware survived the test and showed no signs of degradation. All strain gages remained operable to well above their rated temperatures. One sonic transducer failed during the test. Thermocouple No. 23 on the outer surface of the rock opened on the 28th day of the test. All other thermocouples operated throughout the test. The power supply limit was the only reason for terminating the test at 48 days.

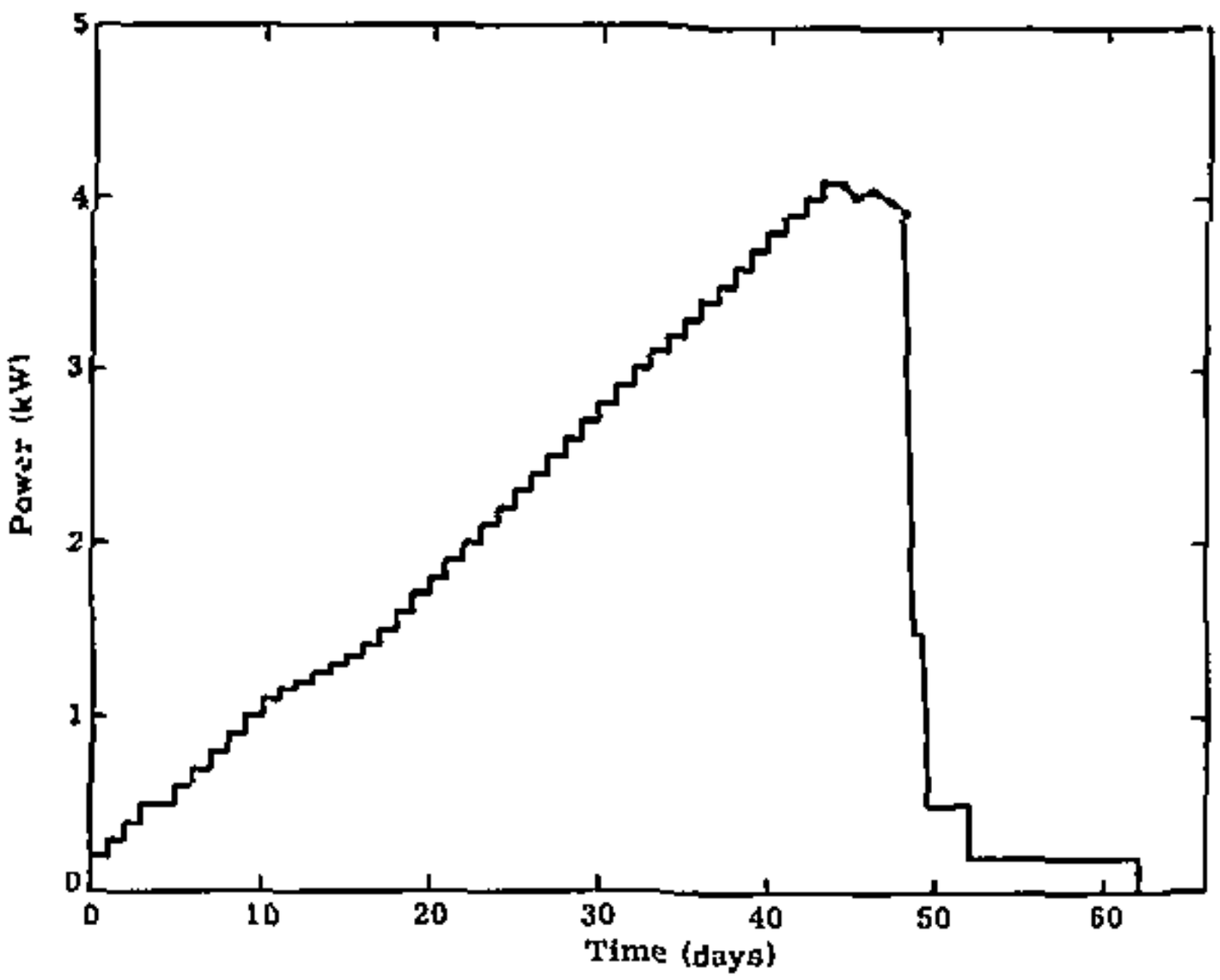

Figure 41. DRD-1 power input

Most of the test data concerning melting, expansion of the melt, mass transport, convection heat transfer, and rock cracking taken during the test were obtained by the probe thermocouple (No. 2) and the four thermocouples attached to the outer surface of the heater tube sheath (Nos. 3, 4, 5, and 6). Daily temperature readings were taken from the strip charts for all the thermocouples. The data for Nos. 3 through 6 are shown in Figure 42. At the beginning of the test when heat was transferred through the rock and simulant by conduction and across gaps by radiation and coeduction, the temperatures of the top and bottom thermocouples (3 and 6) were lower than those of the middle thermocouples because heat was lost out the ends as well as radially. Number 3 had the lowest temperature because heat was also lost out the top by air convection in the expansion volume. Gap sizes around the solid simulant varied; hence, the thermal resistance also varied which accounts for the

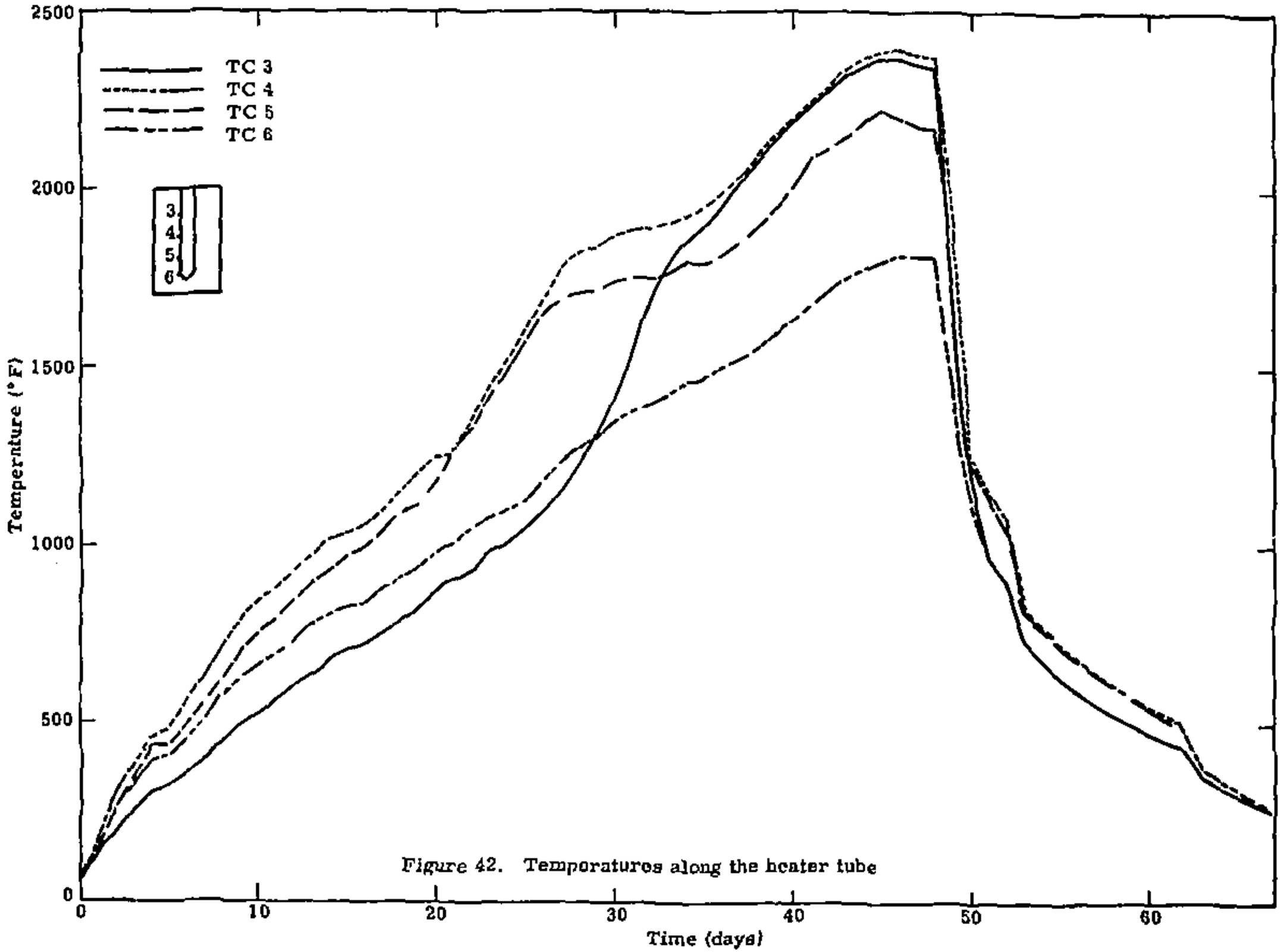

Figure 42. Temperatures along the heater tube

difference in the temperatures of Nos. 4 and 5. On day 21, the simulant began to soften and fill the gaps and the temperatures of Nos. 4 and 5 became nearly equal. The level of the top of the simulant also began to drop at day 21. Convection began at day 26. This is indicated by a sharp rise in the temperature of No. 3 and a reduction in the slopes of Nos. 4 and 5 as heat was being transferred vertically by mass transport from the middle to the top. The slope of No. 6 began to decrease at about day 32 as the convection cell increased in size and reached the bottom of the annulus. By day 37, the top of the rock had heated up and the vertical temperature gradient in the unmelted rock corresponded to the gradient in the circulating melt. At this point, a convection equilibrium was reached where the slopes of the four curves remained nearly constant, and the temperature changes closely followed changes in the heating rate. There was a vertical temperature gradient from 6 to 4. The temperature of No. 3 was slightly lower than 4 because of the end losses. On day 49 during cool down, convection stopped and the two ends once again became cooler than the middle.

Before the simulant was completely melted, the probe thermocouple was used to locate the level of the top of the simulant. After the simulant melted and circulation began, the probe measured temperatures in the melt to locate the top of the convection cell. It was also used to locate any solid materials that entered the annulus. Figures 43 through 48 show the vertical temperature distributions in the melt for the days that significant events occurred. The probe hole was located approximately 0.15 inch out from the thermocouples that were attached to the heat tube. However, there was no way of knowing that the probe stayed at exactly that radius as it was inserted into the melt, so the temperature of thermocouple No. 3 is given as a reference. Figure 43 shows the probe temperatures the 33rd day of the test. The top of the liquid was located by the change in slope of the temperature curve and by the resistance of the viscous liquid. The liquid level had expanded 2 inches up into the expansion volume at that time. As the probe was inserted into the melt, the resistance decreased as the temperature increased. At a depth of 14.25 inches, approximately 0.5 inch below the top of the heater, the slope of the curve reversed, indicating the top of the convection cell. As the liquid moved upward along the heater, the temperature increased, giving the curve a positive slope. Above the convection cell, the temperature decreased as heat was conducted vertically in accordance with the Laplace equation. Early on the 38th day, the top part of the rock cracked and small amounts of sand ran into the expansion volume several times that day. The cracks were probably caused by the large temperature gradients that resulted when convection transferred more heat to the top of the rock. When the relatively cool sand hit the surface of the viscous liquid, there was a small region of mixing which caused a crust to form at the interface between the sand and rock/waste matrix. Early in the day, the crust was too hard to penetrate with the probe, but later in the day it softened enough to permit the probe to be forced through (Figure 44). The viscosity gradually decreased from the top of the crust until the liquid was fluid enough for circulation at a depth of 12.4 inches. The increase in the convection cell size from day 33 was caused by the large temperature increase (and viscosity decrease) at the top of the melt. On day 40 (Figure 45), more sand entered the expansion, possibly caused by the crack opening up more. If vertical cracks had opened up, they would have increased the volume and width of the annulus. This hypothesis is backed up by a lowering of the crust and liquid level, indicating an

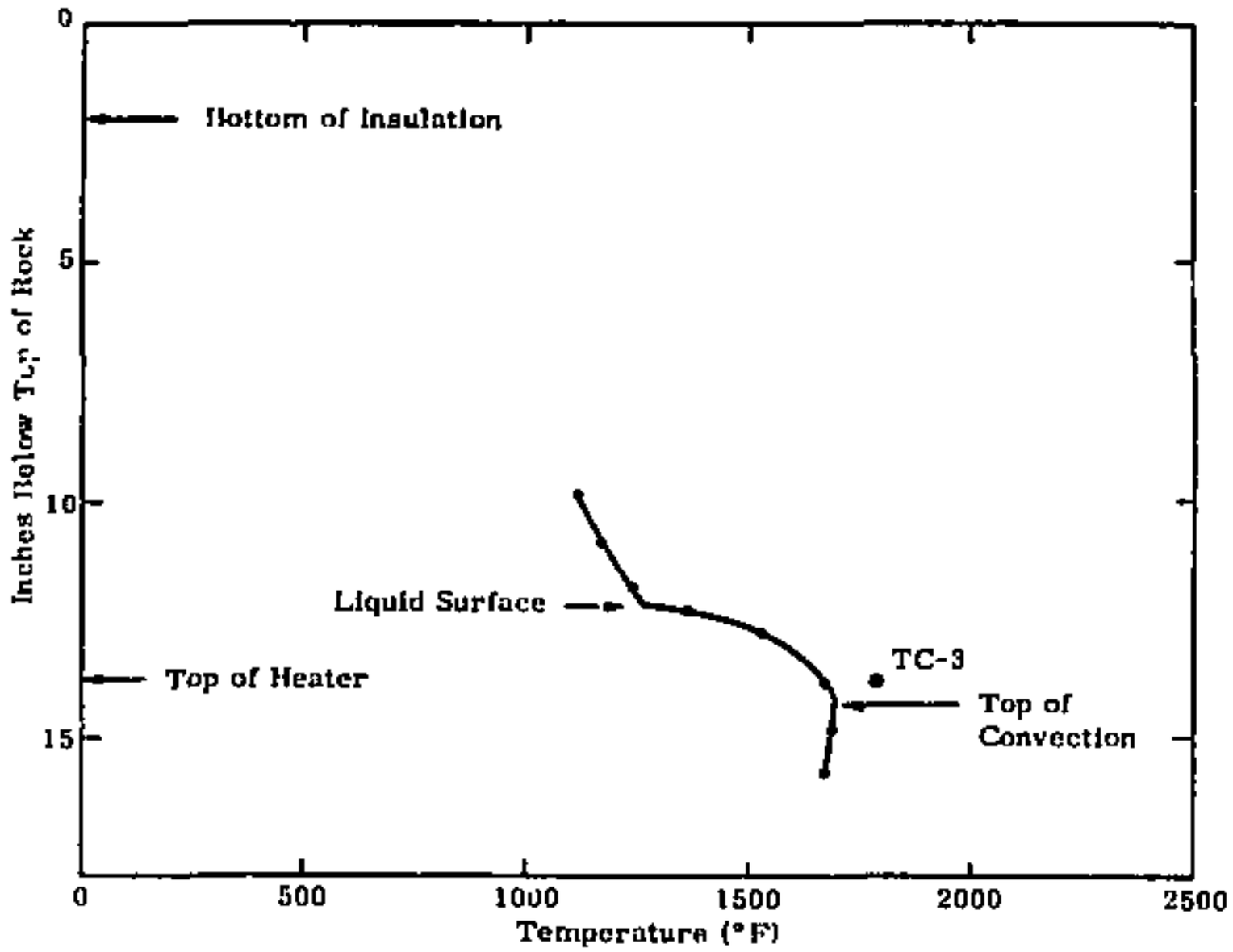

Figure 43. Probe temperatures, day 33

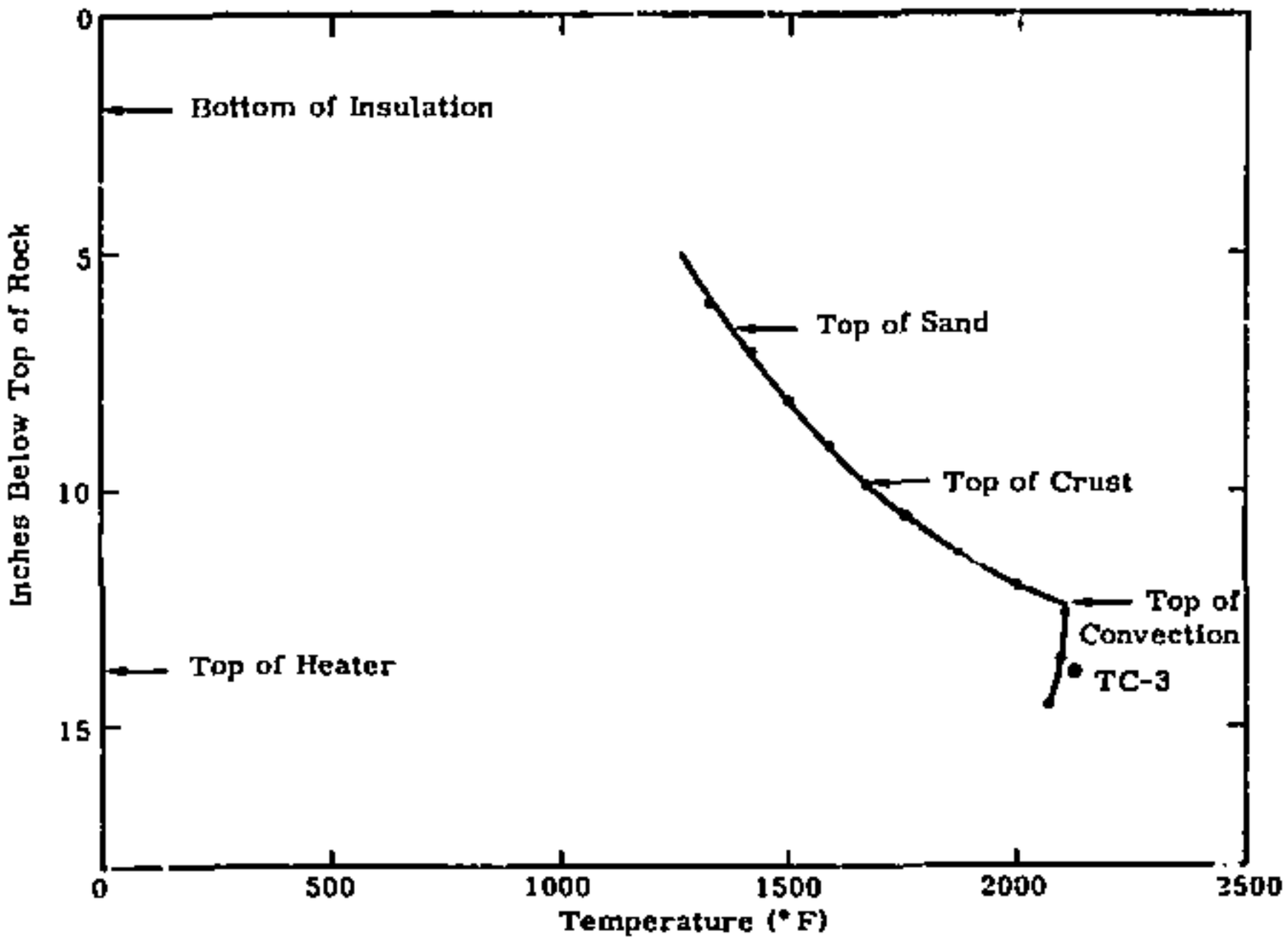

Figure 44. Probe temperatures, day 38

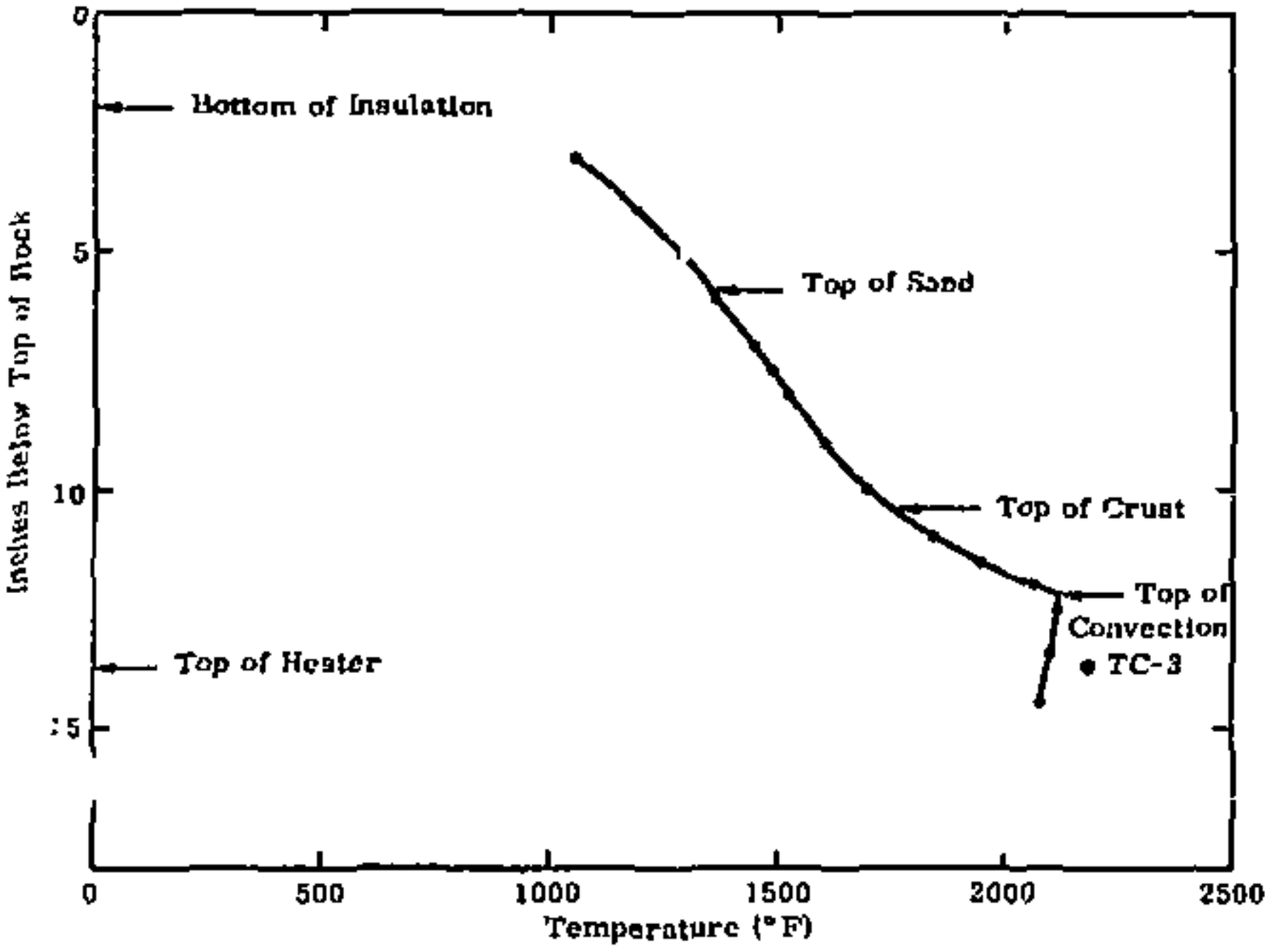

Figure 45. Probe temperatures, day 40

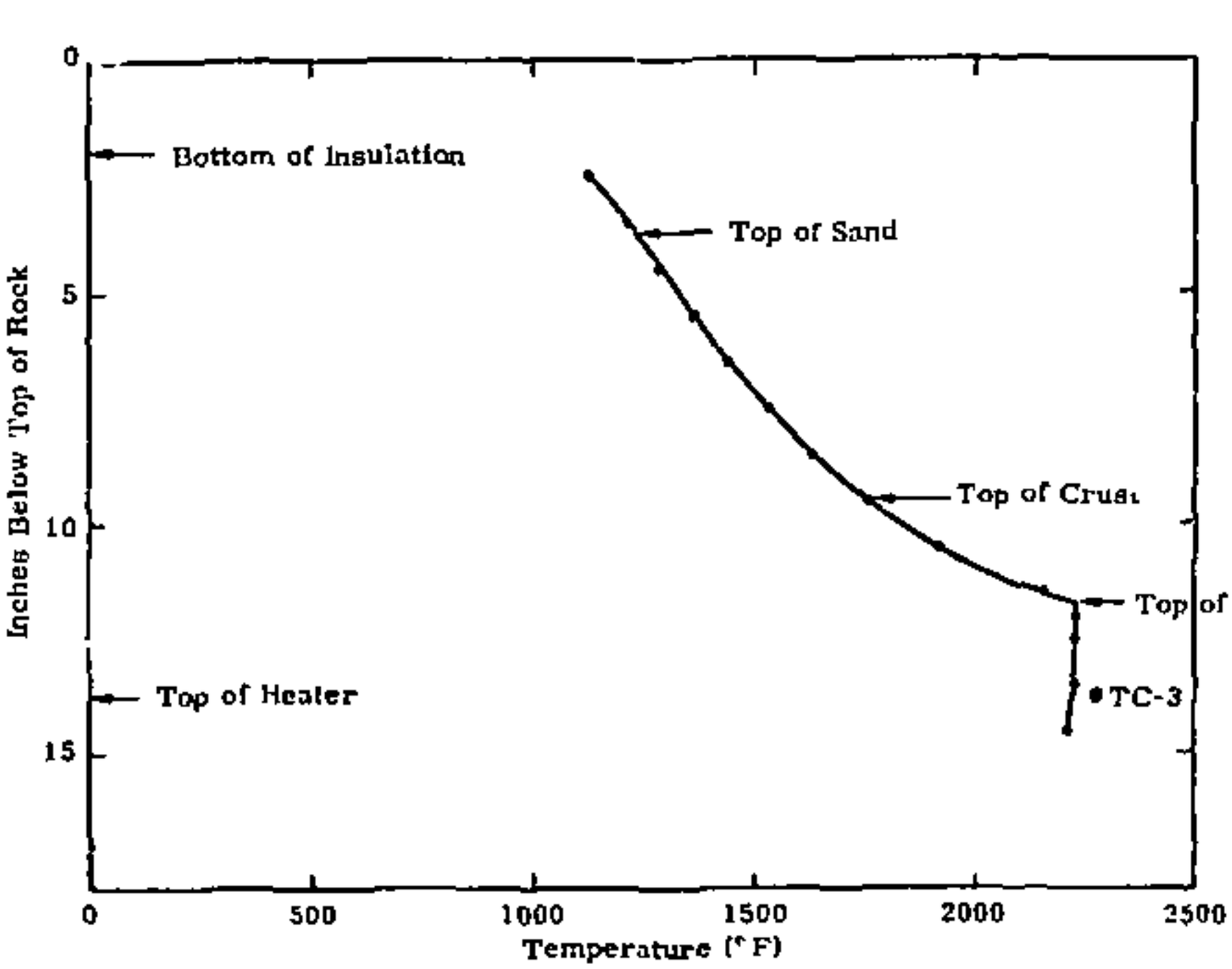

Figure 46. Probe temperatures, day 41

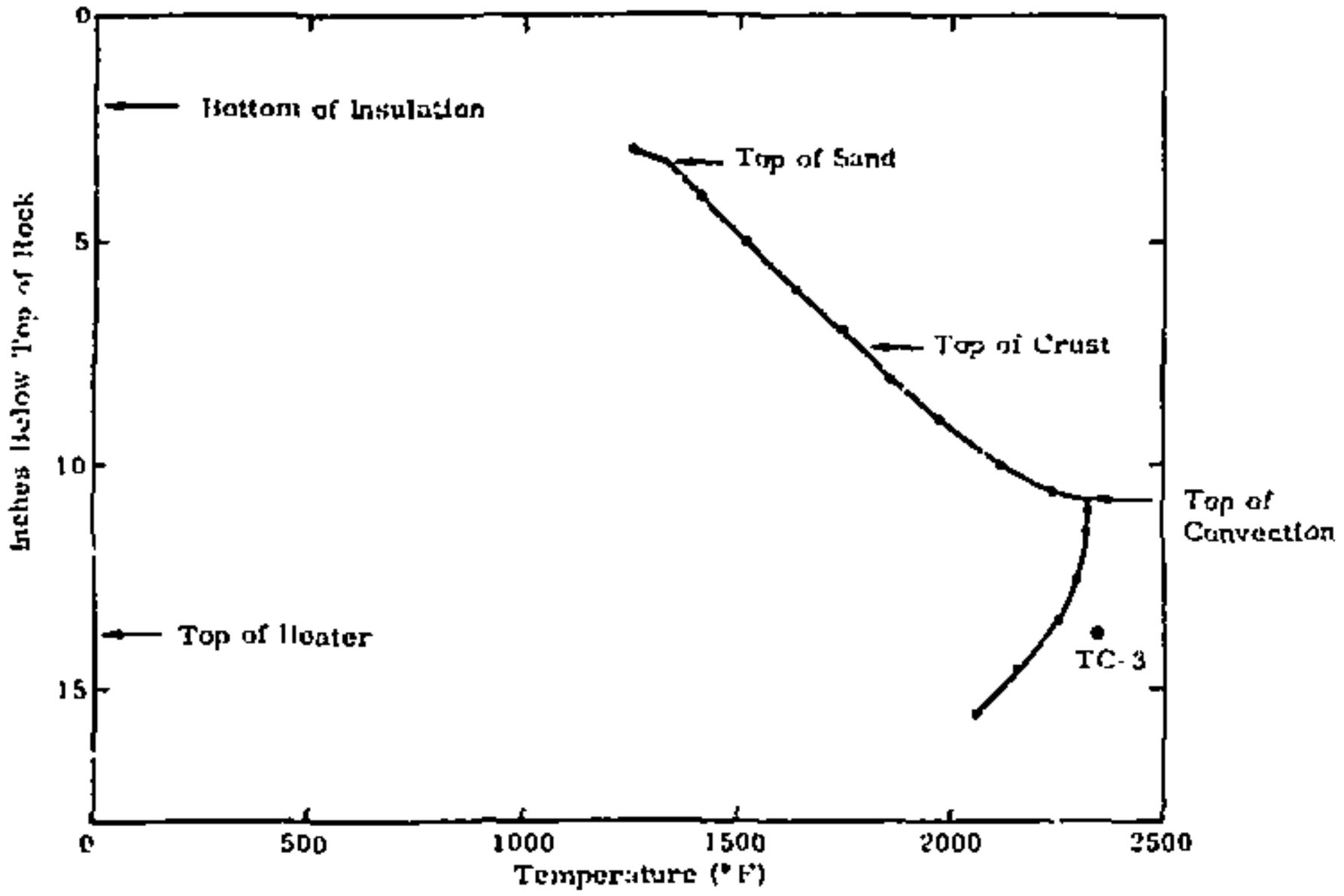

Figure 47. Probe temperatures, day 45

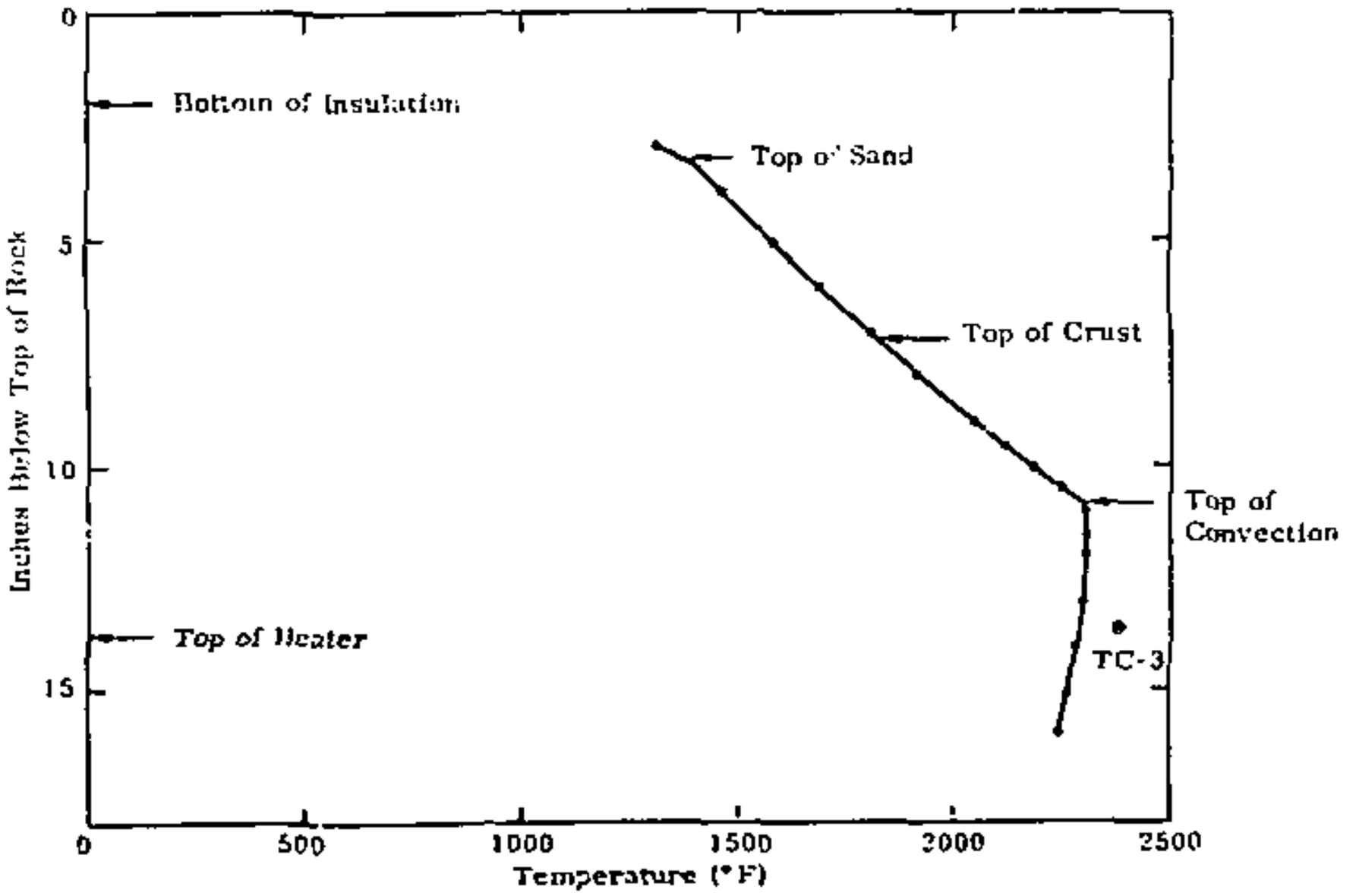

Figure 48. Probe temperatures, day 47

increase in volume. There was practically no increase in the height of the convection cell even though the temperatures increased. This indicates that the annulus width increased. Very little of the melt was expected to enter the cracks because they would be sealed when the viscous liquid resolidified as it reached cooler rock. No more sand entered the annulus after day 40, and on day 41 (Figure 46) the liquid level ferrous began to rise again due to expansion of the melt. The level of the sand also rose as it was pushed up by the crust. The highest temperature at the top of the melt was during day 45 (Figure 47). However, it still required considerable force to push the probe through the crust. The last probe readings were taken day 47 when the heating rates had started to decrease. The result was a decrease in the vertical temperature gradient in the convection cell (Figure 48). Figure 49 summarizes the boundaries that were located with the probe. The decrease in the height of the convection cell near the end of the test was caused by a decrease in heating rates and an increase in the annulus width. The liquid or crust level increased as rock melted and the matrix increased in temperature.

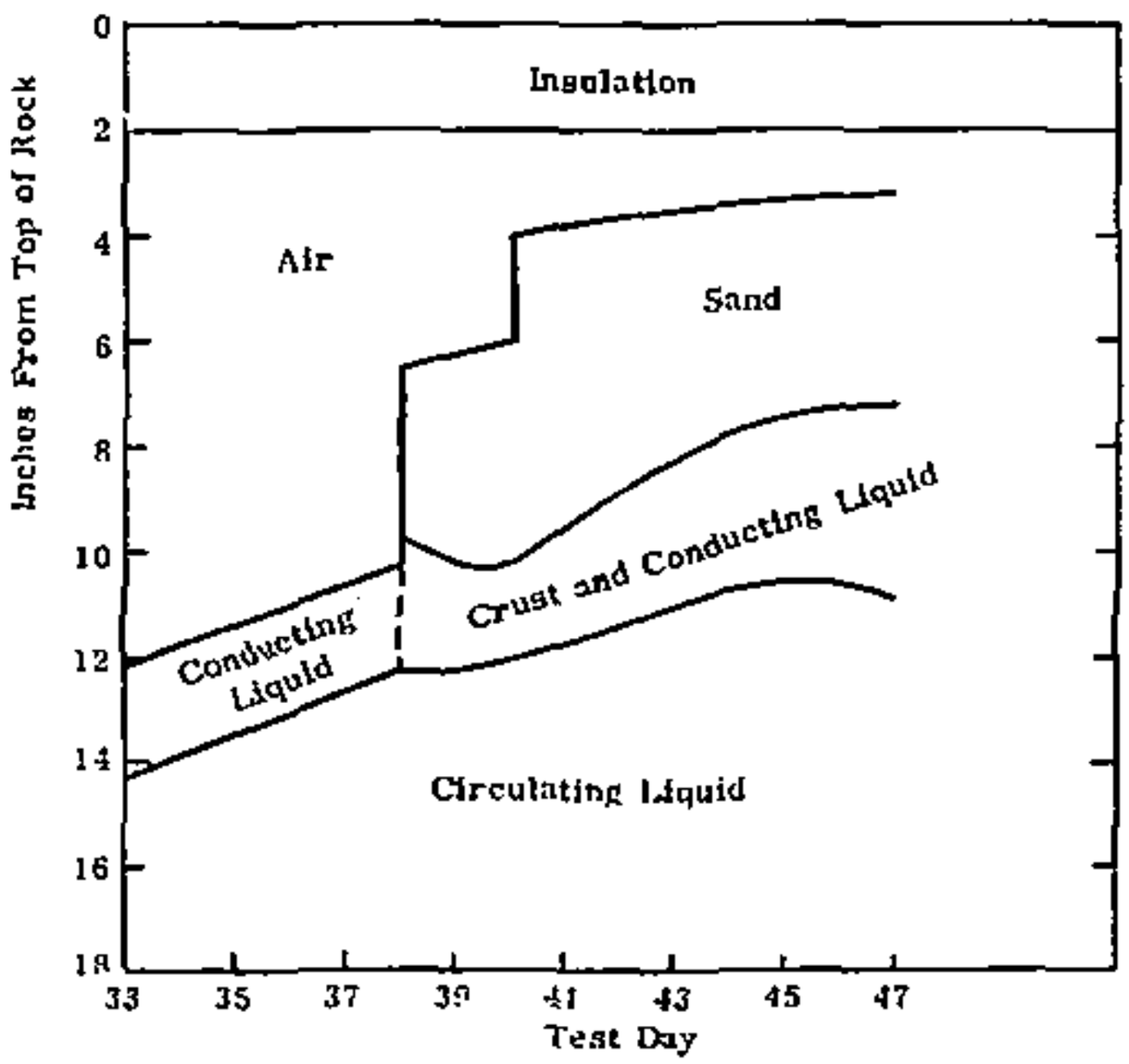

Figure 49. Composition of top section of annulus

Temperatures in the unmelted rock were used to check the accuracy of the CINDA model and will be used in conjunction with posttest chemical, crystallography, and material property tests to determine the effects of temperature in the DRD environment. Figure 50 shows the temperatures at several radii. Note that the changes in the temperature of the melt (thermocouple 4, Figure 42) caused by the initiation of convection are nearly damped out at the surface of the rock (thermocouple 22, Figure 50). Sand temperatures only 1 foot away from the rock never exceeded 525°F, which illustrates the small volume that was affected by the test. The radial temperature plots which were used to check analytical predictions are shown in Figure 51. Interpolation between thermocouples 4 and 9 was aided by the CINDA program. Convection during days 40 and 46 reduced the slope in the melt annulus. Figures 52 and 53 show some of the correlations of test data and predicted temperatures on day 25 before convection started. Correlation was excellent in the radial direction, but predictions were slightly high in the vertical direction. Possible errors in the test data and the predictions, some of which could have been compensating, are (1) heat losses up to expansion volume and heater tube were not included in the model, (2) material properties may not have been correct, (3) the rock model was cylindrical but the rock was a parallel-piped, and (4) inaccuracies in instrumentation. Predictions were not as accurate after convection started, as shown in Figure 54, because vertical mass transport was not included in the model. The maximum error at any location in the rock or melt in predicted temperature rises using the average effective conductivity instead of actual convection was only 19.6 percent.

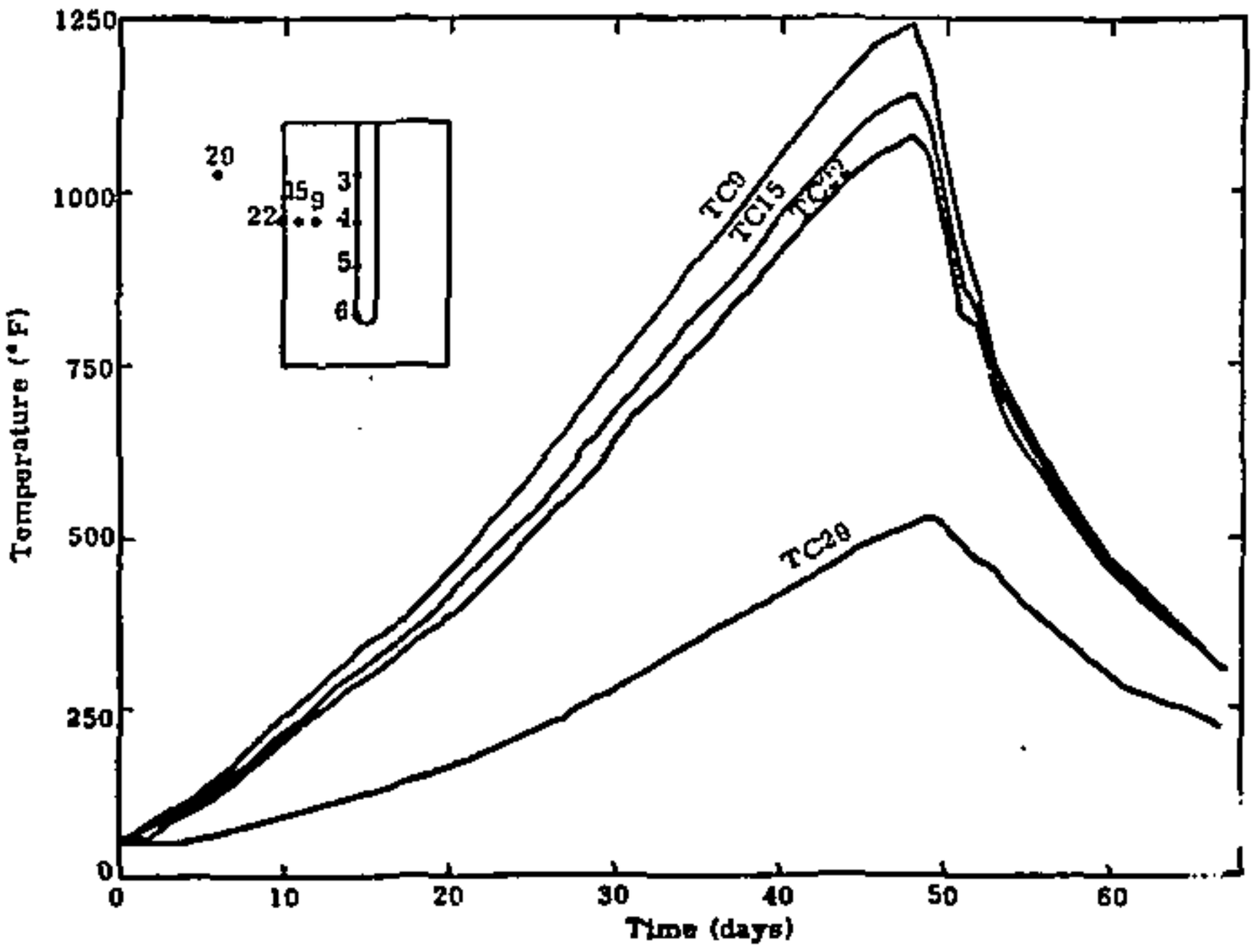

Figure 50. Temperatures in the solid rock and sand

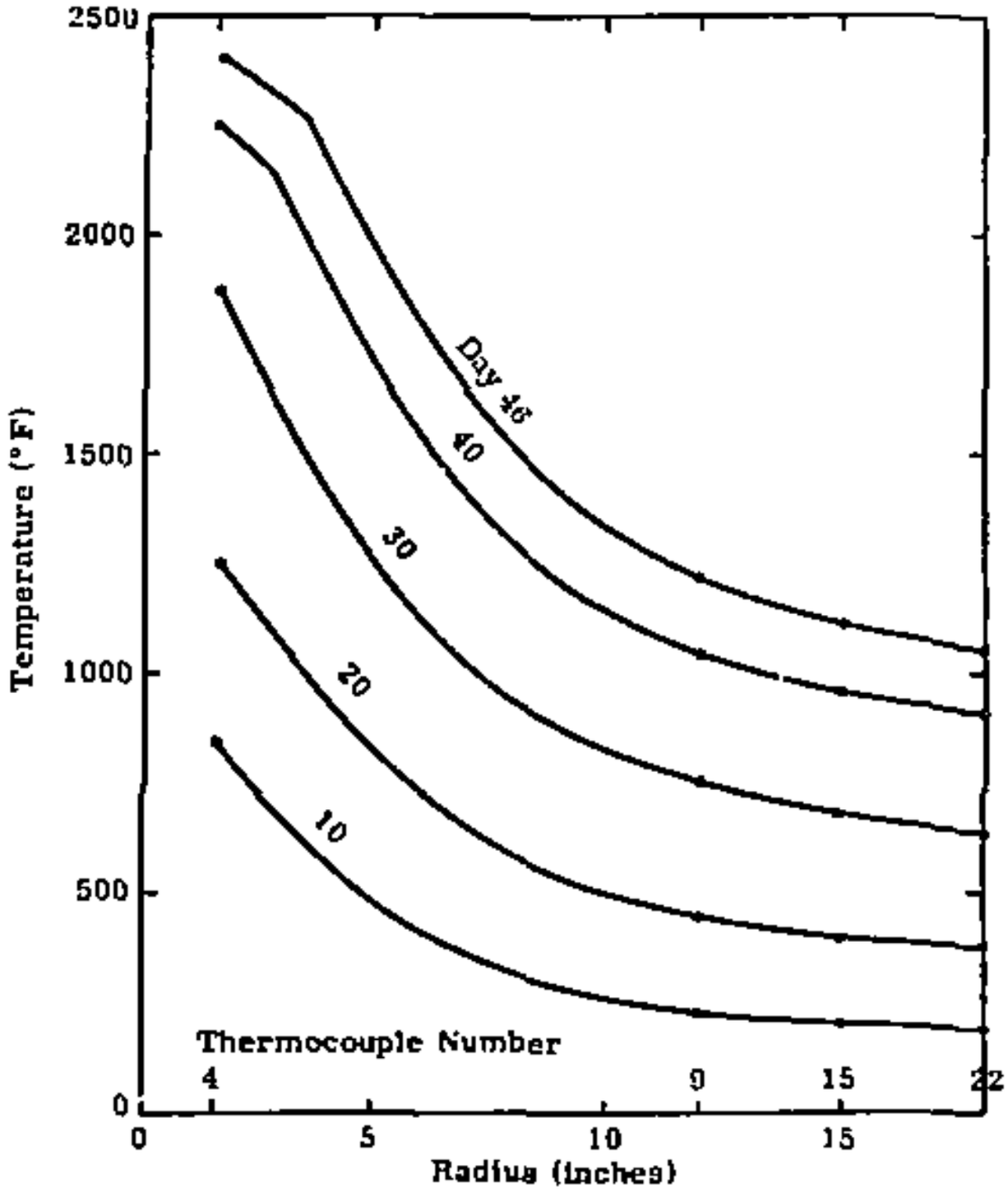

Figure 51. Measured radial temperature distributions

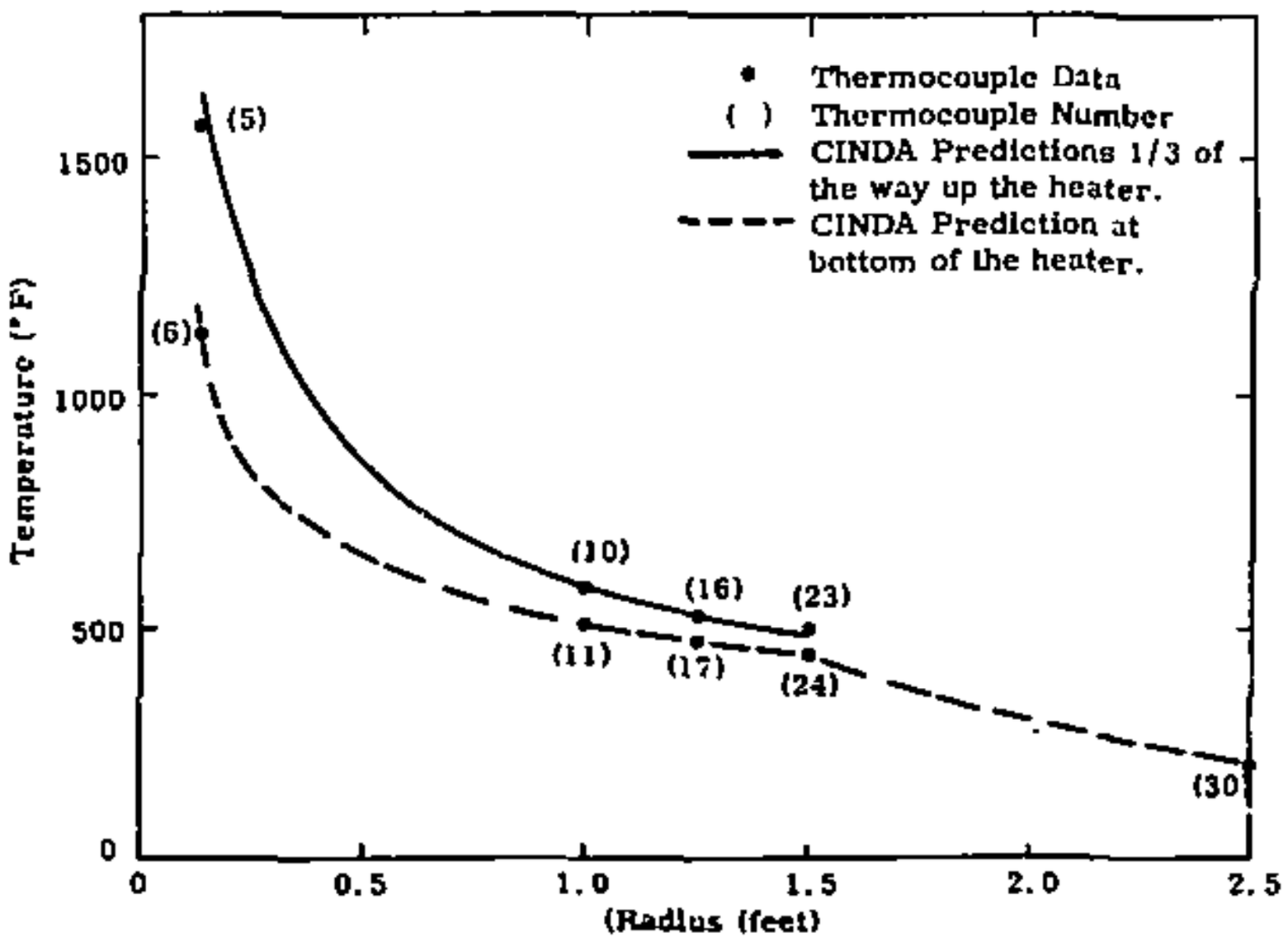

Figure 52. DRD-1 predicted and measured temperatures, 25 days into the test

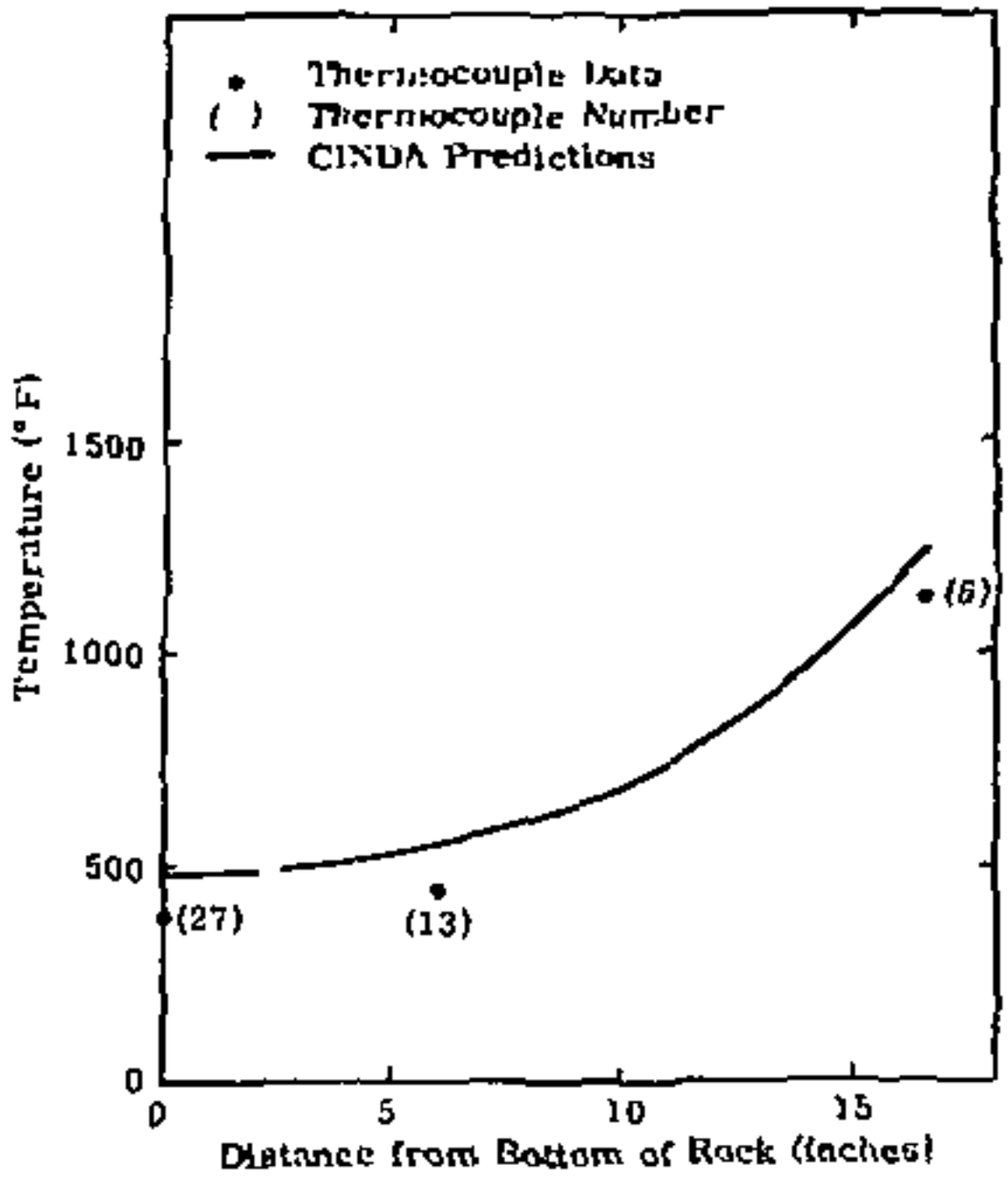

Figure 53. Predicted and measured temperatures, 25th day of the test

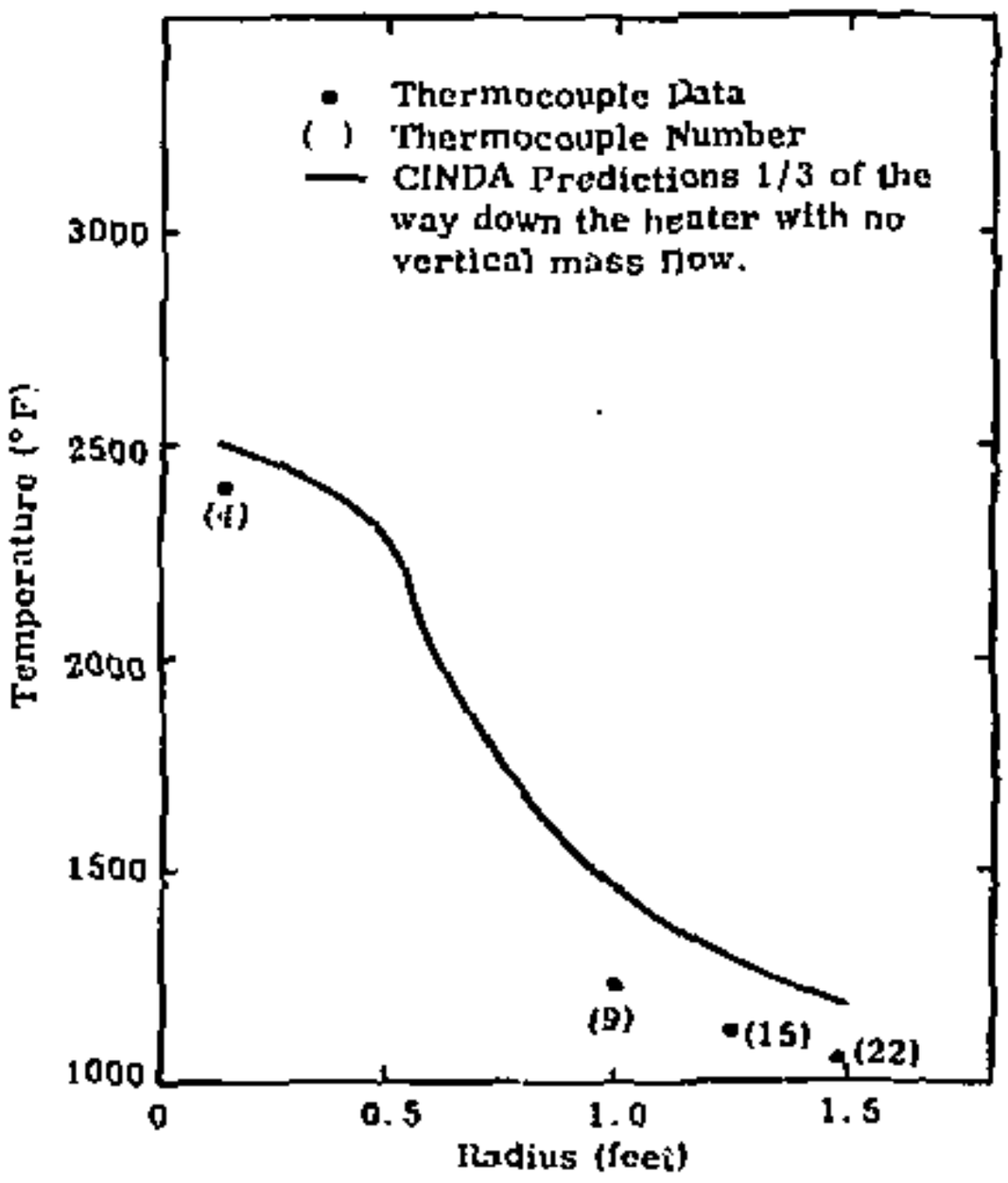

Figure 54. DRD-1 predicted and measured temperatures, 46 days into the test

Cooling air flow rates and inlet and outlet temperatures are given in Figure 55. These data were used to compute heating losses in the access tube and, in conjunction with hygrometer readings, to determine if water liberated from the heated rock would permeate through the melt and exit through the fill port. The average water loss out the access tube for several days when parts of the rock were above the dehydration temperature was approximately 0.5 pound/day. Since the cooling system was not sealed, instrumentation was limited, and sampling was not continuous, this figure should be treated only as a rough approximation, but it does show that moisture did leave the port during the heating phase of the test.

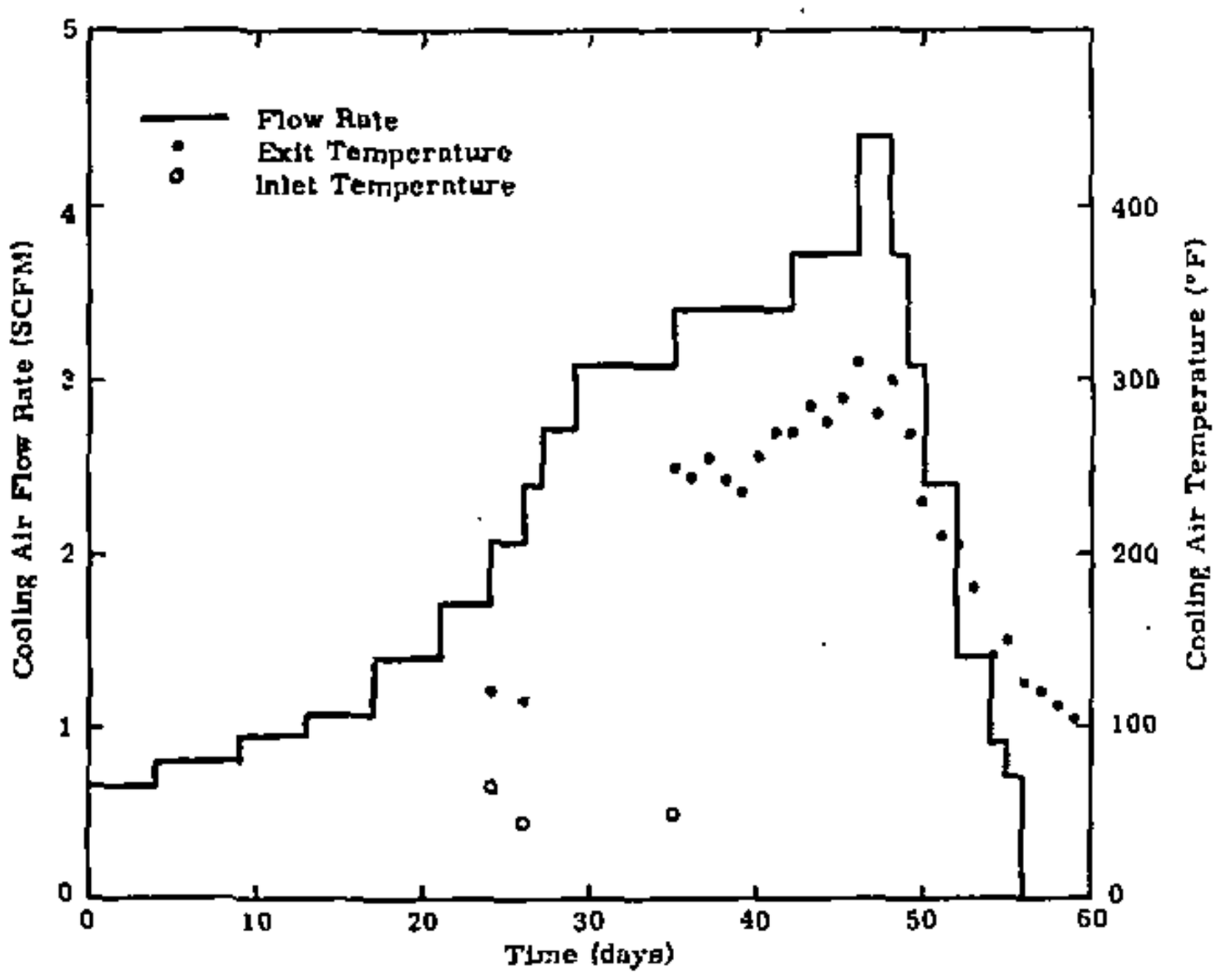

Figure 55. Cooling air flow rates and temperatures

Occasionally during the test, gases came from the access tube that were irritating to the eyes, probably H_2S or HCl, but the times were too short to obtain a sample. On days 42 and 45, gas samples from the access tube were taken but no gases other than water vapor and air were present.

On days 45, 46, and 47, samples of the melt were taken with a steel pipet. The tube was pushed through the crust to a level two inches below the top of the heater. Suction was then applied to the top of the tube to draw a sample of the melt into the pipet. The tube was then withdrawn and sectioned, and the solidified sample was analyzed by X-ray fluorescence, as described in Appendix I. On day 45, the ratio of rock to simulant in the melt was 0.43 to 1. A sample was also taken of

the sand above the crust, and the analysis showed no simulant in the sand. On the 46th day, the ratio of rock to simulant had increased to 1.22 to 1. An analysis of the melt sample taken the 47th day showed a rock to simulant ratio of 5.67 to 1. Although this ratio indicated more rock had melted in one day than had been predicted, there were no visible rock inclusions in the pipet or any other evidence that this was not a representative sample of the melt. Since this was approximately the rock concentration in the melt that was desired and since melting would proceed slowly with the constant maximum heat input, the heat-up phase of the test was terminated the following day.

By the 67th day of the test, all rock temperatures were below 300°F. The rock was then uncovered and allowed to air cool to ambient temperature. The rock was cracked as expected, and sand had entered the cracks, flowed beneath the base plates, and filled the access tube to within 3.2 inches of the top (Figure 56). None of the interior hardware, including the heater, heater tube and sheath, and insulation, showed any signs of degradation. The large vertical tensile cracks formed the 38th day of the test extended from the center of each side to the melt cavity. These cracks did not extend into the resolidified melt. There were also two small radial cracks propagating from the melt cavity toward two of the corners. These cracks, shown in the upper and lower left quadrants of Figure 56, were about 13 and 16 inches long. The large crack patterns are shown in Figure 57. The cracks are largest on top and form inverted T's or Y's one third to two thirds of the way down from the top. One of the upper sections was actually broken free from the rest of the rock, as shown in Figure 57b. Only one side was cracked at the bottom; the rest were similar to Figure 57c. None of the melt ran out the cracks and none could be seen in the cracks. Apparently the cracks and molten glass are self-sealing. An epoxy potting compound was poured into the cracks after they were cleaned and inspected so the rock could be removed from the hole intact and sectioned for posttest analyses.

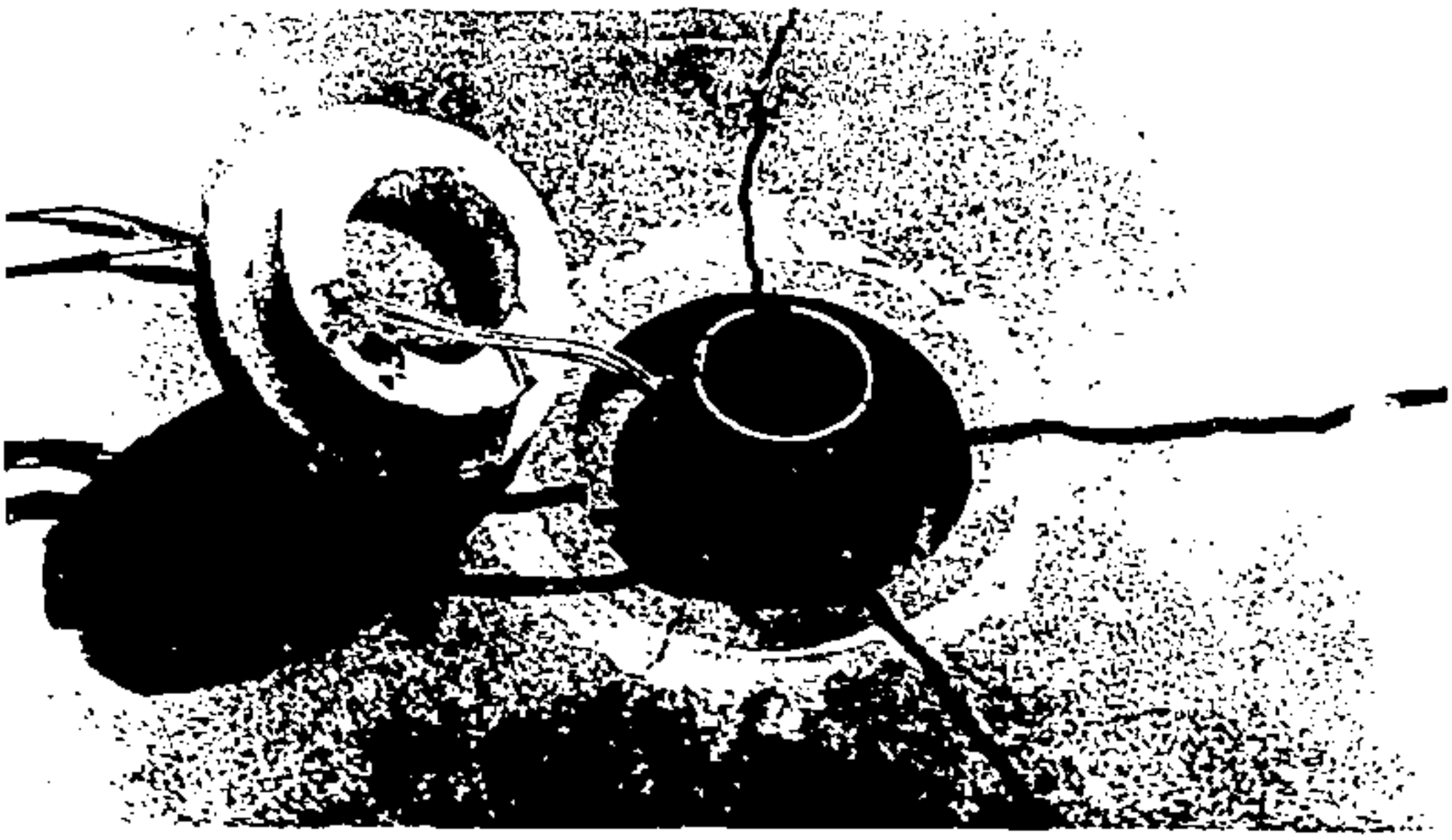

Figure 56. Top of rock after the test showing the cracks and the sand in the annulus

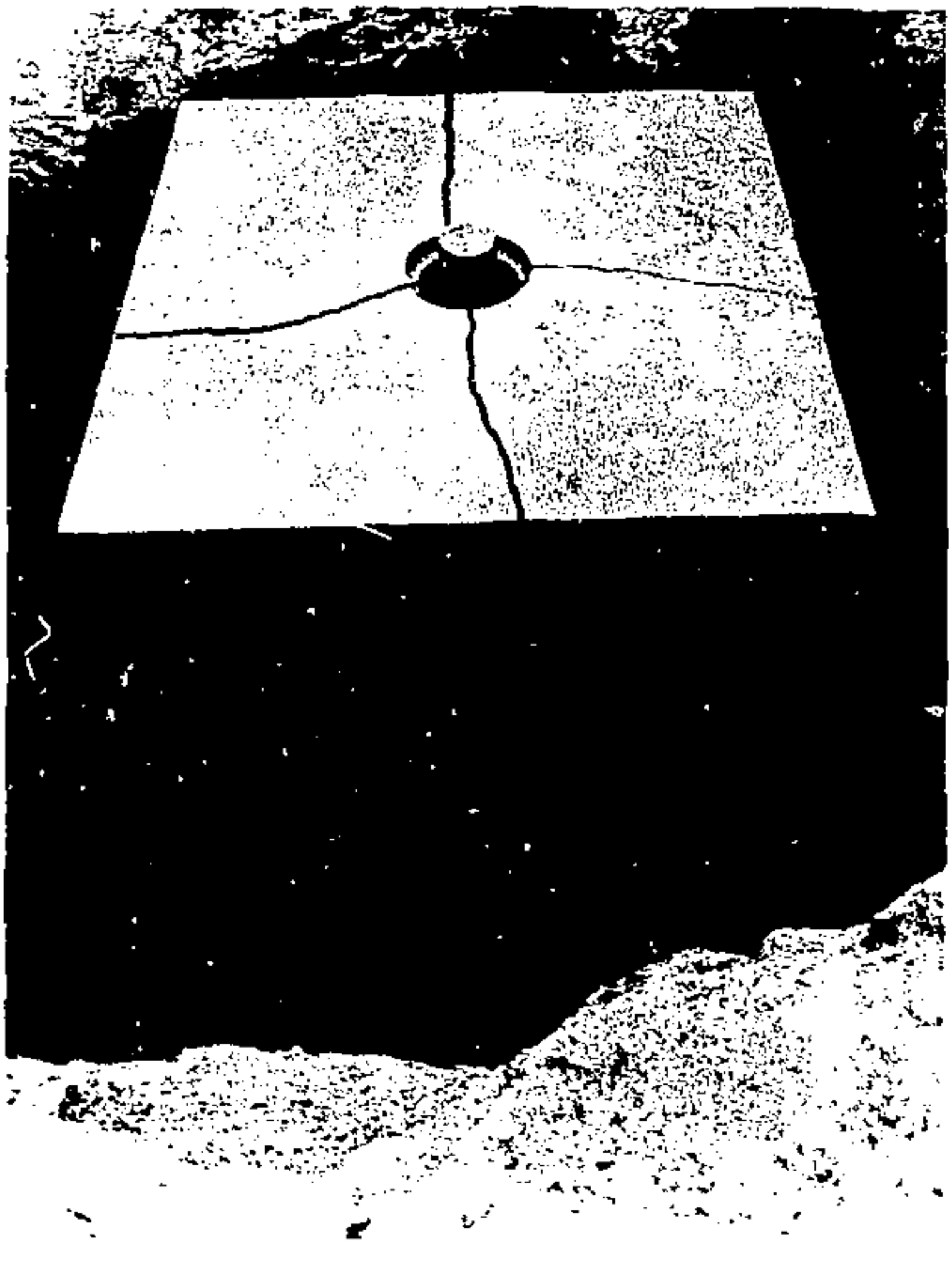

Figure 57a. Uncovered rock showing crack patterns

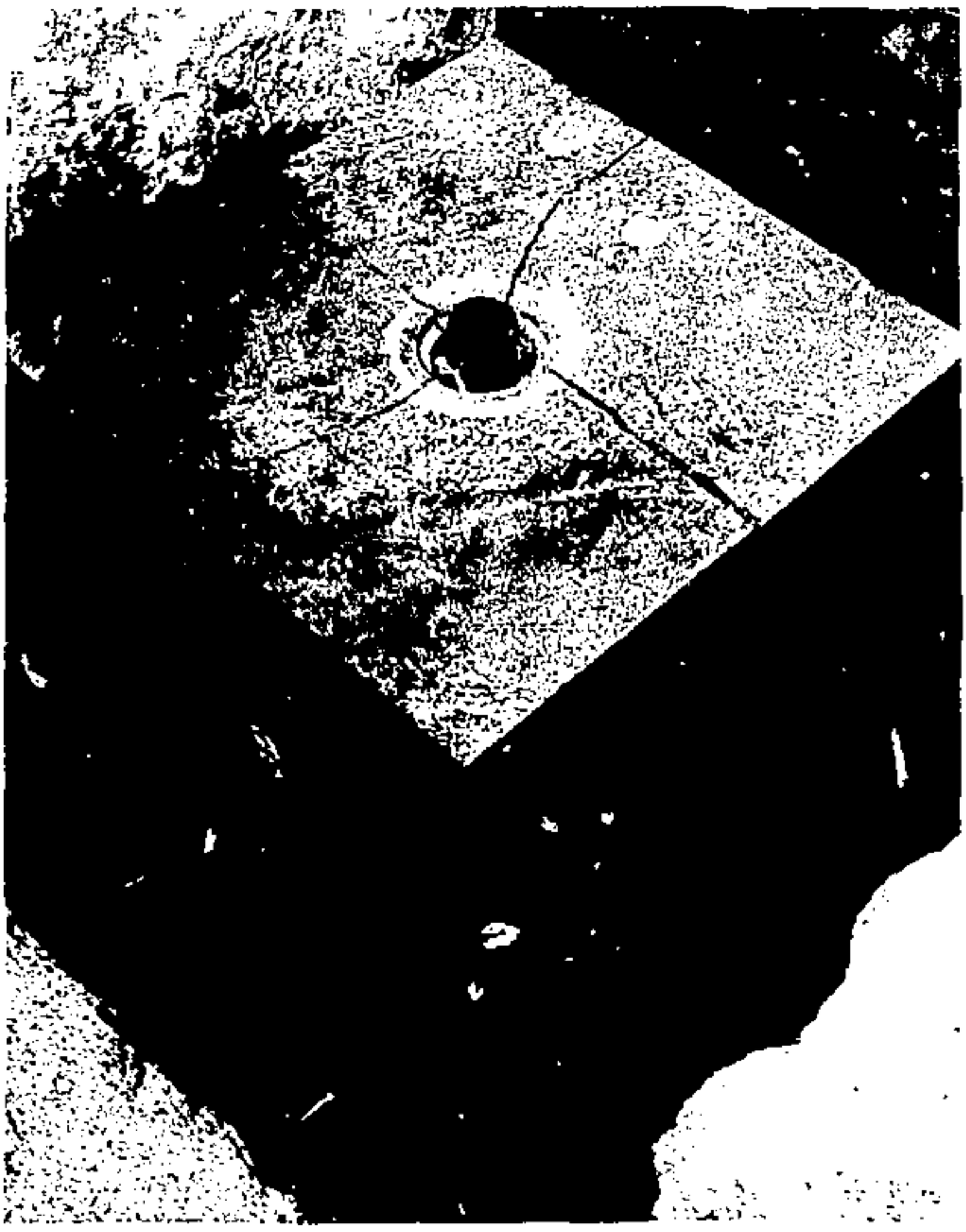

Figure 57b. Uncovered rock showing crack patterns

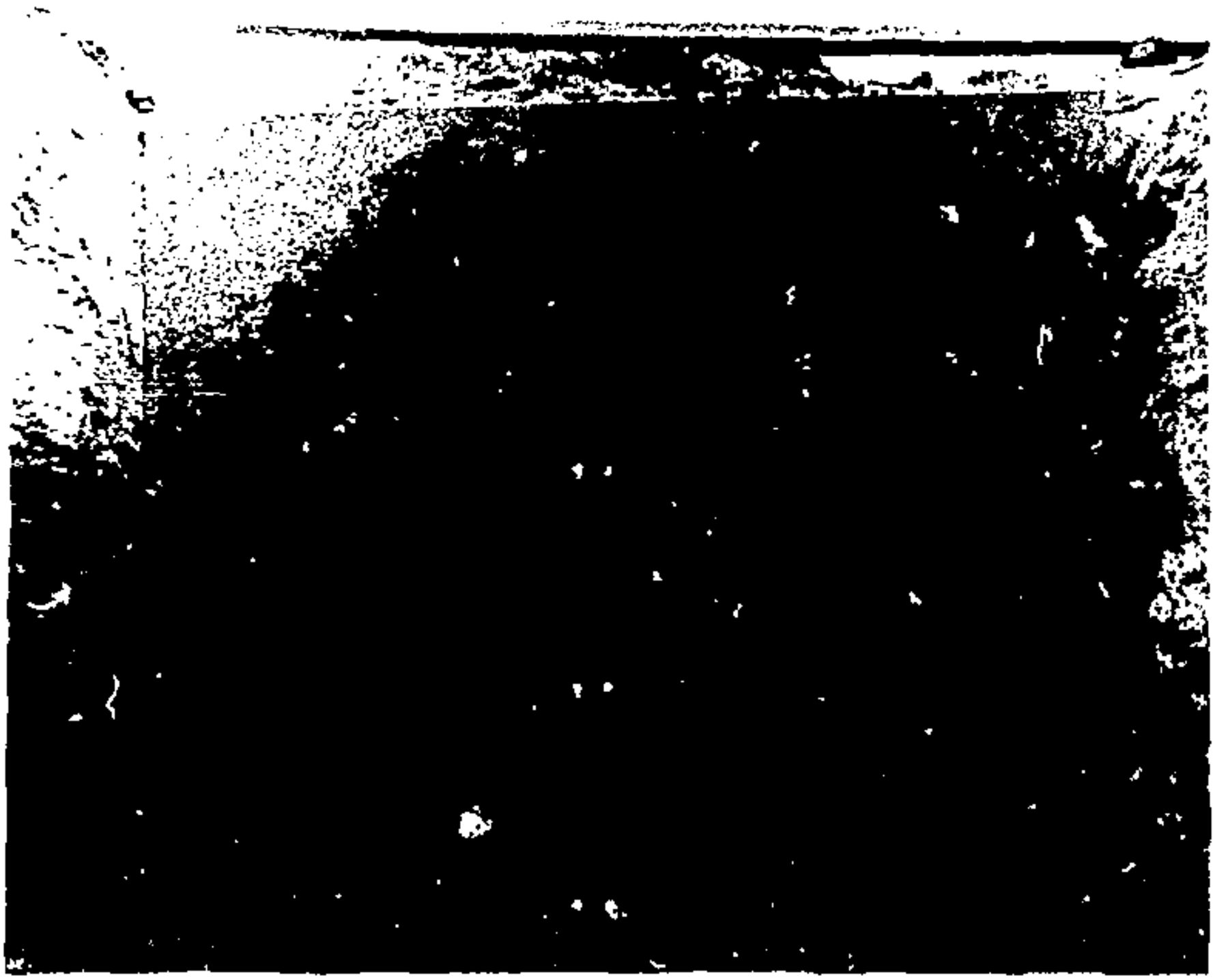

Figure 57c. Uncovered rock showing crack patterns

Posttest, Analyses Outline

The posttest phase of the DRD-1 study will begin by sectioning the rock with a diamond saw. One half will be retained for visual inspection, and the other half will be cut into smaller pieces for laboratory tests. The remainder of the DRD-1 analyses will include the following:

1. Chemical composition of the rock/waste matrix and surrounding porous rock. Samples will be taken from a vertical and radial matrix with several checks on circumferential uniformity. These tests will determine homogeneity, stratification, and the effects of the convection cell. The primary tools for the chemical analyses will be X-ray fluorescence spectroscopy, the electron microprobe, and classified chemistry. Other techniques available for analysis (if it is deemed necessary) include atomic absorption spectrometry, autoradiography, neutron activation analysis, gamma-ray spectroscopy, emission spectrography, electron microscopy, and X-ray and ion backscattering. Descriptions of these techniques are given in Appendix J. Several standard samples containing various rock to simulant ratios were used to calibrate the apparatus which will be used in the chemical analyses (Appendix K).

2. Crystallography of the matrix and surrounding rock. Devitrification and structure will be investigated.

3. Porosity of the matrix and rock. The actual porosity of thin sections will be measured. The apparent open cell porosity will also be measured to determine the amount of water that could be absorbed.

4. Leachability of the matrix.

5. *Thermal conductivity of the matrix, surrounding porous rock, and virgin rock.*

6. Viscosity of the matrix at all locations of different composition.

7. Thermogravimetric analysis to determine the temperatures at which moisture and gases are liberated.

8. Density distributions in the matrix and surrounding rock for input to stratification studies.

9. Circulation patterns and limits of the convection cells.

10. Limits of the melt flow into the thermal stress crack

11. Fracture pattern mapping and strain gage data correlation with thermal stress analyses.

12. Thermocouple data reduction and correlation with analytical and digital models.

13. Sonic data reduction.

14. Integration of all of the above to describe the deep rock nuclear waste disposal process.

The results of these analyses and all the test data will be presented in the final DRD-1 report.

Preliminary Conclusions

A complete set of conclusions will be presented in the final DRD-1 report when all the analyses and tests have been completed. Several conclusions can be made at this time. These are as follows.

1. The DRD-1 test concept and hardware were completely adequate and can apparently be used for higher heating rate and higher temperature tests.

2. Even when average effective convection values are used, the CINDA heat transfer program can give a good approximation of the heat flow in deep rock disposal. When the convection subroutine is added to CINDA, it should be a very effective tool for DRD analyses.

3. The Sandia thermal stress program can be used to predict thermal stress cracks in rock.

4. At least some of the water that is liberated from the rock will exit from the fill tube unless some means to stop it is added.

5. The molten rock/waste matrix expanded up into the fill tube even though the rock cracked. The same type of expansion compensation could possibly be used in an operational configuration.

6. The molten matrix did not flow out into the thermal stress cracks.

7. A long length to diameter cavity for DRD should minimize vertical migration of the melt because the vertical temperature gradient is inversely proportional to the L/D ratio.

8. A low melt temperature glass could be used to seal the fill tube after the rock/waste matrix resolidifies. The surrounding rock would still be hot enough to melt the glass and keep it molten long enough to flow into openings above the matrix. A glass seal should effectively block any ground water leakage that might occur after the surrounding rock cools to below the boiling point of water.

9. The long cylinder, solid high-level waste concept with in place melting would minimize the thermal expansion problem and the time the rock/waste matrix is molten. The concept is also versatile in that waste forms can be tailored to different types of rock and the melt size and duration can be varied by changing the hole diameter and the age and concentration of the waste. As an example, a diluted fresh waste would be molten for a shorter time period than would a full strength aged waste, even though both have the same initial heating rate.

10. Much of the data from the DRD-1 test are applicable for analyses of other deep rock disposal concepts.

All tests and analyses to date have indicated this concept should be feasible even though some engineering problems have been uncovered.

APPENDIX A

STORAGE OF LARGE QUANTITI OF NUCLEAR WASTE IN DEEP SILICA E ROCK

SANDIA LABORATORIES — ALBUQUERQUE, NEW MEXICO; LIVERMORE, CALIFORNIA; TONOPAH, NEVADA

TO : V. L. Dugan - 1734

DATE: March 13, 1973

R. D. Klett

FROM : R. D. Klett - 1734

SUBJECT: Storage of Large Quantities of Nuclear Waste in Deep Silicate Rock

References:

1. J. J. Cohen, A. E. Lewis, and R. L. Braun, "Use of a Deep Nuclear Chimney for the In-Sites Incorporation of Nuclear Fuel-Reprocessing Waste in Molten Silicate Rock," UCRL-51044.

2. R. D. Klett, "Thermal Analysis of the Intact Snap-19/Nimbus B/Agena System," SC-RR-71 0353, July 1971.

3. F. K. Pittman, "Plan for the Management of AEC-Generated Radioactive Wastes," WASH-1202, UC-70, Jan. 1972.

4. Memo, R. D. Klett to V. L. Dugan, "Melting of Rock Around a Column of Reactor Waste Products," dtd, Dec. 14, 1972.

Reference 1 proposes a method of permanent nuclear waste disposal in deep underground nuclear formed chimneys. Chimneys would be formed about 6500 ft. below the surface in silicate rock. The sizes of the chimneys could range from a 35 ft. radius cavity with 48% rubble formed by a 5 KT explosion to a 65 ft. radius cavity with 68% rubble formed by a 30 KT blast. Hopefully, the sequence of events would be as follows. Liquid waste and water would be added to the cavity for 25 years. During the fill period the waste and surrounding rock would be kept at 212°F by the boiling water. The steam would be brought to the surface, condensed, and recycled. At the end of the 25 year fill period when the cavity is filled, the waste would be allowed to boil dry and the inlets would be capped. The temperature would then rise and melt the rubble and surrounding rock. It is assumed that the waste will mix with and dissolve in the melted rock. Melting and mixing would continue for about 90 years until the conduction losses through the solid rock exceed the heat generation rate of the waste. At this time the mixture would gradually begin to solidify from the outer surface. After several thousand years, solidification would be complete and the waste would be in an insoluble silicate rock matrix.

There are several problems that are associated with the burial of large quantities of nuclear waste in a single location that are not mentioned in Reference 1. During the 25 year fill period, radioactive particles, steam, and vapors are continually being circulated above ground. If a leak occurs in any of the plumbing, substantial amounts of radiation could be released because there is no way of turning off the heat that generates the steam. There is also no proof that the cooling water will mix with the waste in such a manner that boiling will be fairly uniform throughout the pool of waste in the cavity.

Temperatures, times, and melt radii presented in Reference 1 may not be valid because of gross simplification used to compute them. It was assumed that after the fill period, the entire liquid core stabilizes at the melt temperature of rock (1920°F) and that all the heat that is generated in the liquid is either conducted away through the solid rock or melts adjacent rock. This could only happen if there was an infinite convection coefficient and either infinite molten rock conductivity or infinite circulation rates driven by a zero potential. The other extreme would be to assume that all the heat in the molten core is transferred by conduction. Using methods derived in Reference 2, it was found that the temperature of the rock and nuclear waste in the center of a non-circulating core would be well above the vaporization temperature of any material. If the waste is not uniformly dispersed in the molten rock, peak temperatures in a large core would become excessive if natural circulation rates are not high. Another possible source of gas in the cavity would be the helium generated by radioactive decay.

Possibly the greatest danger in burying large quantities of waste in one location is the large local thermal expansion of the molten core and surrounding rock. The increase in volume with the smallest quantity of waste mentioned in Reference 1 would be 2.7×10^7 ft^3. This figure was computed assuming no heat transfer to the rock during the 25-year fill period. The volumetric coefficients used for the solid was 1.46×10^{-5} ($°F^{-1}$) and 5.0×10^{-5} ($°F^{-1}$) was used for the liquid. A 10% expansion from a crystaline solid to the liquid phase was used. The thermal expansion could result in two modes of radioactive release. If all motion would be in the upward direction, there would be enough expansion to cause an upheaval of the surface, one mile in diameter with an average height of 1.23 ft. A disturbance of this magnitude could rupture feed lines to the cavity and damage buildings located near cavity. Expansion would also cause stresses in the rock surrounding the cavity and pressures would built up in the cavity. It is conceivable that tensile cracks could propagate from the top of the solid rock down to the molten cavity followed by an excursion of radioactive lava. Even if the molten rock and waste did not breech the surface, but only reached the water table, there could be contamination because it is not known if the waste will be soluble in the rock matrix or even if it will mix.

The current AEC position on permanent storage, as stated in Reference 3, is any concept must be tested using a prototype and the waste must be recoverable in the event of unexpected leakage or indications of future leakage. It would be very difficult to design a meaningful experiment of a large underground storage because of the large physical size of the affected rock and the long transient of time. If anything did go wrong, recovery of 2.2×10^{10} lbs of molten radioactive rock and waste from 6500 ft below the earth surface would be a sizable task.

Most of the potential problems associated with the proposal in Reference 1 stem from the large volume, large quantity of concentrated heat, and the long fill time. The deep hole concept outlined in Reference 4 appears to be a more feasible means of geologic disposal. This method would consist of drilling a deep 10 inch hole into bedrock, placing solidified waste in the bottom part of the hole, and then sealing and refilling the hole. No cooling would be required. The smaller ... coupled with a lower average age of the waste at the time the hole is sealed would greatly reduce the size of the melt zone and the time the rock remains molten. The smaller size reduces the temperature of the molten core and allows a larger percent of the heat to be conducted into the solid rock. The surrounding rock may be able to absorb the smaller change in volume. Although the deep hole concept looks promising, the feasibility study has not been completed.

APPENDIX B

MATERIAL PROPERTIES

APPENDIX B

MATERIAL PROPERTIES

The properties of rocks and soils vary with composition within a given classification, moisture content, confining pressure, compaction, temperature, degree of vitrification, and grain size of crystalline rocks. In addition, the quantity of rock data is very limited. Some of the data presented here were obtained by tests conducted on samples of the rock being used in the DRD-1 experiments (see Appendices F and G). However, most of the data were obtained from References 28 through 30 and 33 through 38 and were for rocks which were similar to those being used in the DRD-1 experiments. Although some of these data are questionable, it is believed that they are the best available at this time.

Granitic Sand

ρ = 120 lb/ft^3

T_m = 2200 to 2400° F

T(°F)	K(Btu/hr ft °F)	C_p(Btu/lb °F)
0	0.53	0.16
400	0.51	0.21
1100	0.46	0.27
1800	0.46	0.29
2200	0.47	0.30
2400	0.49	0.32

Ottawa Sand

ρ = 110 lb/ft^3

T_m = 3100° F

T(°F)	K(Btu/hr ft °F)	C_p(Btu/lb °F)
0	0.225	0.15
400	0.254	0.21
1100	0.353	0.28
1800	0.457	0.30
2200	0.509	0.31

Jet Mist (Dolerite) Rock

ρ = 191 lb/ft^3

H_f = 144 Btu/lb

T_m = 2100 to 2300° F

Speed of Sound = 17,500 ft/sec

Sonic Attenuation = 1 db/cm at 1 MHz

T(° F)	C_p (Btu/lb ° F)
0	0.15
100	0.18
200	0.19
400	0.22
1100	0.27
2000	0.30
2300	0.32
3000	0.34

The reported thermal conductivities of dolerite vary by as much as a factor of three at some temperatures. Reference 29 states that the conductivity of igneous rocks is as dependent on the grain structure as on the chemical composition. The following conductivities are a compilation of data for the high conductivity dolerites which typify fine grain, high density dolerites.

T(° F)	K(Btu/hr ft ° F)
0	1.35
1500	0.74
2000	0.58
2200	0.62
2500	0.96
3100	1.95

Viscosities of liquid basalt and dolerite vary greatly with small changes in composition. Figure B-1 gives the viscosities of two basalts that bracket most of the dolerite viscosity data. Dolerite, which is granular, would follow the crystalline curve until the rock melts. Viscosities below the melt temperatures are not needed for convection studies but are of interest for the analysis of expansion and creep.

T(° F)	Volumetric Expansion from 77° F (%)
212	0.16
392	0.40
752	0.87
1112	1.35
1472	1.91
1832	2.49
2192	3.22

Volumetric expansion during melt = 9 to 13 percent.

Volumetric expansion of melt = 6.8 to 50.2 x 10^{-5} ($°F^{-1}$).

Room temperature compressive strength = 39,400 psi.

Room temperature tensile strength = 3,000 psi.

Room temperature modulus of elasticity = 9.0 x 10^{5} psi.

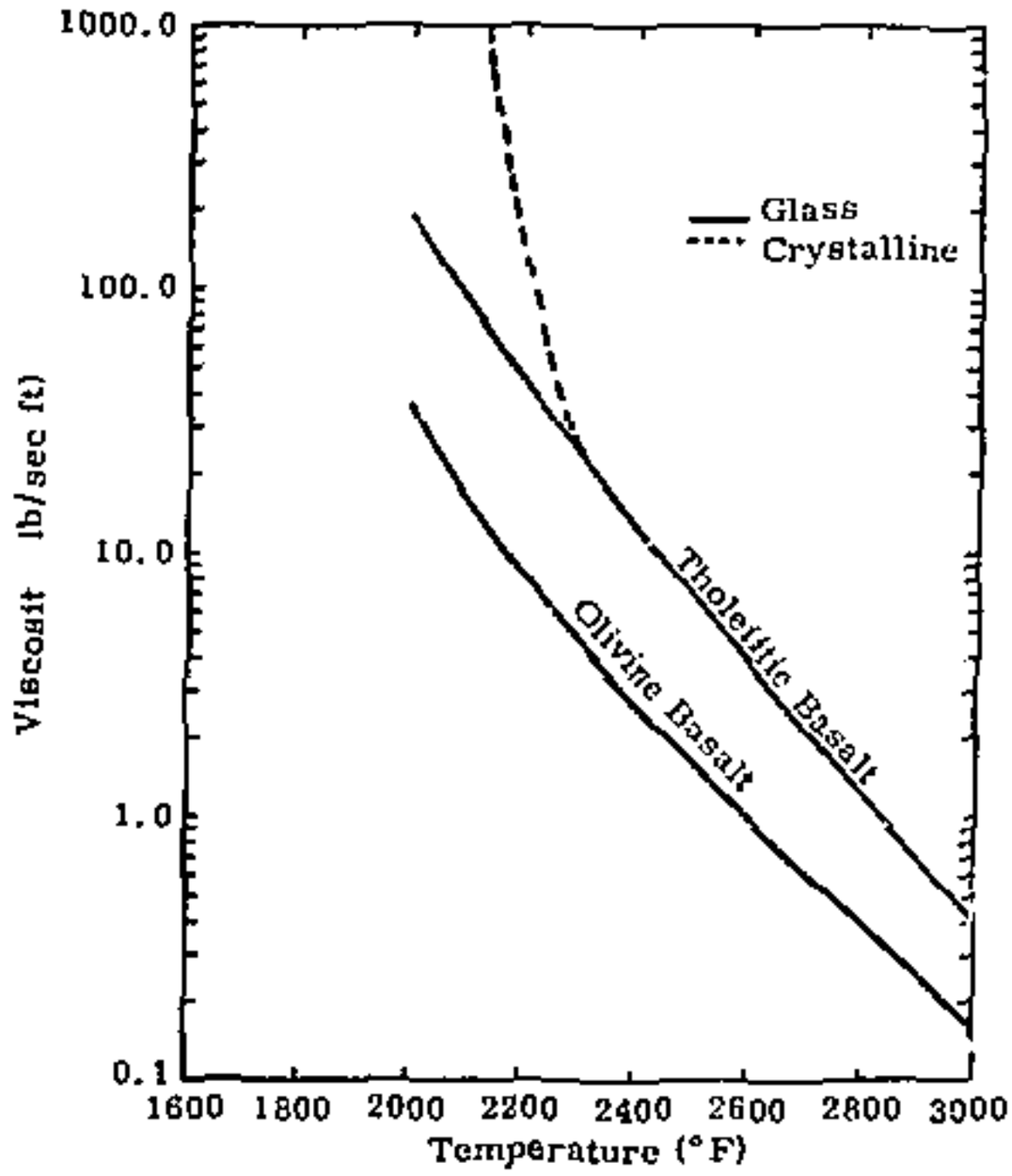

Figure B-1. Viscosities of basalt and dolerite

Salisbury (High Quartz Granite) Rock

ρ = 163 lb/ft^3

H_f = 144 Btu/lb

T_m = 2200 to 2500 °F

Speed of Sound = 17,100 ft/sec

Sonic Attenuation = 3 db/cm at 1 MHz

T(°F)	K(Btu/hr ft °F)	C_p(Btu/lb °F)
0	1.35	0.16
300	0.91	0.20
800	0.68	0.26
1500	0.57	0.28
2000	0.57	0.30
2400	0.62	0.32
3000	0.70	0.34

T(°F)	μ (lb/sec ft)
2370	270 - 60,000
2550	67 - 11,000
2730	23 - 3,300

The values given bracket the viscosities of the various types of granite. Salisbury is probably one of the more viscous types of granite because of the high quartz content.

T(°F)	Volumetric Expansion from 77° F (%)
600	0.72
900	1.32
1063	2.08
1500	2.45
2000	2.86

Volumetric expansion during melt = 7 - 10 percent.

Volumetric expansion of melt = 3.1×10^{-5} ($°F^{-1}$).

Room temperature compressive strength = 30,500 psi.

Room temperature tensile strength = 2,570 psi.

Room temperature modulus of elasticity = 11.2×10^{6} psi.

Platinum

T(°F)	K(Btu/hr ft °F)	Linear Expansion from 77°F (%)	ε
77	41	0	0.10
500	42	0.17	0.11
2000	56	1.10	0.24
3000	64	1.82	0.32

Aluminum Oxide

T(°F)	K(Btu/hr ft °F)	Linear Expansion from 77°F (%)	ε
77	19.0	0	0.75
500	11.6	0.20	0.75
2000	3.6	0.84	0.43
3000	3.6	1.30	0.44

Silicon Carbide

T(°F)	Linear Expansion from 77° F (%)	ε
77	0	0.85
1000	0.26	0.89
2000	0.56	0.87
3000	0.90	0.78

Zirconium Oxide

T(°F)	Linear Expansion from 77° F (%)	ε
77	0	0.77
1000	0.55	0.54
2000	0.90	0.38
3000	1.24	0.47

301 Stainless Steel

T(°F)	Linear Expansion from 77° F (%)
500	0.40
1000	0.90
1500	1.55
2000	2.20

Borosilicate Nuclear Waste Simulant

ρ = 169 lb/ft^3

Slump temperature ≈ 1300° F

Flow temperature ≈ 1650° F

T(°F)	C_p(Btu/lb °F)	K(Btu/hr ft °F)
0	0.16	1.35
500	0.23	1.15
1000	0.26	0.94
1500	0.28	0.74
2000	0.30	0.58
2200	0.31	0.62
2500	0.33	0.96
3100	0.34	1.95

The following viscosities were estimated by visual comparison with liquids of known viscosities.

T(°F)	μ(lb/sec ft)
1800	2.7
2000	1.0
2200	0.40
2400	0.16

T(°F)	Volumetric Expansion from 77°F (%)
212	0.172
392	0.419
572	0.686
752	1.02
880	1.39

Volumetric expansion of melt = 9.0×10^{-5} ($°F^{-1}$).

APPENDIX C

THERMAL ANALYSIS OF DRD-1 EXPERIMENT

APPENDIX C

THERMAL ANALYSIS OF DRD-1 EXPERIMENT

Sandia Laboratories

April 16, 1974

R. D. Klett - 4734

B. M. Brake - 1543

Thermal Analysis of DRD-1 Experiment

Ref: 1. Gaski, J. D., Lewis, D. R., and Thompson, L. R., "Chrysler Improved Numerical Differencing Analyzer for 3rd Generation Computers (CINDA-3G)," TN-AP-67-287, Chrysler Corporation, Space Division, New Orleans, La., October 1967.

2. Gabrielson, V. K., "HEATMESH-71: A Computer Code for Generating Geometrical Data Required for Studies of Heat Transfer in Axisymmetric Structures," SCL-DR-720004, September 1972.

CINDA (Ref. 1) is a dimensionless, multi-option, systems compiler computer program. A network representation of a physical problem presented to the program may be solved by a variety of methods. Subroutines within the program are available for handling variable boundaries, variable material properties and melting phenomena. HEATMESH-71 (Ref. 2) provides a convenient means of constructing the network.

The dolerite rock used in the DRD-1 experiment was modeled as a cylinder with 1.5 ft radius, 2.25 ft long (bottom quarter of rock). Ottawa sand 1.5 fr thick surrounded the rock and granitic soil completed the model to a total radius of 15 ft. A hole for the heater and waste simulant with radius of .2 ft and length of 1 ft at the top of the 2.25 ft length was incorporated into the model. Heat was applied at the inner surface of the simulant (.875 in. thick glass).

A transient thermal analysis using implicit forward-backward differencing (Crank-Nicholson method) was then performed. Variable material properties were used in the analysis. Several heat pulses were used during the course of the analysis in order to predict thermal gradients in the rock and to determine the composition of the melt front as a function of time. CINDA does not include chemical reaction or convection within the cavity and as a result some inaccuracies result. Comparison of CINDA predictions with thermocouple records obtained during the heating phase of the test are within 1 percent. Cool-down predictions after the heater was turned off are more inaccurate probably because 15 ft is no longer infinity.

APPENDIX D

PREDICTED CONVECTION IN DEEP ROCK DISPOSAL EXPERIMENT I

APPENDIX D

PREDICTED CONVECTION IN DEEP ROCK DISPOSAL EXPERIMENT 1

Sandia Laboratories

Albuquerque, New Mexico
Livermore, California

date February 15, 1974

to Distribution

from R. D. Klett - 4734

subject Predicted Convection in Deep Rock Disposal Experiment 1

Ref: 1. Memo, R. D. Klett, 4734, to Distribution, dtd. July 13, 1973, subject, "Deep Rock Disposal Experiment."

2. T. Murase and A. R. McBirney, "Properties of Some Common Igneous Rocks and Their Melts at High Temperatures", Geological Society of America Bulletin, Vol. 84, No. 11, November 1973.

3. S. P. Clark, Jr., "Handbook of Physical Constants", The Geological Society of America, 1966.

4. J. W. Elder, "Laminar Free Convection in a Vertical Slot", Journal of Fluid Mechanics, Vol. 23, Part 1, 1965.

5. J. W. Elder, "Turbulent Free Convection in a Vertical Slot", Journal of Fluid Mechanics, Vol. 23, Part 1, 1965.

6. E. R. G. Eckert and R. M. Drake, Jr., "Analysis of Heat and Mass Transfer", McGraw-Hill, New York, 1972

7. S. T. Hsu, "Engineering Heat Transfer", D. Van Nostrand Company, New York, 1963.

8. E. R. G. Eckert and W. O. Carlson, "Natural Convection in an Air Layer Enclosed between Two Vertical Plates with Different Temperatures", International Journal of Heat and Mass Transfer, Vol. 2, p. 106, 1961.

9. G. K. Batchelor, "Heat Transfer by Free Convection across a Closed Cavity between Vertical Boundaries at Different Temperatures", Quarterly of Applied Mathematics, Vol. 12, No. 3, October 1954.

10. J. W. Elder, "Numerical Experiments with Free Convection in a Vertical Slot", Journal of Fluid Mechanics, Vol. 24, Part 4, 1966.

11. R. L. Curran, "Use of Mathematical Modeling in Determining the Effects of Electrode Configuration on Convection Currents in an Electric Glass Melter", IEEE Trans. on Industry and Gen. App., Vol. IGA-7, No. 1, January-February, 1971.

12. T. S. Chen and R. E. Goodson, "Computation of Three-Dimensional Temperature and Convective Flow Profiles for an Electric Glass Furnace", Glass Technology, Vol. 13, No. 6, December 1972.

Nomenclature:

C_p = Specific Heat (BTU/lb)
D = Annulus Width (ft)
g_o = 32.2 (ft/sec^2)
Gr = Grashof Number = $D^3 g_o \beta \Delta T/\nu^2$
h = Convection Coefficient (BTU/sec ft^2 °F)
K = Thermal Conductivity (BTU/sec ft °F)
K_c = Effective Conductivity across Annulus Due to Convection (BTU/sec ft °F)
L = Annulus Height (ft)
Nu = Nusselt Number = hD/K
Pr = Prandtl Number = $C_p \mu/K$
Q = Heat Transfer (BTU/sec)
r_i = Inner Radius of Annulus (ft)
r_o = Outer Radius of Annulus (ft)
Ra = Rayleigh Number = Gr • Pr = $D^3 g_c \beta \Delta T/\alpha\nu$
ΔT = Temperature Gradient across Annulus (°F)
U = Velocity (ft/sec)
$\bar{U}$ = Average Velocity (ft/sec)
Y = Distance Measured Horizontally across an Enclosure (ft)
α = Thermal Diffusivity = $K/\rho C_p$ (ft^2/sec)
β = Volumetric Thermal Expansion (°F^{-1})
μ = Viscosity (lb/sec ft)
ν = Kinematic Viscosity = μ/ρ (ft^2/sec)
ρ = Density (lb/ft^3)

In the design of the DRD-1 experiment described in Reference 1, it was necessary to know the Nusselt Number (hL/K) or the effective conductivity across the melter annulus. A uniform heat source experiment such as DRD-1 has vertical mass transfer and a vertical temperature gradient resulting in more radial heat transfer and melting at the top of the rock than at the bottom. However, the current version of the GENGA digital heat transfer program used to predict DRD-1 temperatures

can only handle isotropic conduction. This limitation did not hinder the design of this experiment. Average radial conduction computations based on empirical equations were used to find an effective conduction in the melt zone.

Some of the properties of the waste simulant and rock have not as yet been measured. In these cases properties of similar materials were used to compute convection. Since the viscosity of rock varies greatly with small differences in composition, convection was predicted using both the maximum and minimum viscosity of dolerite and basalt melts (Ref. 2 and 3). Viscosities of the simulant were estimated by visual comparison with liquids of known viscosities. The appropriate viscosities of the rock and simulant are shown in Figure 1. Thermal expansion and densities of the simulant were measured by Dr. [illegible] 5326. All other properties were from References 2 and 3.

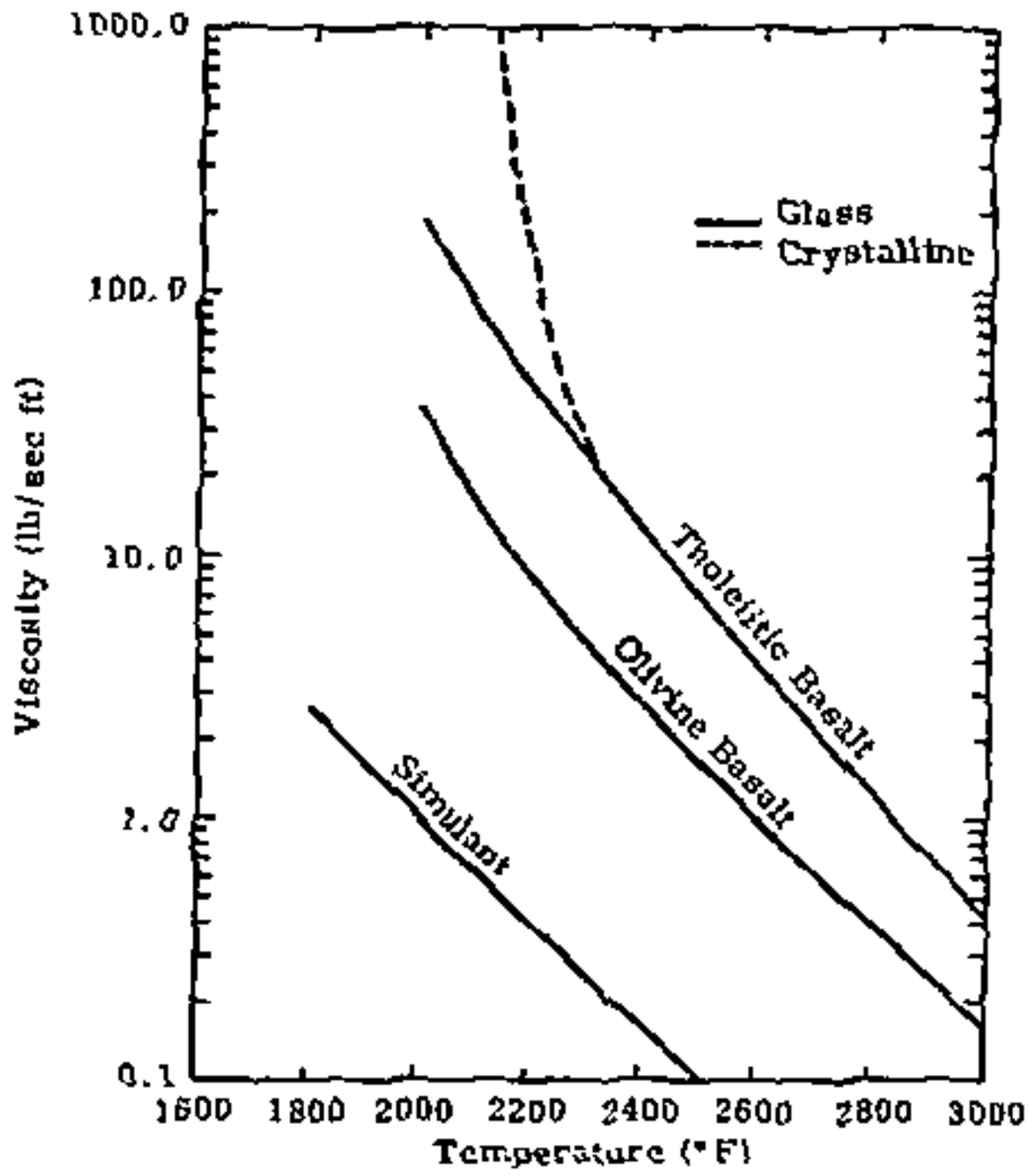

Figure 1. DRD-1 Viscosities

J. W. Elder conducted laboratory tests physically similar to DRD-1 except for fixed boundaries (Ref. 4 and 5). One apparatus consisted of a vertical annulus of fluid with a L/D = 18.2 and a uniform heat flux at the inner boundary wall. Other configurations were parallel vertical uniform temperature plates with L/D ranging from 12 to 60. The fluids were medical paraffin and 2/1 stoke silicone oil. Rayleigh

Numbers ranged from less than 10^3 to 2.3×10^8. Elder found that for $Ra < 10^3$ the temperature field satisfies Laplace's equation but a weak unicellular circulation is present (Fig. 2a). For $10^3 < Ra < 3 \times 10^5$ large temperature gradients grow near the walls and a uniform vertical temperature gradient is established in the interior region. At about $Ra = 4 \times 10^5$ the interior region generates a steady secondary flow starting at the bottom (Fig. 2b). At about $Ra=6 \times 10^5$ the secondary flow occupies the entire interior region (Fig. 2c). Near $Ra = 10^6$ tertiary flow begins. Smaller reverse flow cells develop in the weak shear layer between the secondary cells (Fig. 2d). The flow begins to become unsteady at $Ra \approx 10^7$. Turbulence begins at the walls of the annulus with a critical $Ra = 8 \times 10^8 (D/L)^3 (Pr)^{-5}$. The middle of the interior becomes turbulent near $Ra = 10^{10} (D/L)^3$.

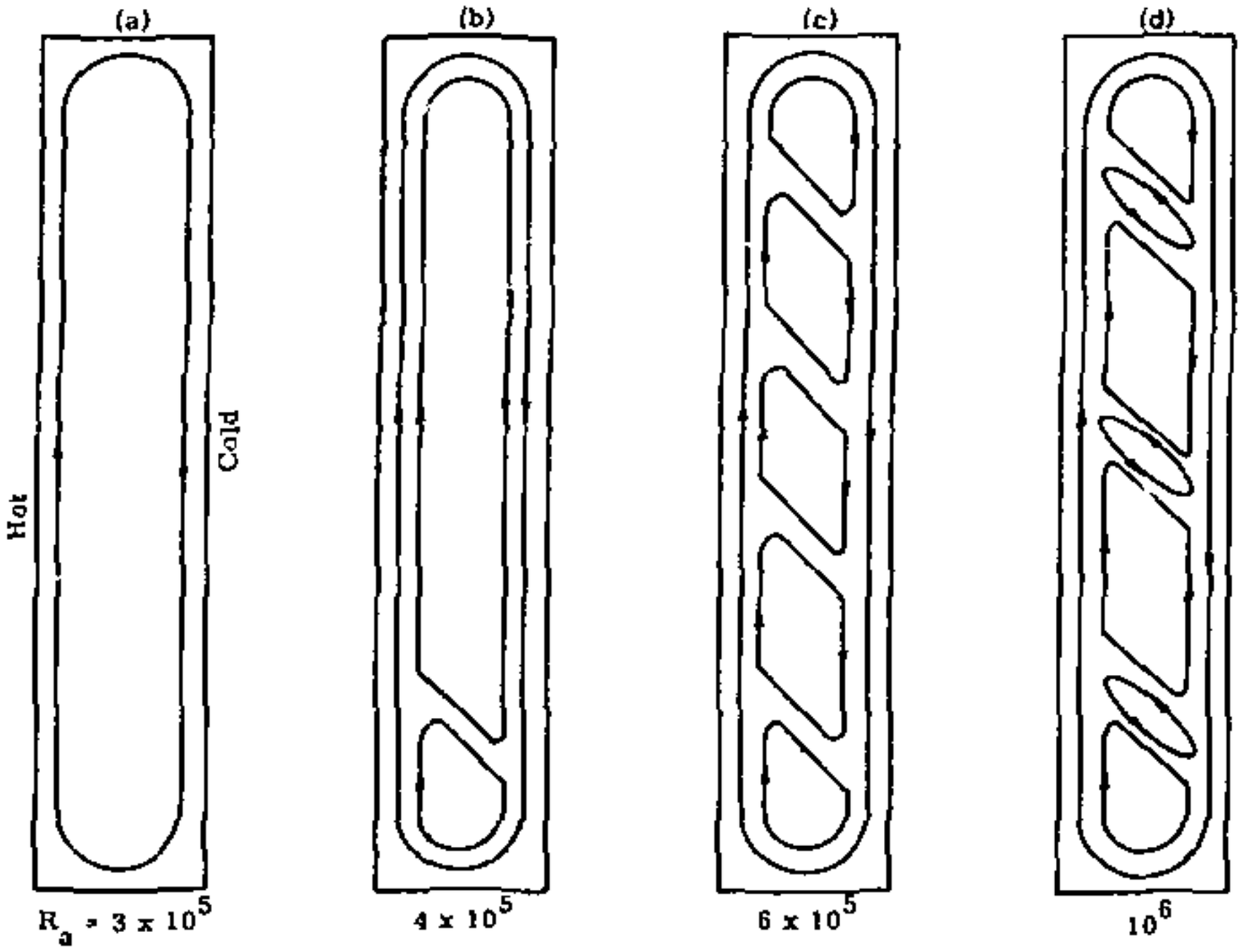

Figure 2. Natural convection stream lines in an annulus with a L/D = 18.3

A good approximation to the average effective radial conductivity across a convecting annulus that agrees well with Elder's experimental and analytical work can be found using Figures 12-14 in Reference 6. An equation (Ref. 7) which gives approximately the same results in the Ra range expected in the DRD-1 experiment is:

$$\frac{K_e}{K} = 0.085 \, (Ra)^{.325} \left(\frac{D}{L}\right)^{1/9} \qquad (1)$$

Several other experiments from References 7, 8, and 9 were conducted using a fluid with a Pr = 1 (i.e., Gr = Ra). Empirical equations from these studies include:

$$\frac{K_e}{K} = 0.22 \, (Gr)^{.25} \left(\frac{D}{L}\right)^{.25} \tag{2}$$

$$\frac{K_e}{K} = 0.119 \, (Gr)^{.3} \left(\frac{D}{L}\right)^{.1} \tag{3}$$

$$\frac{K_e}{K} = 0.065 \, (Gr)^{.333} \left(\frac{D}{L}\right)^{1/9} \quad , \; Gr > 10^5 \tag{4}$$

$$= 0.18 \, (Gr)^{.25} \left(\frac{D}{L}\right)^{1/9} \quad , \; 10^4 < Gr < 10^5 \tag{5}$$

These equations also agree fairly well with Reference 6 if Ra is substituted for Gr. None of these equations account for the vertical variation in heat flow.

In the DRD-1 experiment only a negligible amount of the total heat input goes into the melt as sensible heat above the melt temperature. Therefore, it is possible to find the average melt radius as a function of time and heating rate for a fixed heating profile using CHDA and pure conduction. Since the inner radius of the annulus is fixed, the melt temperature is fixed, and the heating rate is increased very slowly (Fig. 3), the following equation can be solved simultaneously with any of equations 1 through 5 or with Figure 12-14 in Reference 6 to find the effective conductivity (K_e) as a function of temperature for this heat pulse.

$$K_e \, \Delta T = \frac{q \ln \frac{r_o}{r_i}}{2 \pi L} \tag{6}$$

Batchelor (Ref. 9) developed an equation for the velocity profile in fully developed primary flow in a vertical enclosure. Although it is limited to $Ra < 10^5$, uniform viscosity in the enclosure, a linear temperature gradient, and fully developed flow (i.e., no end effects), it is useful to find a rough approximation to the average velocity. Integrating Batchelor's equation

$$U = \frac{Ra}{12} \frac{\alpha}{D} \frac{Y}{D} \left(1 - \frac{Y}{D}\right) \left(1 - 2\frac{Y}{D}\right) \qquad (7)$$

the average velocity is

$$\bar{U} = 0.0052 \frac{Ra\,\alpha}{D} \,. \qquad (8)$$

Velocities and effective conductivities for the DRD-1 experiment were predicted using the following input data.

$$L = 2 \text{ ft}$$
$$r_i = 0.21 \text{ ft}$$

Condition	D (ft)	Q (KW)	Outer T (°F)
Beginning of Simulant Melt	.083	2.5	1800
Beginning of Rock Melt	.083	2.9	2200
50/50 Rock and Simulant	.15	3.9	2200
7.5 Rock to 1 Simulant	.35	4.0	2200

D was found using CINDA and the heat pulse in Figure 3.

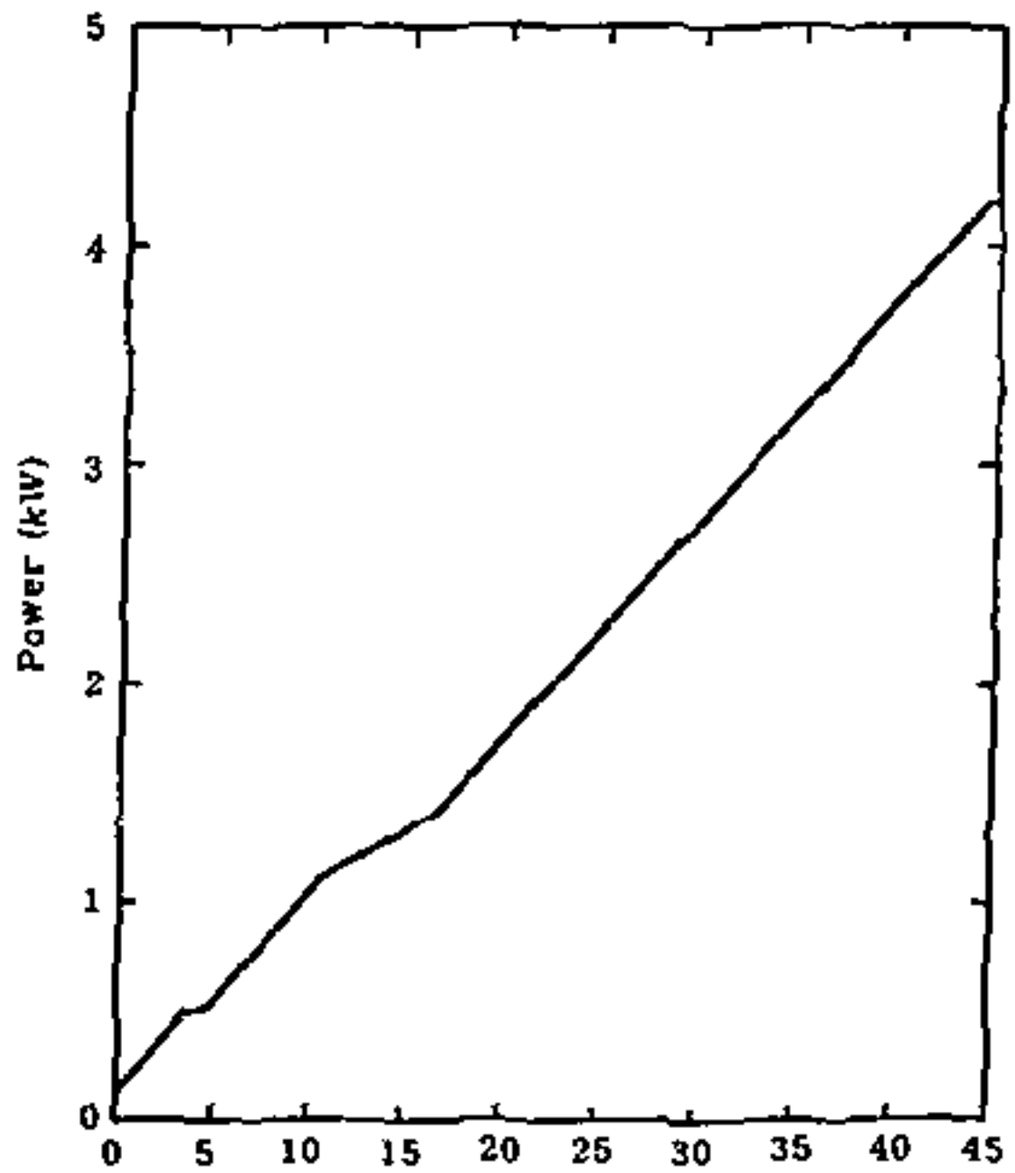

Figure 3. DRD-1 heat pulse

The material properties for the melts were:

Rock

$\rho = 168$ lb/ft^3

$\beta = 1.1 \times 10^{-4}$ °F^{-1}

Simulant

$\rho = 163$ lb/ft^3

$\beta = 9 \times 10^{-5}$ °F^{-1}

Rock and Simulant

μ from Figure 1

T (°F)	K (BTU/hr ft °F)	C_p (BTU/lb °F)
1500	0.74	0.28
2000	0.58	0.30
2200	0.61	0.31
2500	0.95	0.33

The results of the DRD-1 convection study using Reference 6 and Equations 6 and 8 are summarized in the following Table.

Melt	$\bar{T}$ (°F)	ΔT (°F)	Ra	Nu	K_c $\left(\frac{BTU}{hr\ ft\ °F}\right)$	$U\left(\frac{ft}{min}\right)$
Simulant	1940	280	1.54×10^4	1.83	1.17	0.215
Simulant	2305	210	5.54×10^4	2.72	1.96	0.655
50/50 Low μ Rock	2360	320	7.66×10^4	2.95	2.36	0.670
50/50 High μ Rock	2400	400	2.47×10^4	2.10	1.79	0.230
Low μ Rock	2380	360	7.14×10^5	5.70	4.73	2.729
High μ Rock	2420	440	2.25×10^5	4.34	3.51	0.905

These and intermediate data points were used to generate the effective radial thermal conductivity of the molten simulant and rock that were used in the CHNDA program to predict DRD-1 temperatures.

With the heat pulse defined in Figure 3, the rate of increase in K_c due to an increasing annulus width nearly compensates for the increasing heat flux, with the result the inner annulus temperature should never exceed about 2500°F during the test if the rock follows the low viscosity curve or 2600°F for the high viscosity curve.

There are several refinements that are needed before analytical or numerical methods can be used to accurately predict deep rock nuclear waste convection. These include:

1. The ability to handle two materials with different properties that react with each other.

2. The ability to analyze complex shapes with boundaries that change because of melting, chemical reaction, and/or mechanical degradation.

3. Inclusion of vertical heat and mass transfer.

4. Acquisition of better material properties as a function of temperature and pressure.

The numeric methods developed by the glass industry for the analysis of glass furnace convection (Refs. 10, 11, and 12) might be adaptable to deep rock disposal. However, an interim measure that would be useful for analysis and design would be a convection subroutine for CINDA that includes mass transport and the option of switching input data.

As improved methods and better property data become available, they will be checked against the results of the DRO-1 experiment.

APPENDIX E

ULTRASONIC INSTRUMENTATION FOR DEEP ROCK DISPOSAL EXPERIMENT

APPENDIX E

ULTRASONIC INSTRUMENTATION FOR DEEP ROCK DISPOSAL EXPERIMENT

SANDIA LABORATORIES — ALBUQUERQUE, NEW MEXICO; LIVERMORE, CALIFORNIA; TONOPAH, NEVADA

TO . Ralph H. Richards, 4733 DATE. August 8, 1973

FROM . John H. Cieske , 9352

SUBJECT. Ultrasonic Instrumentation for Deep Rock Disposal Experiment

Deep Rock Disposal Experiment #1 will be instrumented with six ultrasonic $LiNO_3$ transducers. The transducers will be positioned on the outside six faces of the rock so that the following three ultrasonic experiments can be carried out during the total time the rock is being heated and cooled: (1) Ultrasonic Pulse Echo, (2) Ultrasonic Through Transmission, and (3) Acoustic Emission.

(1) Ultrasonic Pulse Echo. Two of the six transducers will be placed opposite each other on two opposing vertical faces of the block so that the ultrasonic waves excited by the two transducers will propagate toward the center of the rock. The ultrasonic waves will be reflected back toward the transducers from which they were initiated at the interface of the cylindrical cavity or melt zone at the center of the rock. The same two transducers which initiated the waves are then excited by the returning waves and the delay time for the waves to travel the full round trip from the outside surface of the rock to the inside surface of the melt zone will be measured on an oscilloscope. From the measured delay time and data on the temperature dependence of the velocity in the rock one can then calculate the distance from the outside surface of the rock to the inside surface of the melt zone at any time during the course of the experiment.

(2) Ultrasonic Through Transmission. The remaining four transducers will be placed in opposing pairs one each on the remaining four faces of the block so that they will be in a plane which is perpendicular to the propagation direction of the two pulse echo transducers. These transducers will be used to measure the delay time of the ultrasonic wave excited by one of the transducers and received by the other transducer directly opposite it. In this case, the distance between the two transducers is known and the average velocity of the ultrasonic wave in the rock between the two transducers can be calculated as a function of the temperature which will be read by the thermocouples placed in the rock. This data will be used both for the evaluation of the pulse echo and the acoustic emission data.

(3) Acoustic Emission. All six transducers will be used as receivers during the time the pulse echo and through transmission determinations are not being made. If and when an internal crack occurs at any time during the experiment and at any location in the rock, acoustic waves will be sent in all directions of the rock at the same time. The ultrasonic waves arrive at different times at each of the six transducers and the delay time differences of the waves between each of the transducers will be recorded. From the delay time differences and the data of the velocity versus temperature in the rock, the location of the root of the crack will be ascertained by triangulation techniques.

APPENDIX F

HIGH TEMPERATURE BEHAVIOR OF CANDIDATE ROCKS

APPENDIX F

HIGH TEMPERATURE BEHAVIOR OF CANDIDATE ROCKS

Sandia Laboratories

Albuquerque, New Mexico
Livermore, California

date November 7, 1973

to R. D. Klett - 4734

from R. J. Eagan and E. K. Beauchamp - 5316

subject High Temperature Behavior of Candidate Rocks

To assist in the selection among the candidate rocks for the Deep Rock fuel waste disposal test, a number of high-temperature tests were performed. The tests included a "slump" test, hot-stage microscopic examination, and differential thermal analysis (DTA).

Slump Tests

The slump test, in which a bar is allowed to deform in flexure under its own weight, is intended only to provide a rough idea of the viscosity and other mechanical behavior of the materials at high temperature. (If the bars were glasses or other materials with a linear stress-strain rate dependence, this test could provide a quantitative viscosity determination.)

The experiments were run w' amples 1/8-inch thick and approximately 1/4-inch wide. The were supported on the ends, with a 2-1/2-inch unsupported length. The bars were held in a zirconia setter box which was placed in the furnace entrance and gradually moved into the furnace to reduce thermal shock of the samples.

The samples are identified as follows:

1A - Jet Mist
1B - Berkeley
A - Academy Black
B - Dark Pearl
C - Sierra White
D - Cold Springs Green
E - Charcoal Black
F - Salisbury Pink (1200°C test only)

The first run was at 800°C for 1 hour. No deformation was observed in any sample. Color changes were observed, particularly in B and D, which turned light brown.

The samples from the first run were rerun at 900°C for 105 minutes. Examination in situ showed that only the Sierra White had deformed (~1/16-inch beam deflection). When the samples were cooled it was apparent that the deformation was not caused by plastic flow. The bar simply became so friable that it fractured under its own weight. The 1B, A, and B samples were also friable but somewhat stronger than the C sample. All samples showed color changes. Most looked bleached.

Measurement of the thickness of the C bar showed that it had expanded from .1261 to .1305 inch. Similar, but smaller, expansions were observed in all other samples except 1A. Evidently the mica phase had decomposed and expanded to fracture the granites.

For run number 3, samples were held at 1000°C for 1 hour. As in the 900°C run, the C sample deformed and became very weak. Beam deflection was ~.100 inch. The bar also warped. All other samples except 1A were very friable at the end of the run. Samples B and D were slightly warped. In a highly subjective test in which the bars were twisted between the fingers, the samples ranked in strength as follows: 1A highest; then D, A, E, B, 1B, and C. Again, measurements of thickness changes showed that all samples except 1A had expanded.

In run number 4, at 1100°C, the C sample slumped all the way to the container. On cooling, the material was very friable. The B sample also sagged (~1/8-inch) but was stronger than after the 1000°C run. Apparently enough of the material had melted to bond the grains together. Samples A and E did not sag but were friable. Sample D did not sag but warped. Sample 1B sagged about 1/16-inch. Sample 1A did not slump but was substantially weaker than for lower temperature runs, though stronger than the other materials. It was also the only sample which did not expand during the run.

The results of run number 5 (at 1200°C for 1 hour) can be seen in Figure F-1. No A sample was available for this run. Samples 1B, B, C, and E all slumped to the bottom of the container. Sample D warped but did not sag. All but sample 1A were glossy after the run, indicating that some of the crystalline material had melted and formed a glass. All samples were clearly less friable than after the 1100°C run, apparently because of the glass bonding. Sample E was obviously the most fluid, to the point that surface tension rounded all edges and corners.

In a separate run at 1200°C a sample of Salisbury Pink slumped to the floor of the zirconia container after 30 minuates. Subsequent examination of the cooled sample showed large melted areas surrounding large unmelted crystalline grains.

Hot Stage Microscopy and DTA

A hot stage microscope was used to determine the temperatures at which substantial liquid is formed. The temperature was determined by placing a Pt-Pt10Rh thermocouple in contact with a fragment of granite. The melting of the rock was observed near the point at which the thermocouple contacted the granite at a magnification of ~65X so that individual grains could be easily resolved. Since granite is composed of several types of crystaln it does not have a well defined "melting point." The data in the accompanying table notes the temperature at which "substantial" liquid is present. This may be interpreted as the point at which many of the more refractory grains are surrounded by a melted phase or at which a large number of grains have bubbles formed in them indicating that they have melted. The flow temperature indicates the temperature at which movement of the grains occurred.

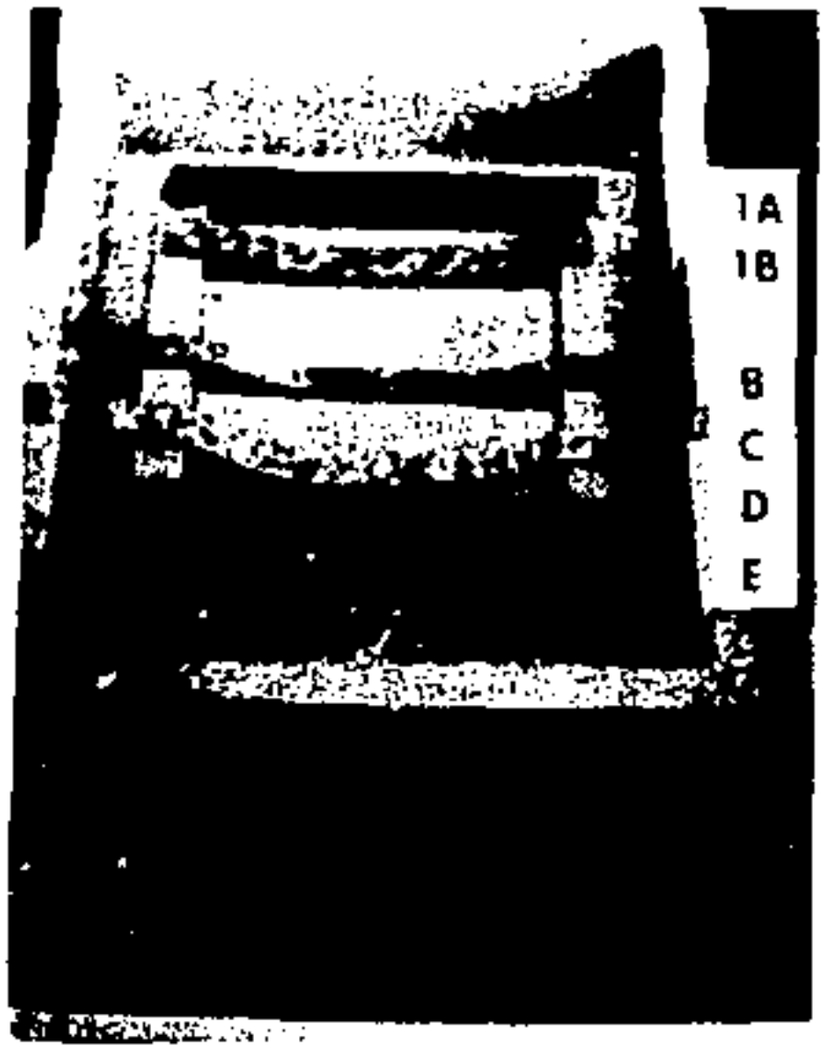

Figure F-1. Slump test at 1200°C for 1 hour

Table F-I. Summary of Hot Stage Microscope Observations

Granite	Substantial Liquid Temperature °C	Flow Temperature °C
Jet Mist	1150 - 1175	1250
Salisbury	1230	>1300
Academy	1175	1275
Cold Springs Green	1150	>1300
Sierra White	1210	>1300
Charcoal Black	1200	1250
Dark Pearl	1170	1270
Berkeley	1150 (Black areas)	>1300

Another way to determine the melting points of the rocks is to measure the heat effect associated with melting using differential thermal analysis (DTA). Generally, a peak corresponding to adsorption of heat at the melting point of a particular crystalline phase will be observed for each crystalline phase. The DTA curves for Salisbury Pink Granite and Jet Mist are shown in Figures F-2 and F-3. In a complex material, such as granite, the peaks may not be well defined. The endothermic peaks associated with melting of some crystalline phases in the Salisbury Pink granite, for example, are not resolved because the crystals melt very slowly. The abrupt changes in the curve are associated with a change in the effective thermal diffusivity of the specimen brought about by melting of one of the constituents.

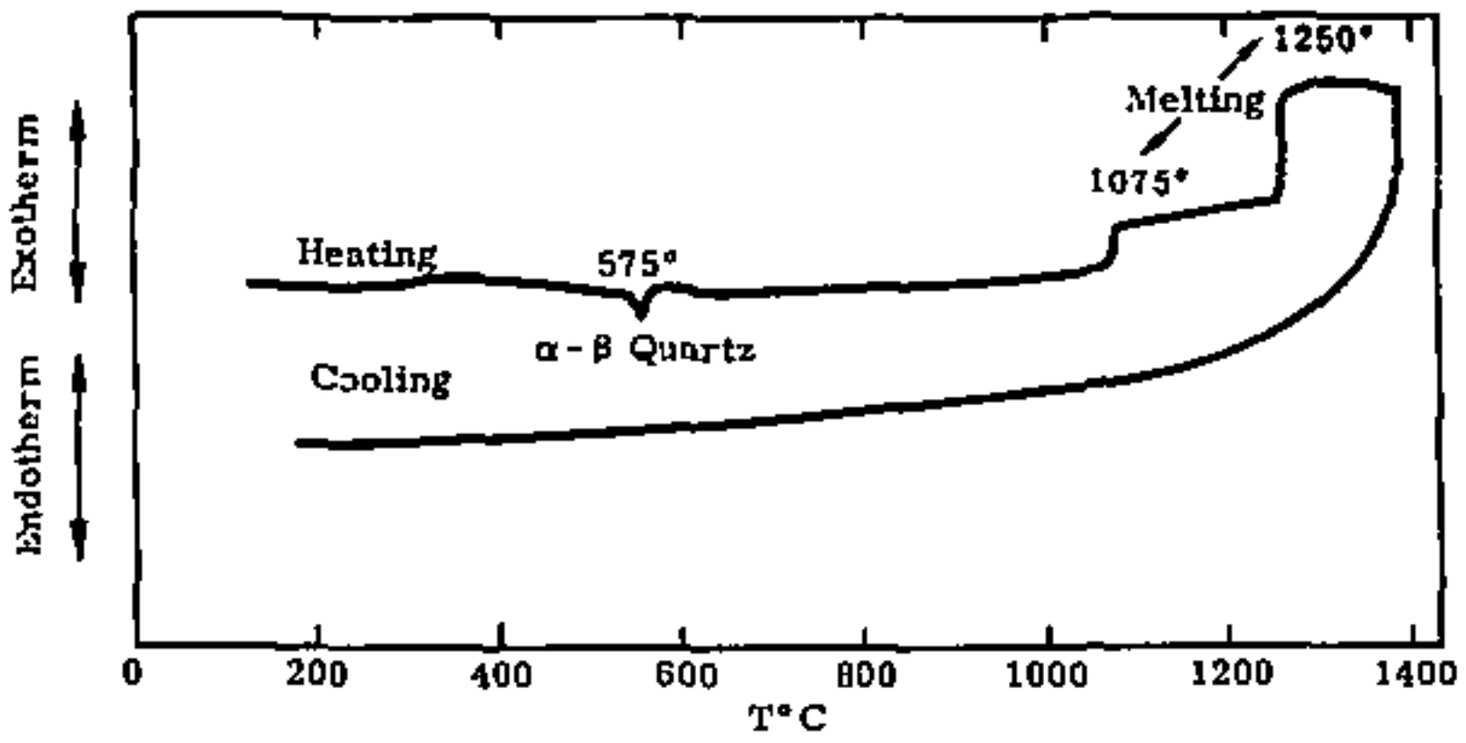

Figure F-2. DTA trace of Salisbury Pink Granite. Heating rate 10°C/min.

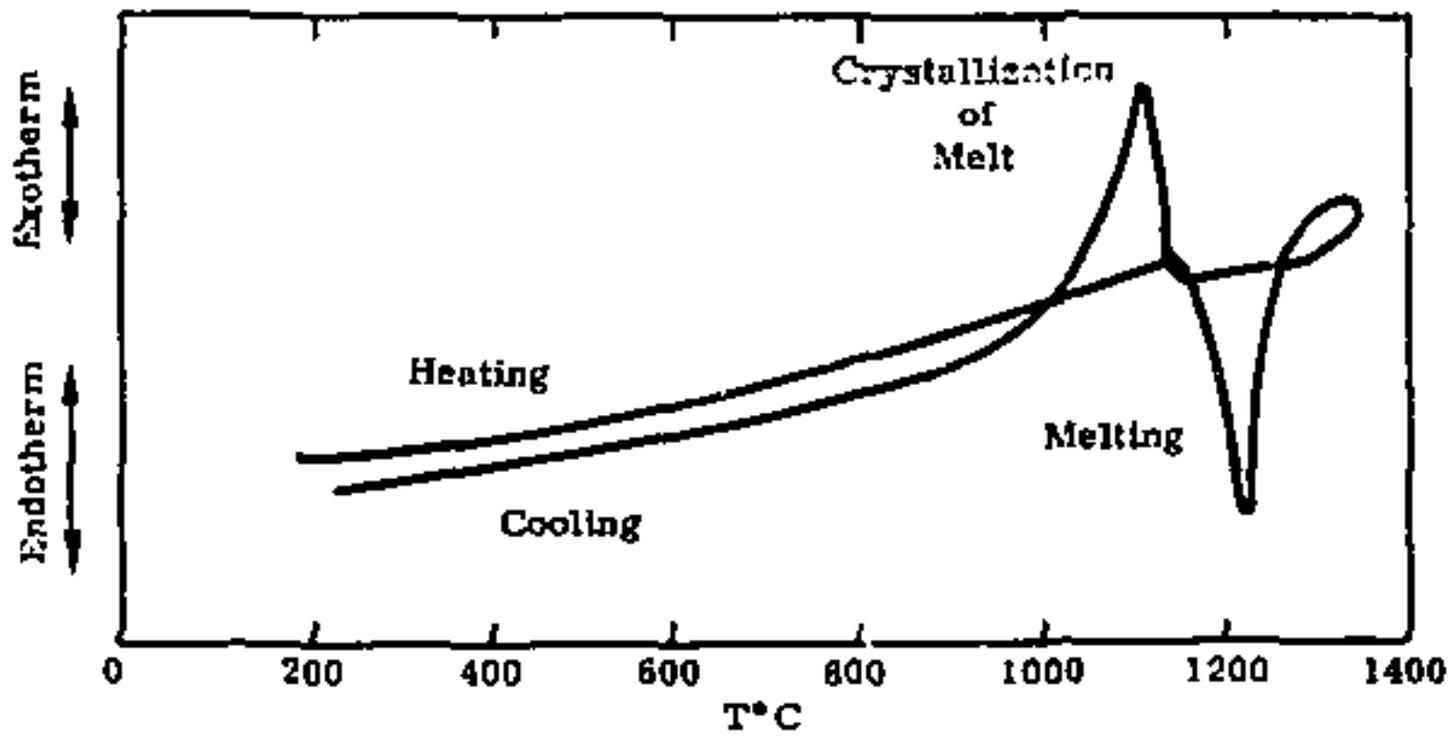

Figure F-3. DTA trace of Jet Mist Dolerite. Heating rate 10°/min.

Samples of Jet Mist and Salisbury Pink were examined by X-Ray Diffraction to determine the crystalline phases (G. Gay - 5525). Owing to the complexity of the rock, identification of each mineral shown in Table F-II is not absolutely certain.

Table F-II. Composition of Granitic Rocks

Salisbury Pink	Jet Mist
α quartz	Diopside (Pyroxene)
Oligioclase (Potassium Feldspar)	Hedenbergite (Pyroxene)
Microcline (Potassium Feldspar)	Bytownite (Plagioclase Feldspar)
Biotite (Mica)	
Bytownite (Plagioclase Feldspar)	

Density of Melted Rock

Tabular values for granitic rocks indicate that volume increases of the order of 10% occur on melting. Since this volume increase will increase the melt level in the Deep Rock Test, it is important to determine the magnitude of change. Samples of the Jet Mist were melted, held at temperature long enough to eliminate most bubbles, and then quenched. The resultant glass density was 2.69 gm/cm^3. Initially, the Jet Mist had a density of 3.05 gm/cm^3.

Comments

On the basis of the slump tests alone, it might be assumed that the lowest melting granite was the Sierra White. However, when the results of the experiments in the hot-stage microscope are considered, it is clear that although the Sierra White and the other granites which deformed easily contain low melting phases, they also contain refractory materials which prevent complete melting at lower temperatures. On the other hand, the Jet Mist does not deform even at 1200°C but melts essentially completely at 1250°C to give a fluid melt. (It also is the strongest of the materials at high temperature, apparently because it contains little or no mica.) If the choice among these materials was made on the basis of maximum fluidity at the lowest temperature, the Jet Mist is the best material. Charcoal Black is apparently next best (with Academy Black a close third).

APPENDIX G

SYNTHESIS OF FUEL WASTE SIMULANT AND REFRACTORY COMPATIBILITY

APPENDIX G

SYNTHESIS OF FUEL WASTE SIMULANT AND REFRACTORY COMPATIBILITY

Sandia Laboratories

Albuquerque, New Mexico
Livermore, California

date October 5, 1973

to R. D. Klett - 4734

from E. K. Beauchamp and H. J. Gregory - 5316

subject Synthesis of Fuel Waste Simulant and Refractory Compatibility

Glass Melting Experiments

Presently, fission products are generally removed from reactor fuel (after "burning" only a small fraction of the fuel) by the Purex process. The waste is initially in the form of an aqueous solution of (primarily) nitrate salts. The composition of the solution varies with reactor type and with the time the fuel is exposed to the reactor environment. A typical composition, and the one chosen by Battelle Northwest (BNW) for most of their experiments on solidification of waste, is shown in Table I.

The primary consideration in synthesizing a fuel waste simulant for the first deep rock disposal experiment is that the simulant have low viscosity so that convective heat transfer can be promoted. The first trial melts were made using a phosphate addition to give a glass with the composition shown in Table II. This approximates the orthophosphate melts examined by BNW for use in stainless steel containers.

The phosphate glass melted easily and was very fluid above 1000°C. However, it vigorously attacked most of the oxide refractories that it contacted and destroyed the molybdenum disilicide heating elements in the melting furnace apparently by vapor transport of P_2O_5. The platinum crucible used to melt the glass showed no signs of attack. Since there was also some concern that the relatively high solubility of phosphate glasses in water might make it difficult to handle samples in post-melt analysis, it appeared worthwhile to try melting a borosilicate glass.

Table I

REFERENCE WASTE COMPOSITION PW-6

(Excluding High Vapor Pressure Materials)

Process Waste

Element	Na	Fe	Cr	Ni
Moles	2.0	0.5	0.045	0.020

Fission Products

Element	Mo	Tc(Mo)	Sr	Ba	Cs(K)	Rb(K)
Moles	0.095	0.022	0.027	0.027	0.054	0.010

Element	Y+Re(Ce)	Zr	Ru(Fe)	Rh(Co)	Pd(Ni)	Te
Moles	0.208	0.106	0.059	0.010	0.032	0.012

Element	Ag	Cd
Moles	0.002	0.002

Actinides

Element	Np(U)	U+Pu(U)	Am+Cm(Ce)
Moles	0.0085	0.054	0.0022

Table II

PROPOSED FUEL WASTE SIMULANT (ORTHOPHOSPHATE MELT)

Oxide	Moles	Batch Additive
Na_2O	1.0	Na_2CO_3
Fe_2O_3	0.280	Fe_2O_3
Cr_2O_3	0.022	Cr_2O_3
NiO	0.052	NiO
MoO_3	0.117	MoO_3
SrO	0.027	$SrCO_3$
BaO	0.027	$BaCO_3$
K_2O	0.032	K_2CO_3
ZrO_2	0.106	ZrO_2
CoO	0.010	$CoCO_3$
UO_2	.0625	$UO_2(U_3O_8)$
Y_2O_3	0.021	Y_2O_3
CeO_2	0.162	CeO_2
PO_4	2.017	$NH_4H_2PO_4$

The choice of the composition for the borosilicate glass was made on the basis of the ternary phase diagram for the Na_2O-B_2O_3-SiO_2 system. As seen in Fig. 1, the lowest melting point for the system is a ternary eutectic at 540°C. The borosilicate melt was made by replacing the Na_2O at the composition of the eutectic with an equivalent mole fraction of the mixture of oxides in the fuel waste. The melt composition is the same as that shown in Table II except that the PO_4 is replaced with 1.5 moles of B_2O_3 and 3.0 moles of SiO_2.

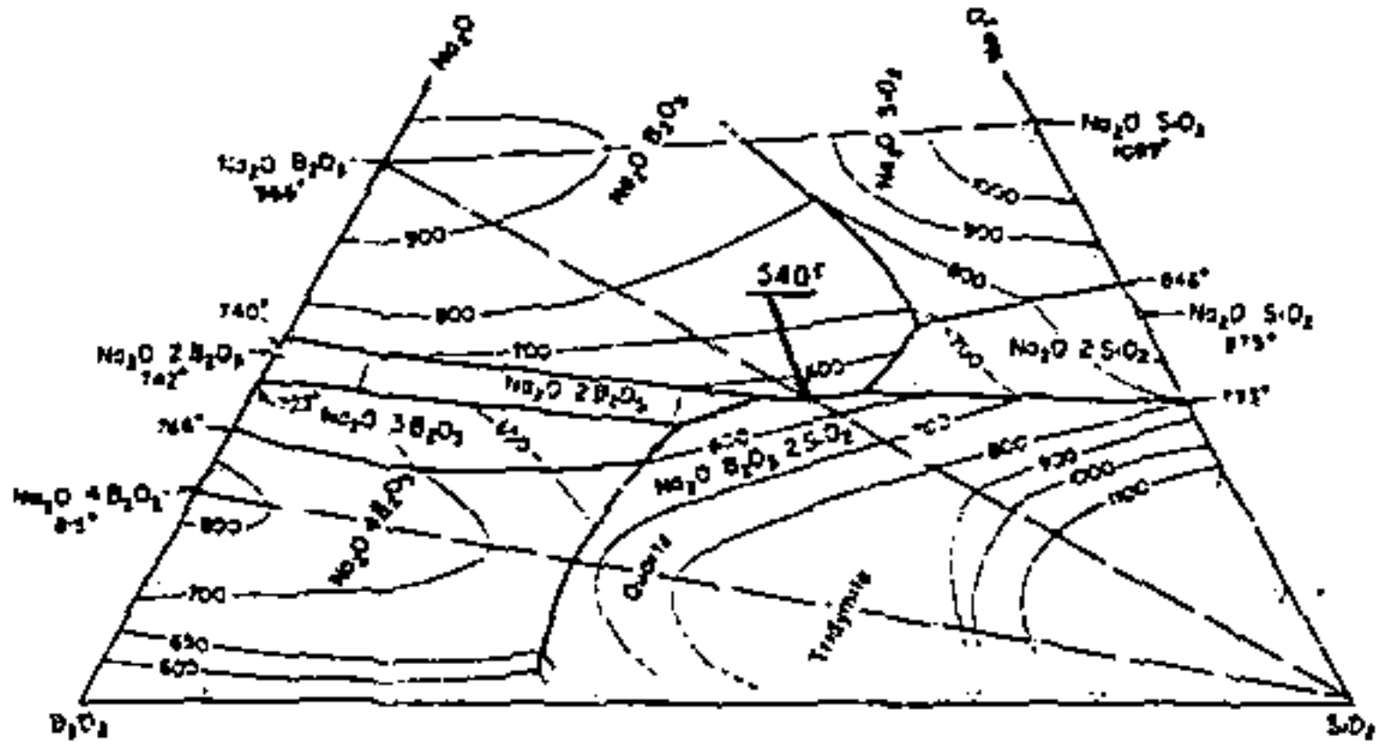

Figure 1. System Na_2O-B_2O_3-SiO_2

Like the phosphate glass, the borosilicate glass is very fluid at 1000°C, with a viscosity estimated at 50 poise. The change in viscosity with temperature is not extremely rapid -- at 800°C the glass is probably still above the softening point, i.e., less than 10^7 poise.

Generally the borosilicate glass quality is good. No devitrification (crystallization) has been observed and seed (bubble) content has been low. In the first melt, some segregation occurred, apparently because of settling of high density batch constituents to the bottom of the crucible in the early stages of melting. However, with manual stirring at intervals, the glass homogeneity was greatly improved in subsequent melts. The glass is nearly black; thin sections are dark brown with a green tint. The expansion curve for the glass is shown in Figure 2.

Glass-Refractory Compatibility

In the deep rock test, the molten fuel simulant will be contacting the heater tube and several thermocouple protection tubes. In an attempt to find a suitable refractory material for these interfaces, some simple compatibility tests were performed by immersing candidate materials in the borosilicate glass and observing their erosion. The materials tested included 96% and 99.8% (AD-99) alumina, porous zirconia, dense (hot-pressed) zirconia, silicon carbide from a broken Globar element, boron nitride (HPBN), molybdenum disilicide flame-sprayed on a molybdenum rod, tin oxide and platinum. The glass was held in a platinum crucible.

The alumina and zirconia behaved similarly. All samples showed moderate to severe attack after 24 hrs. at 1200°C and 1300°C. Typically for glass attack on refractory oxides, erosion was enhanced at the glass-air interface.

The molybdenum disilicide and SiC samples completely dissolved within a few hours of immersion. The boron nitride also dissolved rapidly. However, neither the tin oxide nor the platinum showed any sign of attack.

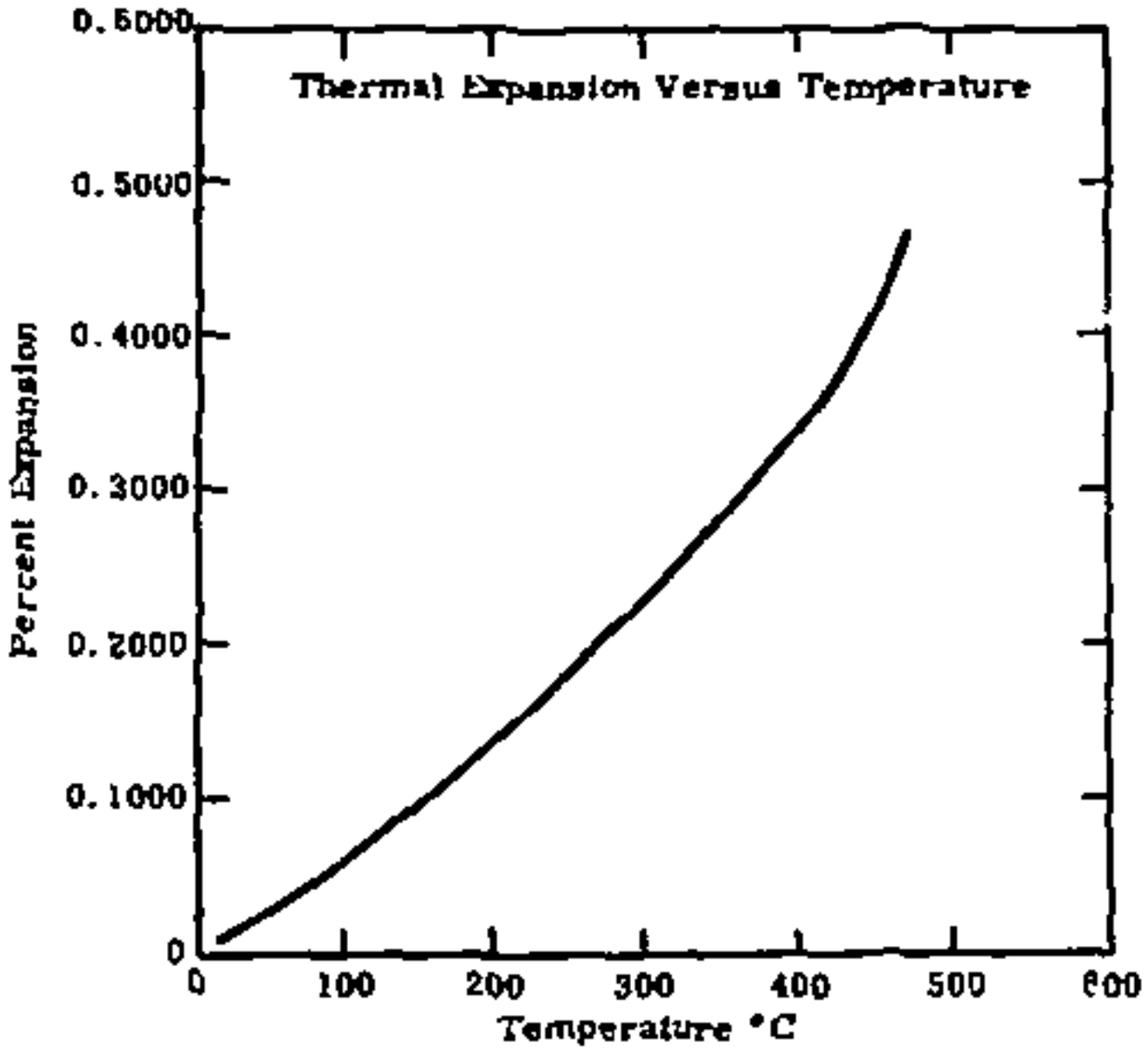

Figure 2. Expansion curve for borosilicate waste simulant glass

On the basis of these results it was recommended that platinum-sheathed thermocouples be used and that the protection tube for the heater be alumina with a platinum sheath. (The oxide is not available in tube form.)

Production of Glass for the Deep Rock Test

The volume of the glass required for the Deep Rock Test is slightly more than six liters. (With a glass density of 2.7, that amounts to >16kg). The crucible size limits the volume of a melt to less than 0.4 liters, so that at least 16 melts are required.

The glass is being melted in platinum crucibles at 1100°C. Initially, it appeared that the easiest way to load the glass into the granite block would be as a free flowing frit. Therefore, after melting, the molten glass was "dri-gaged," i.e., poured in a stream into water so that thermal stresses would break the glass into small particles.

The particle size from this treatment averaged about 1/8-inch diameter. However, the packing density for the particles was only 50-55%. The limited volume in the test cavity requires a packing density of >65% to produce the desired level of glass after remelting. An attempt was made to dry mill the glass frit, but only marginal improvement in packing density was obtained. Milling the glass to a very fine powder, especially with water as a vehicle, is undesirable since absorbed water could cause foaming of the glass in remelting.

To put the glass in a form which could be easily packed into the test cavity, it was remelted at 1000°C and then pressed into the simple mold shown in Figure 3. The resultant ring section of glass is also shown. Since some cracking of the pressed parts could be tolerated only perfunctory annealing (at 450°C) was performed.

Figure 3. Mold and fuel simulant ring section

APPENDIX H

PRELIMINARY THERMAL STRESS ANALYSIS OF THE DEEP ROCK NUCLEAR WASTE DISPOSAL EXPERIMENT

APPENDIX H

PRELIMINARY THERMAL STRESS ANALYSIS OF THE DEEP ROCK NUCLEAR WASTE DISPOSAL EXPERIMENT

Sandia Laboratories
Albuquerque, New Mexico
Livermore, California

date October 1, 1973

to R. D. Klett - 4734

John T Schomaeun

from J. T. Schomaeun - 1544

subject Preliminary Thermal Stress Analysis of the Deep Rock Nuclear Waste Disposal Experiment

A preliminary thermal stress analysis of the granite rock for the "deep rock nuclear waste disposal experiment" was completed. Both the 36" and 60" diameter geometries were considered. The stresses were calculated for a two-dimensional circular slice from the granite block. Due to symmetry, the problem is mathematically dependent only upon the radial dimension.

Analyses were made based on both the following assumptions:

1) Temperature independent material properties - A closed form solution is available for this type of thermal stress problem for temperature independent material properties. This solution was used to rapidly study the various temperature and geometry conditions.

2) Temperature dependent material properties - A finite element computer program was used to determine the effects of temperature dependent material behavior. For this preliminary study, the material was considered to be elastic. The material property definition used is given in Table 1.

The thermal profiles used are given in Figures 1 through 3. The two temperature profiles in Figure 3 are representative of two proposed heat pulses for the 36" diameter model (7 kw constant heat pulse, 2 days and Pulse A, 20 days).

The calculated hoop stresses for the two temperature profiles are given in Figure 4. The inner material is in compression and the outer material is in tension. The reduction in stress near the inner surface is due to the effect of temperature dependent material properties. A complete summary of the results is given in Table 2. The effect of temperature dependent material properties can be seen by comparing similar conditions. The 7 kw heat pulse

is considerably more severe than the Pulse A environment. The ultimate tensile strength of the granite is only about 3,000 psi.

The structural significance of these results is difficult to assess. If the granite material behaves in a linear manner having the properties given in Table 1, the rock will fracture at the outer surface and the crack will progress inward. In reality, the granite material behavior is probably viscoelastic (creep) or plastic (nonlinear). Both of these effects will reduce the magnitudes of the hoop stress. The analysis methods are available to include either viscoelastic or plastic material behavior when material properties are determined. The present two-dimensional analysis can be easily extended to the three-dimensional, axisymmetric geometry when desired. I feel that the simple two-dimensional analysis is adequate for this preliminary evaluation.

Table 1

Granite Material

Temperature °F	Modulus of Elasticity psi x 10^6	Coefficient of Expansion in/in°F x 10^{-6}
0	9.0	4.6
600	9.0	4.6
900	4.5	5.6
1500	2.25	5.5
2300	.45	4.6

Table 2

Summary of Results

Thermal Profile	Figure Number	Geometry	Material	Tensile Hoop Stress (psi)
A	1	60"D	Constant	29,200
B	1	60"D	Constant	11,700
C	1	60"D	Constant	6,10[illegible]
50 Hours	1	60"D	Table 1	12,200
D	2	36"D	Constant	25,800
E	2	36"D	Constant	23,500
F	2	36"D	Constant	16,400
7 kw Constant	3	36"D	Table 1	20,700
Pulse A	3	36"D	Table 1	14,650

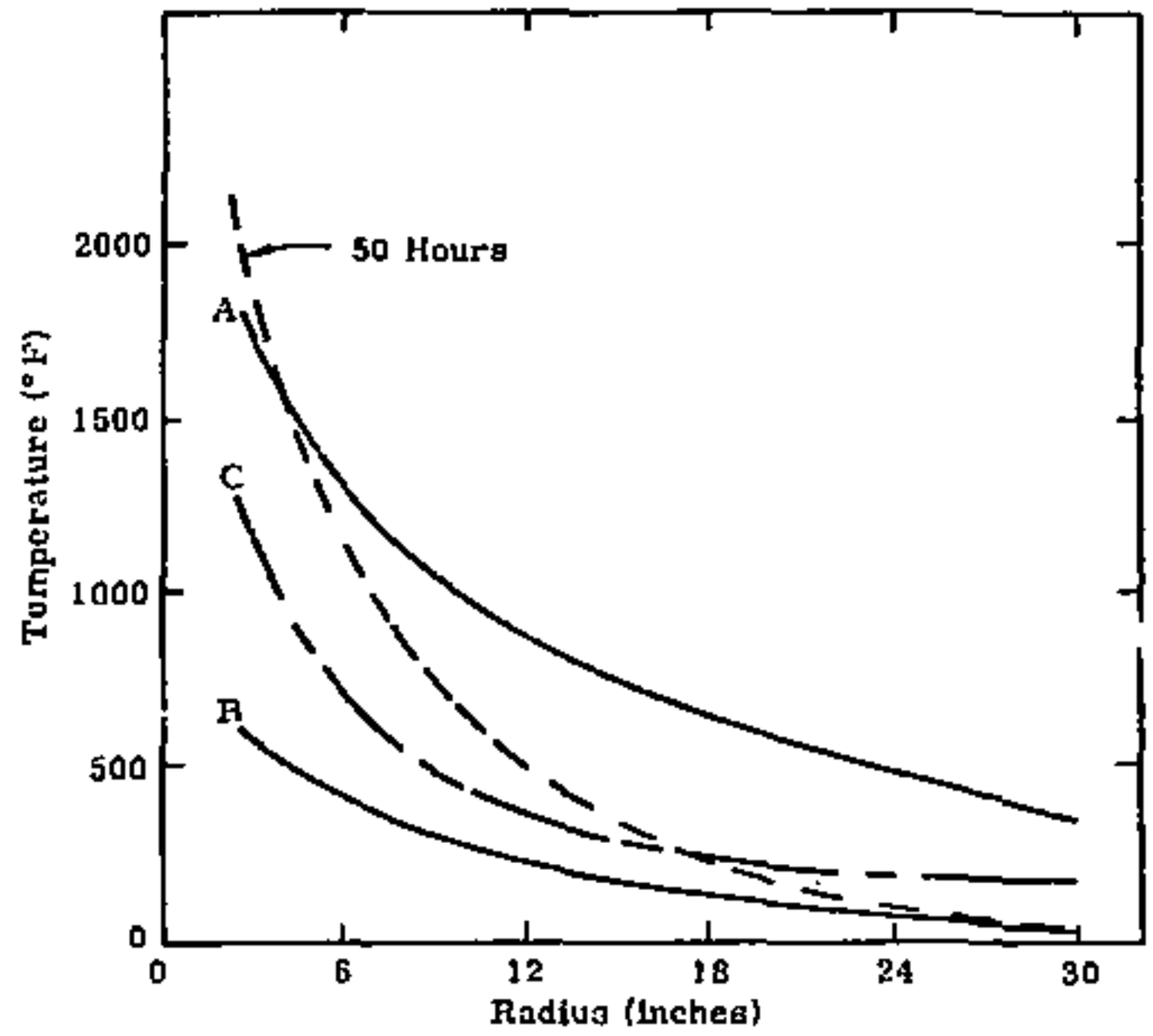

Figure 1. Temperature profiles, 60-inch diameter

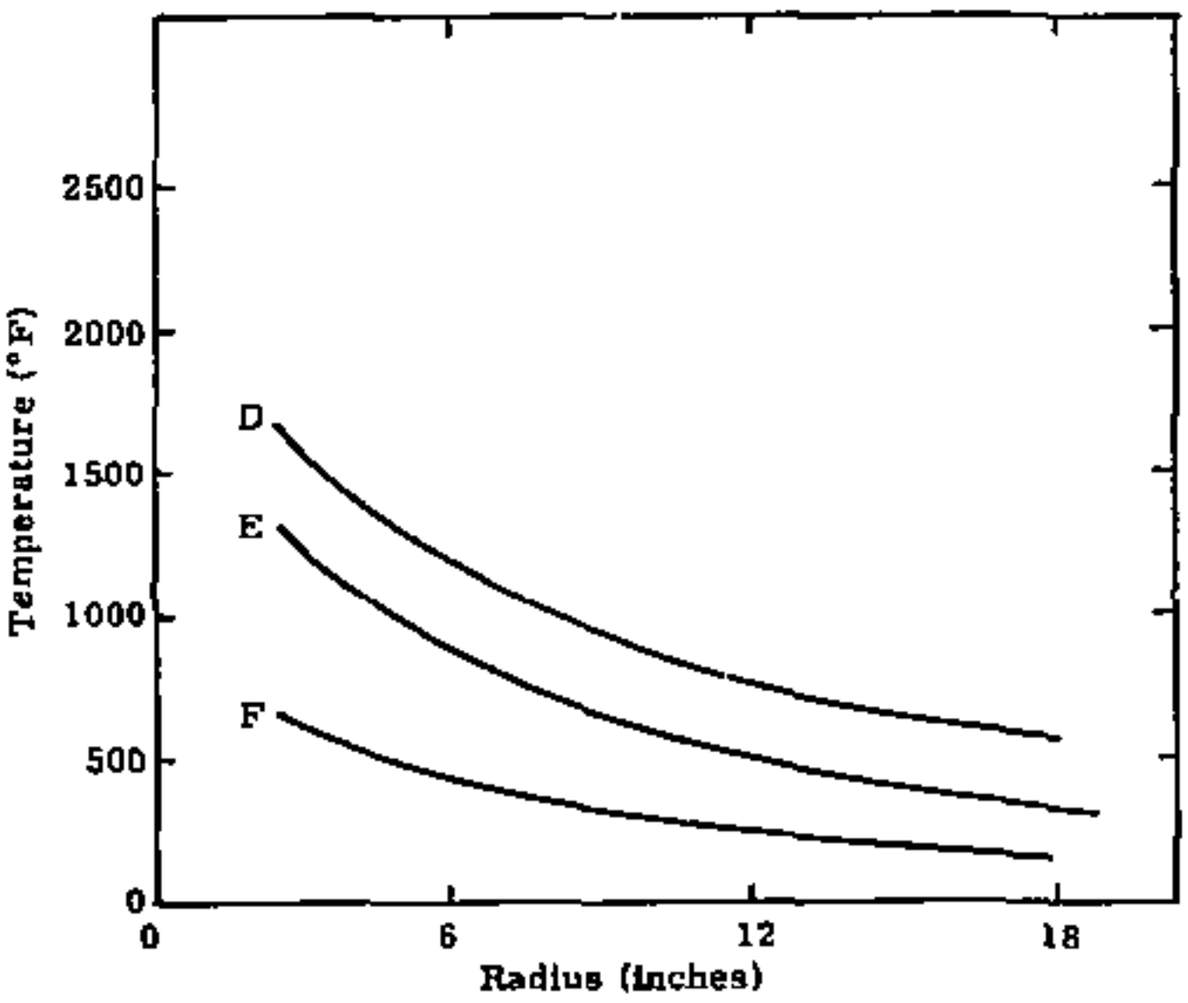

Figure 2. Temperature profiles, 36-inch diameter

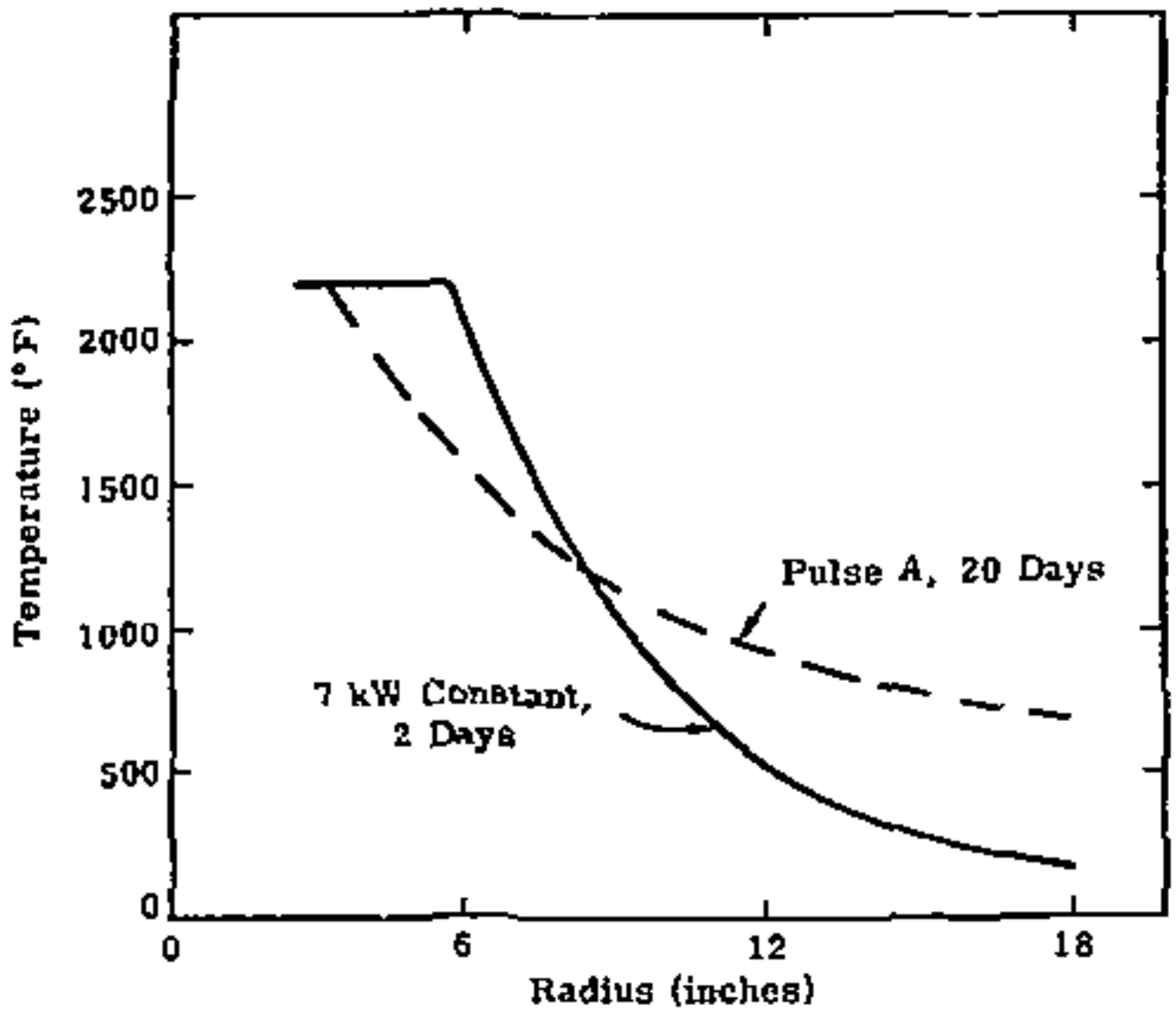

Figure 3. Temperature profiles, 36-inch diameter

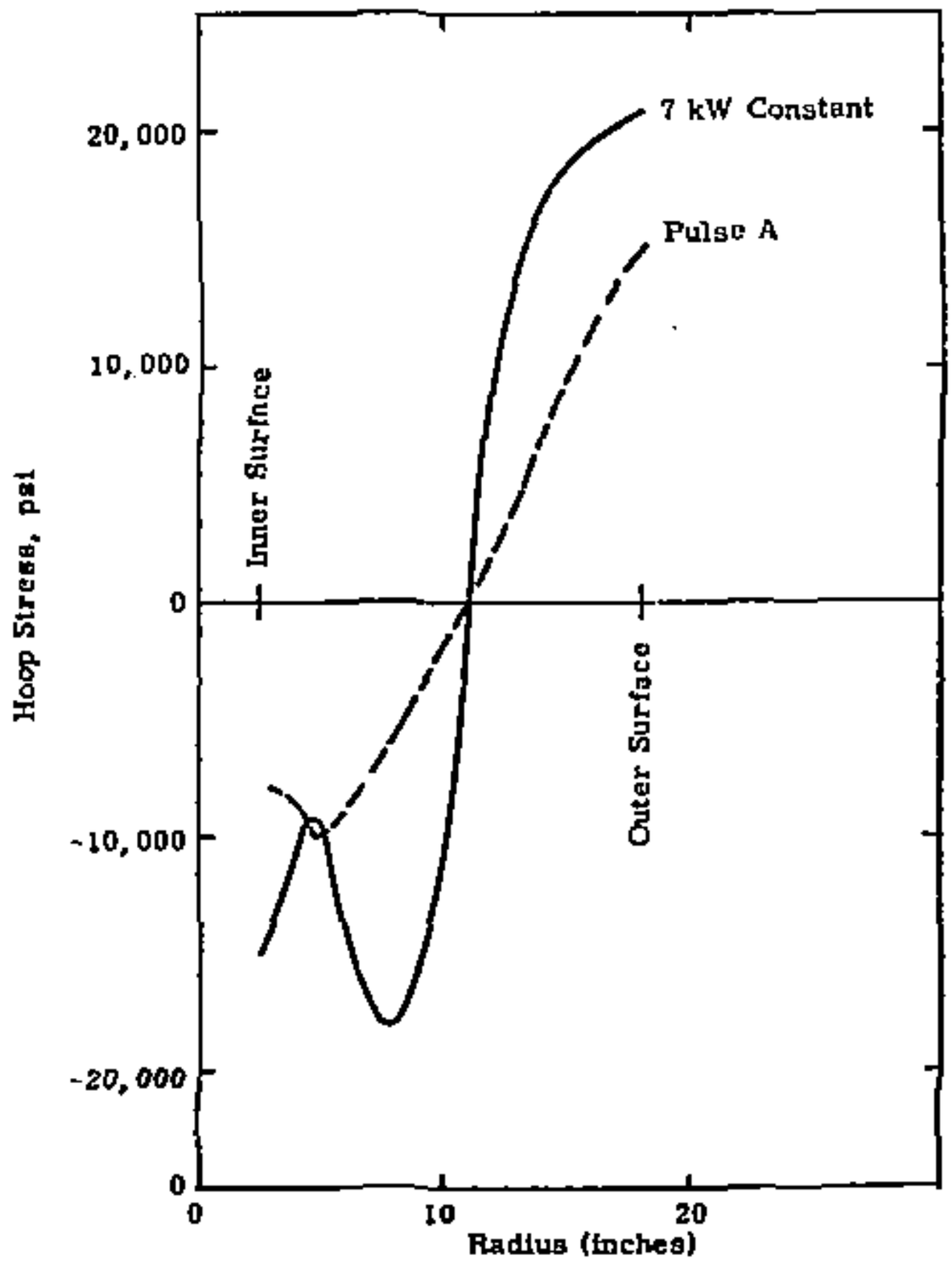

Figure 4. Stress profiles

APPENDIX I

DEEP ROCK WASTE DISPOSAL EXPERIMENT #1 (DRD-1)

APPENDIX I

DEEP ROCK WASTE DISPOSAL EXPERIMENT #1 (DRD-1)

Sandia Laboratories

Albuquerque New Mexico
Livermore California

date February 12, 1974

to Memorandum of Record

B. T. Kenna

from B. T. Kenna - 5822

subject *Deep Rock Waste Disposal Experiment #1 (DRD-1)*

Ref: Memo, B. T. Kenna to R. D. Klett, "Analyses of Samples from Deep Rock Waste Disposal Experiment," dtd 1/2/74*

The DRD-1 experiment, described in the referenced memo, has been in progress for about a month and has proceeded in accord to pre-experimental planning. However, the maximum power available at the experimental site meant that only a slow, undeterminable, melting rate could be obtained and, therefore, theoretical calculations of the melt composition were difficult at best. Small samples of the melt could be obtained by inserting a steel tube (1/4" O. D., 1/8" I. D.) into the center of the melt and applying suction to draw a small amount of molten mass into the tube. After cooling, the tube was sectioned and the black, glassy-like material removed for analysis by x-ray fluorescence. Four samples were obtained: (1) a small blob sticking to the end of a thermocouple placed in the melt for a short period, date 2/4/74; (2) a large-grain, sandy-like material which stuck to the sides of the thermocouple, data 2/4/74; (3) a sample collected in a steel pipette as described above, data 2/5/74. Because the samples were powdered rather than solid and also varied in quantity, it was not possible to ensure that similar volumes in each sample would be used in the analyses. Peak intensity ratios, using an element (such as Fe) indigenous to the rock as the normalizing factor, alleviate this problem. These ratios can then be compared to peak intensity ratios derived from the solid standards described in the reference.

As shown in Table I, the analysis of samples 1, 3, and 4 indicated progressive diluting of the simulant by rock, i. e., 60-80% simulant, 40-50% simulant, and ~15% simulant, respectively. Perturbation of the Fe content of samples 3 and 4 perhaps could have occurred during the time the molten mixture was in contact with the interior of the steel tube. However, the time duration of this contact before solidification of the melt was on the order of a few minutes, and any perturbation should be minimal. Nonetheless, a longitudinally sectioned sample of steel pipette with the solidified glass in place will be studied with the electron microprobe to determine that interior leaching or melting of the steel tube was not a problem. Sample 2 apparently was granulated rock only with <1% simulant included.

---

*Appendix K.

Since ca. 20% simulant was approximately the composition desired at the end of the test, increases in the thermal input were discontinued and the cooling cycle has begun. This will involve about a month's time to ensure that the rock does not suffer severe thermal shock. The maximum temperature reached was 1320°C.

Table I. Analysis of Samples from DRD-1

Sample	Intensity Ratio Mo/Fe	U/Fe	Sr/Fe	Ce/Fe	% Simulant
10% simulant	0.00851	0.0063	0.00469	0.00825	10
30% simulant	0.0254	0.0213	0.0168	0.0238	30
50% simulant	0.0282	0.0262	0.0160	0.0200	50
70% simulant	0.0387	0.0395	0.0235	0.0350	70
90% simulant	0.0477	0.0495	0.0307	0.0603	90
#1	0.0296	0.0347	0.0243	0.0495	~70
#2*	0	0	0	0	<1
#3	0.0241	0.0249	0.0157	0.0373	~45
#4	0.00691	0.00773	0.00453	0.0145	~15

*None of the elements included in the simulant were detected, but the elements included in the rock were found.

APPENDIX J

SAMPLE ANALYSES IN SUPPORT OF THE DEEP ROCK DISPOSAL EXPERIMENT

APPENDIX J

SAMPLE ANALYSES IN SUPPORT OF THE DEEP ROCK DISPOSAL EXPERIMENT

Sandia Laboratories

Albuquerque, New Mexico
Livermore, California

date October 4, 1973

to R. D. Klett - 4734

B. T. Kerma

from B. T. Kerma - 5525

subject Sample Analyses in Support of the Deep Rock Disposal Experiment

The initial deep rock disposal experiment will provide a sample ca. 3 ft by 4.5 ft by 0.25 in. for elemental analyses. This memo summarizes the primary methods to be used for elemental analyses and the methods available to answer specific questions regarding the sample if required.

The initial objective is to determine the extent of diffusion by the borosilicate-fuel simulant in the dolerite matrix during the liquid phase. Analysis of each element present in the sample slab is not necessary to obtain this information. At the outset, it is suggested that we look at one or two elements having fast (Na or K), intermediate (Sr or Ba), and slow (Y, Zr, Ce or U), diffusion rates. Although a final decision must wait until analyses are completed *on standard pre-test samples, an educated guess suggests that we* determine K, Ba, Zr, and U.

The following analytical methods are being considered for use. It is not intended that all these methods be used on each specimen; rather, the methods would be used to complement each other as needed.

1) X-ray fluorescence spectroscopy. Both energy dispersive and crystal dispersive fluorescence capabilities are available. This would be the simplest method since neither mechanical nor chemical destruction of the sample is required. Profiles of element concentrations can be obtained by scanning the sample surface in a step-wise manner. This is expected to be the main technique used.

2) Atomic absorption spectrometry. By dividing the sample surface into a grid network and taking a sample from each grid (e.g., by drilling), atomic absorption spectrometry can be used to provide more precise quantitative data for specific elements. This method would be used for determining the exact concentrations of elements at locations thought to be particularly significant.

3) Classical chemistry. By dissolving samples taken from the grid network, the exact concentration of elements throughout the sample can be obtained by standard gravimetric, volumetric, or electrochemical means. These methods are generally considered to be the most accurate, and they will be used as a reference for the more rapid instrumental techniques.

4) Autoradiography. Since uranium is naturally radioactive, autoradiography should be an excellent means for determining uranium distribution in the sample slab. Other naturally radioactive elements such as ^{40}K do not emit sufficient radiation to interfere with this; however, gamma ray spectroscopy may be applicable for determining their abundances.

Items such as density and porosity can generally be determined by direct radiography.

5) Neutron activation analysis and gamma ray spectroscopy. For less complex matrices, activation analysis and gamma ray spectroscopy can define element concentrations. However, in a system this complicated, radiochemical separations will almost certainly be necessary. Although this technique is applicable for determining major concentrations of elements, its applicability will more probably be in the area of trace analyses.

6) Emission spectrography. For detecting a large number of elements at one time, emission spectrography has no peer. However, it generally is not used for quantitative determinations of elements present in high concentrations (> 5%). It would be used for semiquantitative determinations of minor or trace elements as necessary.

7) Electron microscopy. Although both scanning and transmission electron microscopes are available, probably only scanning electron microscopy would be used. This technique would permit us to define the sample surface in terms of grain size, elements present in grains, and general surface morphology.

8) Electron microprobe. Under computer control, this instrument provides quantitative analyses as a function of distance. Each individual analysis is representative of a minute volume of material and only a small area can be done at a time. However, its capability for defining spatially resolved elemental distributions may be of real significance.

9) Other techniques which may find use include x-ray (diffraction, spectrography, etc.) and ion backscattering. Although these methods are not presently considered immediately applicable, they are available should the need arise.

With the analytical equipment and expertise available, the elemental analyses planned should not present any severe problems. With the experience gained from this first experiment it is probable that additional methods of characterization will be recognized, and these can be made available for use on future tests.

APPENDIX K

ANALYSIS OF SAMPLES FROM DEEP ROCK WASTE DISPOSAL EXPERIMENT

APPENDIX K

ANALYSIS OF SAMPLES FROM DEEP ROCK WASTE DISPOSAL EXPERIMENT

Sandia Laboratories

Albuquerque, New Mexico
Livermore, California

date January 2, 1974

to R. D. Klett - 4734

from B. T. Kenna - 5822

subject: Analysis of Samples from Deep Rock Waste Disposal Experiment

Ref: Memo, B. T. Kenna to R. D. Klett, "Sample Analysis in Support of the Deep Rock Waste Disposal Experiment," dtd Oct. 4, 1973 *

The Deep Rock Waste Disposal experiment is beginning and samples should be available for analysis about February of this year. This memo summarizes the sample configuration we would like to have and the analytical procedures we have planned. The initial analytical objective is to determine the relative extent of mixing and diffusion by the borosilicate-fuel simulant in the dolerite matrix during the liquid phase. The elements we will determine semiquantitatively are Ni, Sr (fast to intermediate diffusion rates), Y, Ce, and U (slow diffusion rates). We had hoped to also determine either Na or K, but this will not be possible due to interferences.

As we understand, our gross sample will be a slab between 0.25 in. and 2.0 in. thick with a height (4.5') equal to the height of the original dolerite ("Jet Mist") block (4.5') and the width will be equal to the width of the block (3.0 ft). It is important that our gross sample be from the center of the block so that elemental distributions and/or mixing patterns can be properly established. The samples for our analysis then would be cut from the gross sample slab in such a way that they would represent a matrix of the slab and would be indexed according to their position in the slab. The samples can be either square or circular in shape; their individual width could be either 1 or 2 in.

The primary analytical technique to be used will be energy dispersive x-ray fluorescence. Use will be made of atomic absorption and perhaps neutron activation analysis when deemed necessary to provide baseline analysis and to answer troublesome questions. The electron microprobe is also available to investigate any particularly interesting areas.

E. K. Beauchamp, 5846, has provided us with standards comprised of a mixture of "Jet Mist" rock and varying amounts of simulant material. Although the fluorescent x-ray spectrum is complicated, K_α and L peaks

---

*Appendix J

of six elements (Ni, Sr, Y, Mo, Ce, and U) can be isolated unambiguously for semiquantitative analysis. Atomic absorption analysis of these elements in the standards have verified the stated composition. Figures 1a, and b show the standard working curves developed from these standards which will be used for x-ray fluorescence analysis of the Deep Rock Waste Disposal samples. We estimate our analysis time will be about 3-4 weeks after receiving the samples.

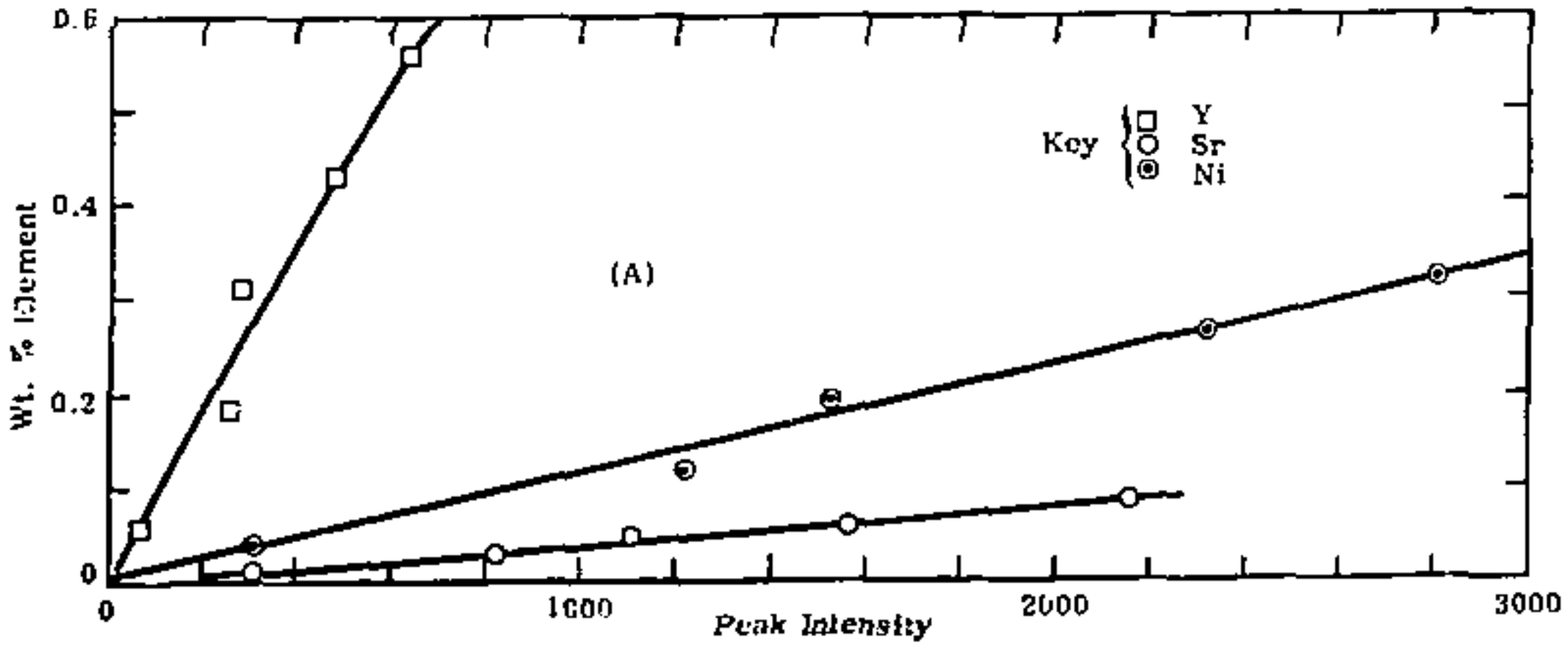

Figure 1. X-ray fluorescence peak intensity versus concentration standard curves for selected elements in deep rock waste disposal experiment

REFERENCES

1. A. S. Kubo and D. J. Rose, "Disposal of Nuclear Wastes," Science, December 21, 1973, p. 1205.

2. J. O. Blomeke, J. P. Nichols, and W. C. McClain, "Managing Radioactive Wastes," Physics Today, August 1973, p. 36.

3. J. O. Blomeke and C. W. Kee, "Projections of Radioactive Wastes from the Nuclear Fuel Cycle," Trans. Am. Nuclear Soc., November 1973, p. 324.

4. J. H. Rubin, "Evolving U. S. Policies in Radioactive Waste Management," AIF/ANS International Conference, November 12-16, 1972, Washington, D. C.

5. "Siting of Fuel Reprocessing Plants and Related Waste Management Facilities," Federal Register 35, No. 222, 17530, November 14, 1970.

6. K. J. Schneider, "Solidification and Disposal of High-Level Radioactive Wastes in the United States," Reactor Technology, Vol. 13, No. 4, Winter 1970-71.

7. "Waste Solidification Program Summary Report Vol. II," BNWL-1667, June 1972.

8. J. E. Hansen, "Advanced Waste Management Studies," Progress Report, October-November 1972, BNWL-B-223-3.

9. C. A. Mawson, Management of Radioactive Wastes, D. VanNostrand, Princeton, New Jersey, 1965.

10. "Overview of High-Level Radioactive Waste Management Studies," Battelle Pacific Northwest Laboratories, Nuclear Waste Technology Department, BNWL-1758, August 1973.

11. K. Duursma and M. K. Gross, "Marine Sediments and Radioactivity," Radioactivity in the Marine Environment, Nat. Academy of Sc. Publication, 1971.

12. R. S. Lewis, "The Radioactive Salt Mine," Bulletin of the Atomic Scientists, June 1971.

13. J. Donea, "Operation Hot Mole," Euro Spectra, Vol. II, No. 18, December 1972.

14. S. E. Logan, "Deep Self-Burial of Radioactive Wastes by Rock Melting Capsules," American Nuclear Society Annual Meeting June 10-14, 1973.

15. "An Evaluation of the Concept of Storing Radioactive Wastes in Bedrock below the Savannah River Plant Site," National Academy of Sciences, Washington, D. C., 1972.

16. "Disposal of Radioactive Wastes into the Ground," Symposium on the Disposal of Radioactive Wastes into the Ground, May 29 - June 2, 1967.

17. W. DeLaguna, "Radioactive Waste Disposal by Hydraulic Fracturing," Nuclear Safety, 11, 391, 1970.

18. J. J. Cohen, A. E. Lewis, and R. L. Braun, "In Situ Incorporation of Nuclear Waste in Deep Molten Silicate Rock," Nuclear Technology, April 1972.

19. H. S. Carslaw and J. C. Jaeger, Conduction of Heat in Solids, Oxford Press, New York, 1950.

20. J. A. Angelo, R. S. Post, F. E. Haskin, and C. Lewis, "Nuclear By-Product Long-Term Heat Generation Rates," Trans. Am. Nuclear Soc., November 1972, p. 663.

21. R. W. Bayley and W. R. Muehlberger, "Basement Rock Map of the United States," U. S. Geological Survey, 1968.

22. E. C. Jenkins and W. Thordarson, "Potential Sites for High Level Radioactive Waste Disposal, Nevada Test Site, Nevada," U. S. Geological Survey, July 12, 1972.

23. E. M. B. Dagum and K. P. Heiss, "An Economic Study of Small and Intermediate Size Diameter Drilling Costs for the United States," PNE-3012, June 1968.

24. "A Feasibility Study of a Plowshare Geothermal Plant," PNE-1550 (TID-4500), April 1971.

25. H. C. Hardee and W. N. Sullivan, "Ice Melting Experiments - A Model Study for Burial of Radioactive Wastes," SLA-73-0942, January 1974.

26. H. C. Hardee, "Natural Convection in a Spherical Cavity with Uniform Internal Heat Generation," SLA-74-0089, April 1974.

27. C. R. Longwell, R. F. Flint, and J. E. Sanders, Physical Geology, J. Whiley and Sons, Inc., New York, 1969.

28. S. P. Clark, Handbook of Physical Constants, The Geological Society of America, 1966.

29. U. I. Moiseyenko, L. S. Sokolova, and V. Ye Istomin, "Electrical and Thermal Properties of Rocks," NASA-TT-F-871, November 1970.

30. T. Murase and A. R. McBirney, "Properties of Some Common Igneous Rocks and Their Melts at High Temperature," Geo. Soc. of Amer. Bulletin, Vol. 84, No. 11, November 1973.

31. J. W. Elder, "Laminar Free Convection in a Vertical Slot," Journal of Fluid Mechanics, Vol. 23, Part 1, 1965.

32. J. W. Elder, "Turbulent Free Convection in a Vertical Slot," Journal of Fluid Mechanics, Vol. 23, Part 1, 1965.

33. D. R. Flynn and T. W. Watson, "Measurements of the Thermal Conductivity of Soils to High Temperatures," SC-CR-69-3059, April 1969.

34. M. S. Kersten, "Thermal Properties of Soils," Bulletin No. 28, University of Minnesota, Institute of Technology, Vol. 52, No. 21, June 1, 1949.

35. J. F. Schatz and G. Simmons, "Thermal Conductivity of Earth Materials at High Temperatures," Journal of Geophysical Research, Vol. 77, No. 35, December 10, 1972.

36. V. Ya. Leonidov and V. I. Vernadskiy, "Heat Capacities of Rocks at High Temperatures," Geokhimiya, No. 4, 1967.

37. H. C. Heard, "The Influence of Environment on the Inelastic Behavior of Rocks," UCRL-72164, December 12, 1969.

38. B. V. Baidyuk, "Mechanical Properties of Rocks at High Temperatures and Pressures," Consultants Bureau, New York, 1967.